AD 742005

Columbus Division
North American Rockwell

NR72H-12

EXPLORATORY INVESTIGATION OF PULSE BLOWING FOR BOUNDARY LAYER CONTROL

By

T. E. Oyler
W. E. Palmer

Columbus Aircraft Division/North American Rockwell Corporation

Prepared Under

Contract N00014-71-C-0259, NR215-183 (Code 461)

Sponsored By

The Office of Naval Research, Aeronautics

"Reproduction in whole or in part is permitted for any purpose of the U.S. Government"

Approval for Public Release;
Distribution Unlimited.

Reproduced by
NATIONAL TECHNICAL
INFORMATION SERVICE
Springfield Va 22151

87

UNCLASSIFIED
Security Classification

DOCUMENT CONTROL DATA - R&D

(Security classification of title, body of abstract and indexing annotation must be entered when the overall report is classified)

1. ORIGINATING ACTIVITY (Corporate author) Columbus Aircraft Division/North American Rockwell Corp. - 4300 E. Fifth Avenue, Columbus, Ohio 43216	2a. REPORT SECURITY CLASSIFICATION UNCLASSIFIED 2b. GROUP

3. REPORT TITLE

EXPLORATORY INVESTIGATION OF PULSE BLOWING FOR BOUNDARY LAYER CONTROL

4. DESCRIPTIVE NOTES (Type of report and inclusive dates)

Technical Report (April 1971 through January 1972)

5. AUTHOR(S) (Last name, first name, initial)

Oyler, Ted E.
Palmer, William E.

6. REPORT DATE 15 January 1972	7a. TOTAL NO. OF PAGES 84	7b. NO. OF REFS 5
8a. CONTRACT OR GRANT NO. N00014-71-C-0259 b. PROJECT NO. c. d.	9a. ORIGINATOR'S REPORT NUMBER(S) NR72H-12 9b. OTHER REPORT NO(S) (Any other numbers that may be assigned this report)	

10. AVAILABILITY/LIMITATION NOTICES

Approval for Public Release;
Distribution Unlimited.

11. SUPPLEMENTARY NOTES	12. SPONSORING MILITARY ACTIVITY Office of Naval Research Aeronautics Code 461 Arlington, Virginia 22217

13. ABSTRACT

Description of results of an experimental investigation to determine the feasibility of intermittent jet blowing to achieve reduced air flow rates as compared with steady blowing for prevention or delay of flow separation on a trailing edge flap. The jet was directed tangential to the flap surface in a downstream direction. The results show that significant reductions in mass flow rate could be realized at a given flap lift effectiveness.

Details of illustrations in
this document may be better
studied on microfiche

DD FORM 1 JAN 64 1473

UNCLASSIFIED
Security Classification

UNCLASSIFIED

Security Classification

14 KEY WORDS	LINK A ROLE	LINK A WT	LINK B ROLE	LINK B WT	LINK C ROLE	LINK C WT
Boundary Layer Control (BLC)						
Pulsing Jet						
High Lift Devices						
Experimental						

INSTRUCTIONS

1. ORIGINATING ACTIVITY: Enter the name and address of the contractor, subcontractor, grantee, Department of Defense activity or other organization *(corporate author)* issuing the report.

2a. REPORT SECURITY CLASSIFICATION: Enter the overall security classification of the report. Indicate whether "Restricted Data" is included. Marking is to be in accordance with appropriate security regulations.

2b. GROUP: Automatic downgrading is specified in DoD Directive 5200.10 and Armed Forces Industrial Manual. Enter the group number. Also, when applicable, show that optional markings have been used for Group 3 and Group 4 as authorized.

3. REPORT TITLE: Enter the complete report title in all capital letters. Titles in all cases should be unclassified. If a meaningful title cannot be selected without classification, show title classification in all capitals in parenthesis immediately following the title.

4. DESCRIPTIVE NOTES: If appropriate, enter the type of report, e.g., interim, progress, summary, annual, or final. Give the inclusive dates when a specific reporting period is covered.

5. AUTHOR(S): Enter the name(s) of author(s) as shown on or in the report. Enter last name, first name, middle initial. If military, show rank and branch of service. The name of the principal author is an absolute minimum requirement.

6. REPORT DATE: Enter the date of the report as day, month, year, or month, year. If more than one date appears on the report, use date of publication.

7a. TOTAL NUMBER OF PAGES: The total page count should follow normal pagination procedures, i.e., enter the number of pages containing information.

7b. NUMBER OF REFERENCES: Enter the total number of references cited in the report.

8a. CONTRACT OR GRANT NUMBER: If appropriate, enter the applicable number of the contract or grant under which the report was written.

8b, 8c, & 8d. PROJECT NUMBER: Enter the appropriate military department identification, such as project number, subproject number, system numbers, task number, etc.

9a. ORIGINATOR'S REPORT NUMBER(S): Enter the official report number by which the document will be identified and controlled by the originating activity. This number must be unique to this report.

9b. OTHER REPORT NUMBER(S): If the report has been assigned any other report numbers *(either by the originator or by the sponsor)*, also enter this number(s).

10. AVAILABILITY/LIMITATION NOTICES: Enter any limitations on further dissemination of the report, other than those imposed by security classification, using standard statements such as:

(1) "Qualified requesters may obtain copies of this report from DDC."

(2) "Foreign announcement and dissemination of this report by DDC is not authorized."

(3) "U. S. Government agencies may obtain copies of this report directly from DDC. Other qualified DDC users shall request through _____."

(4) "U. S. military agencies may obtain copies of this report directly from DDC. Other qualified users shall request through _____."

(5) "All distribution of this report is controlled. Qualified DDC users shall request through _____."

If the report has been furnished to the Office of Technical Services, Department of Commerce, for sale to the public, indicate this fact and enter the price, if known.

11. SUPPLEMENTARY NOTES: Use for additional explanatory notes.

12. SPONSORING MILITARY ACTIVITY: Enter the name of the departmental project office or laboratory sponsoring *(paying for)* the research and development. Include address.

13. ABSTRACT: Enter an abstract giving a brief and factual summary of the document indicative of the report, even though it may also appear elsewhere in the body of the technical report. If additional space is required, a continuation sheet shall be attached.

It is highly desirable that the abstract of classified reports be unclassified. Each paragraph of the abstract shall end with an indication of the military security classification of the information in the paragraph, represented as: (TS), (S), (C), or (U).

There is no limitation on the length of the abstract. However, the suggested length is from 150 to 225 words.

14. KEY WORDS: Key words are technically meaningful terms or short phrases that characterize a report and may be used as index entries for cataloging the report. Key words must be selected so that no security classification is required. Identifiers, such as equipment model designation, trade name, military project code name, geographic location, may be used as key words but will be followed by an indication of technical context. The assignment of links, roles, and weights is optional.

UNCLASSIFIED

Security Classification

Columbus Division
North American Rockwell

NR72F-12

EXPLORATORY INVESTIGATION OF PULSE BLOWING FOR BOUNDARY LAYER CONTROL

By

T. E. Oyler

W. E. Palmer

Columbus Aircraft Division/North American Rockwell Corporation

Prepared Under

Contract N00014-71-C-0259, NR215-183 (Code 461)

Sponsored By

The Office of Naval Research, Aeronautics

"Reproduction in whole or in part is permitted for any purpose of the U.S. Government"

Approval for Public Release;
Distribution Unlimited.

15 January 1972

Details of illustrations in this document may be better studied on microfiche

FOREWORD

This report is submitted to comply with the requirements of Contract No. N00014-71-C-0259 entitled "Pulsing Boundary Layer Control," dated 1 March 1971. The effort was conducted during the period from April 1971 to January 1972 and was monitored for the U.S. Navy by Mr. T. L. Wilson of the Aeronautics Branch of the Office of Naval Research.

The authors wish to express their appreciation for the use of the Army Air Mobility Research and Development Laboratory's 7' x 10' wind tunnel facility. The cooperation of its staff, under the direction of Mr. A. Morse, was excellent. Acknowledgement is also made of the services of Mr. T. Wynn who ably directed the conduct of the experimental test program.

ABSTRACT

This report describes the results of an experimental investigation to determine the feasibility of intermittent jet blowing to achieve reduced air flow rates as compared with steady blowing for prevention or delay of flow separation on a trailing edge flap. The jet was directed tangential to the flap surface in a downstream direction. The results show that significant reductions in mass flow rate could be realized at a given flap lift effectiveness.

SUMMARY

The results of an experimental investigation to determine the relative merits of both steady and pulsing boundary layer control (BLC) systems are presented.

Wind tunnel tests were conducted in the U.S. Army Air Mobility Research and Development Laboratory's 7' x 10' low speed wind tunnel located at Ames Research Center, Moffett Field, California.

A semi-span model with an advanced airfoil shape and two large end plates that produced a two-dimensional test channel of one-foot span was utilized. Experimental data consisting of pressure distributions for the center span station of the quasi two-dimensional test channel are compared for both pulsing and steady blowing cases. Instantaneous velocity measurements were made over the upper surface of a plain trailing edge flap by means of a hot wire anemometer. Conditions of no blowing, steady blowing, and intermittent blowing (pulsing) were investigated and compared for effectiveness. In addition, the pressure measurements were integrated to obtain wing, flap, and total airfoil section normal force coefficients.

The effectiveness of the steady versus the pulsing BLC method is compared for the range of momentum coefficients normally found for BLC application. In this range it is shown that at the most favorable condition the same increment of lift can be realized by pulsing with only 50 percent of the weight flow rate required for steady blowing.

TABLE OF CONTENTS

Section		Page
I	INTRODUCTION	1
II	SYMBOLS	2
III	EXPERIMENTAL INVESTIGATION	4
	Model Description	4
	Test Procedure	4
	Data Reduction	6
IV	TEST RESULTS	8
	Force Data	8
	Velocity Distributions	10
	Pressure Distributions	11
	Flow Visualization	13
	Time Dependent Data	13
V	CONCLUSIONS	14
VI	RECOMMENDATIONS	15
VII	REFERENCES	16
VIII	TABLES AND FIGURES	17

FORM 351-F REV 3-71

LIST OF TABLES AND FIGURES

Table No.	Title	Page No.
I	Airfoil Coordinates (Unflapped)	18
II	Flap Coordinates	19
Figure No.		
1	Installation Sketch	20
2	View of Model Installed in the Test Section, $\delta_F = 0$	21
3	Aft View of Model in the Test Section, $\delta_F = 40°$	22
4	Sketch of Pulsing Valve	23
5	Photograph of Pulsing Valve Mechanism	24
6	Typical Wave Shapes	25
7	Front View of Traversing Mechanism	26
8	Aft View of Traversing Mechanism	27
9	Schematic of Bench Test Set-up	28
10	Spanwise Pressure Variation for BLC Nozzle	29
11	Instrumentation Sketch	30
12	Flow Channel Spanwise Pressure - $\alpha = 0$, $\delta_F = 0$	31
13	Flow Channel Spanwise Pressure Variation (Pulsing)	32
14	Photograph of Recording Equipment	33
15	Sketch of Probe Assembly	34
16	Variation of Lift Coefficient With Angle of Attack, $C_\mu = 0$	35
17	Variation of Lift Coefficient With Angle of Attack, $C_\mu = .165$	36
18	Variation of Section Normal Force Coefficient With Angle of Attack - $C_\mu = 0$	37
19	Variation of Section Normal Force Coefficient With Angle of Attack - $C_\mu = .165$	38
20	Variation of Incremental Lift With Flap Deflection - $C_\mu = 0$	39
21	Variation of Incremental Lift With Flap Deflection - $C_\mu = .165$	40
22	Variation of Incremental Section Normal Force Coefficient With Flap Deflection - $C_\mu = 0$	41
23	Variation of Incremental Section Normal Force Coefficient With Flap Deflection - $C_\mu = .165$ (Steady Blowing)	42

FORM 351-F REV 3-71

LIST OF TABLES AND FIGURES (CONT.)

Figure No.	Title	Page No.
24	Variation of Incremental Section Normal Force Coefficient With Pulse Frequency	43
25	Variation of Incremental Section Normal Force Coefficient With Momentum Coefficient - $\alpha = 0$, $\delta_F = 40°$	44
26	Variation of Incremental Section Normal Force Coefficient With Weight Flow - $\alpha = 0$, $\delta_F = 40°$	45
27	Variation of Incremental Section Normal Force Coefficient With Momentum Coefficient - $\alpha = 20°$, $\delta_F = 40°$	46
28	Variation of Incremental Lift Coefficient With Momentum Coefficient - $\alpha = 0$, $\delta_F = 0$	47
29	Variation of Incremental Lift Coefficient With Momentum Coefficient - $\alpha = 20°$, $\delta_F = 0°$	48
30	Variation of Section Normal Force Coefficient With Angle of Attack	49
31	Variation of Section Normal Force Coefficient With Angle of Attack With and Without End Plates - $\delta_F = 40°$	50
32	Variation of Lift Coefficient With Angle of Attack	51
33	Variation of Drag Coefficient With Lift Coefficient	52
34	Variation of Pitching Moment Coefficient With Lift Coefficient	53
35	Longitudinal Velocity Distribution Normal to the Flap Chord Plane - Flap Chord Station - 9.5% c_w, $\alpha = 0$, $\delta_F = 40°$	54
36	Longitudinal Velocity Distribution Normal to the Flap Chord Plane - Flap Chord Station - 17% c_w, $\alpha = 0$, $\delta_F = 40°$	55
37	Longitudinal Velocity Distribution Normal to the Flap Chord Plane - Flap Chord Station - 27% c_w, $\alpha = 0$, $\delta_F = 40°$	56
38	Effect of Flap Deflection - $C_\mu = 0$, $\alpha = 0°$	57
39	Effect of Flap Deflection - $C_\mu = 0$, $\alpha = 16°$	58
40	Effect of Flap Deflection - $C_\mu = .16$, $\alpha = 0°$	59
41	Effect of Flap Deflection - $C_\mu = .16$, $\alpha = 16°$	60

FORM 351-F REV 3-71

LIST OF TABLES AND FIGURES (CONCLUDED)

Figure No.	Title	Page No.
42	Effect of Pulse Frequency - $C_\mu = .16$, $\alpha = 0°$	61
43	Effect of Pulse Frequency - $C_\mu = .160$, $\alpha = 20°$	62
44	Effect of Momentum Coefficient - Steady Blowing - $\alpha = 0°$, $\delta_F = 40°$	63
45	Effect of Momentum Coefficient (C_μ) - Pulsing BLC - $\alpha = 0$, $\omega = 60$ Hz, $\delta_F = 40°$	64
46	Comparison of Steady and Pulsing BLC - $\alpha = 0$, $\delta_F = 40°$	65
47	Comparison of Steady and Pulsing BLC - $C_\mu = .06$, $\alpha = 20°$, $\delta_F = 40°$	66
48	Comparison of Steady and Pulsing BLC - $\alpha = 20°$, $C_\mu = .08$, $\delta_F = 40°$	67
49	Effect of End Plates for Steady and Pulsing BLC - $\alpha = 0$	68
50 a, b	Typical Flow Visualization Photographs	69 & 70
51 a-g	Typical Outputs From Dynamic Transducers and Hot Wire Anemometer	71-77

Section I

INTRODUCTION

Tangential blowing boundary layer control (BLC) has been utilized many times to increase the flap effectiveness of military aircraft (Reference a).

The penalties, however, of BLC in a design are loss in engine thrust and efficiency. Nominally up to 5 per cent compressor bleed can be extracted from turbojet engines without large penalties; however, for turbofan engines with large bypass ratios the penalties can be large for bleed rates greater than 1 to 2 per cent. Weight and size of the ducting also constitutes a penalty in the aircraft, particularly for thin wing aircraft. These penalties could be reduced in direct proportion to a reduction in the required mass flow rates.

One concept for increasing the BLC effectiveness is to blow intermittently. The pulsing of a jet to delay flow separation over a trailing edge flap is of interest because of the potential saving in weight flow in boundary layer control for conventional aircraft wing flaps. It may also be applicable to augmentor wing and jet flap configurations.

The pulse jet acts to produce a greater degree of mixing with the boundary layer than does the steady jet. This has been investigated both theoretically and experimentally for a flat plate with no pressure gradient by Verhoff (Reference b) who found that the rate of mixing with a pulsing jet was an order of magnitude greater than that of a steady jet.

Unpublished results of exploratory tests in a flow channel with an adverse pressure gradient indicate that this increased jet mixing may permit greater BLC effectiveness in maintaining flow attachment, particularly for a moderately thick approaching boundary layer. There were instances wherein the external stream was separated even though the steady BLC jet was not. These results were encouraging and showed that as much as 25 per cent reduction in momentum coefficient could be realized for preventing flow separation as compared to steady blowing. The next step to consider was how the pulse jet would react in the real world of adverse pressure gradient with circulation lift. Tests were conducted in a 7' x 10' low speed wind tunnel to compare steady and pulsing blowing for various flap deflections, pulsing rates, flow coefficients, and angles of attack on a quasi two-dimensional flapped airfoil. This report presents the results of these tests.

Section II

SYMBOLS

A	axial force - lbs - in chordwise direction
c_w	local wing chord = 3 ft
C_L	lift coefficient - $\frac{\text{Lift}}{q_o S}$
c_{n_t}	total section normal force coefficient $c_{n_w} + c_{n_f} \sin \delta_F$
c_{n_w}	wing section normal force coefficient (See page 6)
c_{n_f}	flap section normal force coefficient (See page 6)
c_{c_w}	wing section chord force coefficient (See page 6)
c_{c_f}	flap section chord force coefficient (See page 6)
C_D	drag coefficient = $\frac{\text{Drag}}{q_o S}$
C_μ	momentum coefficient - $\frac{W V_j}{q_o S}$
g	acceleration due to gravity = 32.2 ft/sec^2
h	distance from flap surface normal to flap chord - inches
q_o	free stream dynamic pressure - lb/ft^2
S	reference area = 12 ft^2
V_o	free stream velocity - ft/sec

V	local velocity - ft/sec
V_j	isentropically expanded jet velocity from P_{T_c} to P_o
W	weight flow - lb/sec
x	longitudinal distance from wing nose in chordwise direction - inches
z	vertical distance from wing chord line - inches
P_o	free stream static pressure - lb/ft^2
P_T	free stream total pressure - lb/in^2
P_{T_n}	nozzle total pressure - lb/in^2
P_{T_c}	plenum total pressure - lb/in^2
C_p	pressure coefficient - $\frac{P_n - P_o}{q_o}$
P_n	= local static pressure - lb/ft^2
δ_F	flap deflection - degrees
ω	pulse frequency - Hz
α	airfoil angle of attack - degrees

Section III

EXPERIMENTAL INVESTIGATION

MODEL DESCRIPTION

The model consisted of an untapered semi-span wing of four-foot semi-span and three-foot chord. The airfoil was of 17 per cent thickness ratio. The airfoil and flap coordinates are listed in Tables I and II. The wing was fitted with a .42 c_w plain flap. Flap deflections of 0 to 60 degrees were available in 10-degree increments. Two wrap-around end plates were mounted to form a 12-inch span, two-dimensional flow channel in the center of the semi-span wing. A sketch of the model is shown in Figure 1 and photographs of the installation in the test section are shown in Figures 2 and 3 . The valve consisted of three 4-inch sliding teflon valve plates that were opened and closed by an eccentric cam driven by a variable frequency electric motor. A sketch of the valve is shown in Figure 4 and a photograph of the sliding plate is shown in Figure 5 . The valve plates being at the nozzle exit produced good square wave pulse shapes. A sample of the nozzle total pressure for various pulse frequencies is shown in Figure 6 . The nozzle height could be varied from .014 inches to .048 inches to produce different mass flow rates for a given plenum chamber pressure level. High pressure air was supplied to the valve plenum from a channel built into the wing running full model span with four circular inlets tapped into the valve plenum. The model construction was of a basic steel structure with a wood filler layup and a final contour of epoxy resin.

A remotely controlled traversing probe rig was attached to the flap. Photographs of the rig mounted on the flap are shown in Figures 7 and 8 . The probe was remotely controlled in the vertical direction only, with the longitudinal motion being manual. The maximum vertical travel was approximately 11-inches from the flap surface.

A plexiglass end plate was also provided to be used for flow visualization studies. The photographs were shot through the tunnel ceiling windows.

TEST PROCEDURE

Prior to shipping the model to the test site, the valve was bench tested for leakage, for nozzle calibration, and for spanwise variation of nozzle flow. The test setup is shown in Figure 9 . High pressure (100 psia) air was supplied to the valve plenum with the valve completely closed. Leakage occurred at the junction of the teflon plates and at each end. The leakage was measured and found to be 1.47 per cent of the total weight flow with the valve

full open and was considered to be acceptable. The leakage rate was verified again at the completion of the test and found to be 1.53 per cent of the total open-valve weight flow.

The spanwise variation of the nozzle flow was checked by means of a .07-inch diameter diaphram pressure transducer mounted in a holder and moved laterally along the nozzle span. The transducer output was displayed on an oscilloscope. Variation of the ratio of nozzle total pressure to plenum total pressure with spanwise station is shown in Figure 10 for a representative pulsing and steady blowing condition.

The experimental investigation was performed in the 7' x 10' low speed wind tunnel of the U.S. Army Air Mobility Research and Development Laboratory, Ames Research Center. Tests were conducted at a free stream Mach number of 0.166 and a corresponding Reynolds number of 3.55×10^{-6}. All data were obtained with boundary layer transition strips consisting of No. 70 Carborundum grit located on both upper and lower surfaces at .11 c_w and extended over the entire model span.

The model was mounted in the test section on the six-component external balance system. This provided total model lift, drag, and pitching moment data. The balance data were filtered to obtain average values during the pulsing tests. The primary data, however, were pressure and velocity measurements. Pressure orifices were installed on the centerline of the two-dimensional section formed by the end plates as shown in Figure 11. Four spanwise orifices were located at 90 per cent c_w to check on the two-dimensionality of the flow between the end plates. Figures 12 and 13 present the variation of the spanwise pressure coefficients for no blowing and pulsing BLC conditions. The data for the no blowing indicate a constant spanwise pressure coefficient over the entire channel except for a point near the left end plate. This change in C_p represents a change in the static pressure of only .39 psf which is considered to be within the accuracy of transducer measurement. The pulsing BLC shows an increase in C_p near each end plate, but there is no evidence of flow separation. The two-dimensionality of the flow in the channel between the end plates was determined to be good for all test conditions. The static pressure orifices were connected to a scanivalve located beneath the tunnel floor. These data were considered average values during the pulsing runs due to the natural damping of the tube length required to connect to the scanivalve. In addition, five diaphram-type (Kulite) transducers were flush-mounted on the upper surface of the airfoil for measuring the dynamic response of the flow at the flap surface. Another dynamic transducer was located on the upper wing surface at 12.5 per cent c_w to evaluate the extent of the effect of the pulsing flow upon the airfoil pressures upstream of the trailing edge flap. The nozzle exit total pressure was monitored with a .07-inch diameter diaphram-type transducer mounted 4-inches from the centerline and approximately .01-inch behind the nozzle exit plane.

The transducer outputs were recorded on a direct writing oscillograph and also on a Honeywell magnetic tape system. A photograph of the recording equipment is shown in Figure 14. All runs were recorded on the oscillograph except those conducted only for flow visualization studies. Flow field measurements were conducted on magnetic tapes.

Flow field measurements through the jet were made by means of both a total head transducer and a one-component hot wire anemometer. The total head transducer was mounted in a tube which was flattened to give an inlet height of 0.030-inch. This probe was mounted on a carriage as shown in Figure 15. The carriage was guided vertically by two rods mounted on linear bearings. A screw jack driven by a small d.c. motor provided the vertical motion. The longitudinal position was set manually. The vertical position readout on the mechanism was found to be inadequate for positioning the probes. This problem was solved by use of a transit which was set up outside the tunnel and each position measured in against a scale mounted on one of the end plates. This method allowed for probe deflections and provided precise positioning. Accuracy was approximately $\pm$.010 inch. The flow survey using the traversing mechanism was initially conducted with the total head transducer probe. Four chordwise stations along the flap upper surface was traversed vertically. Three of the same stations were repeated using the hot wire anemometer probe. The outputs recorded on the direct writing oscillograph and on the Honeywell magnetic tape system. The initial instrumentation contained a two-component hot wire anemometer to define the vortex location. The two-component anemometer had a platinum coated quartz sensor element which proved extremely fragile. Two probes of 0.001-inch and 0.002-inch diameter sensors were installed, and in both instances, the sensors broke prior to obtaining any valid data. The Ames one-component hot wire probes were selected as the best alternative.

DATA REDUCTION

The test progress was monitored by selected on-line data reduced on an IBM 1800 system and printed by typewriter in the tunnel control room. The printed data consisted of the external balance lift, drag, and pitching moment coefficients, and the momentum coefficient. The final data were punched on cards and reduced as time permitted on the 1800 computer. The equations and methods used in the data reduction procedures are as follows:

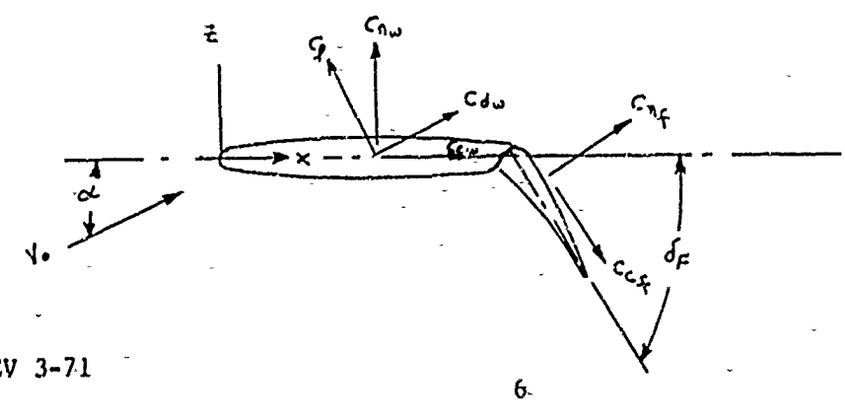

Force Coefficients

$$c_{n_w} = \frac{1}{c_w} \int_o^{c_w} C_p \, dx$$

$$c_{n_f} = \frac{1}{c_f} \int_o^{c_f} C_p \, dx$$

$$c_{n_t} = c_{n_w} + \frac{c_f}{c_w} \left[c_n \cos \delta_F - c \quad \sin \delta_F \right]$$

$$C_\ell = c_{n_t} \cos \alpha - c_{c_t} \sin \alpha$$

Pressure Coefficient

$$C_p = \frac{P_n - P_o}{q_o}$$

Momentum Flow Coefficient

$$C_\mu = \frac{W V_j}{g q_o S}$$

W = weight flow, lb/sec

V_j = jet velocity (ft/sec), expand isentropically to free stream static pressure

Section IV

TEST RESULTS

FORCE DATA

The initial runs were conducted on the plain flap configuration to determine the flap deflection that was most effective with no blowing and with steady blowing. This configuration was then tested for the intermittent blowing. The optimum flap deflection was chosen using the external balance, or total model coefficient data. Figures 16 through 19 show the variation of lift coefficient and section normal force coefficient with angle of attack for various flap deflections. Section normal force coefficient data were derived from the integrated pressure distributions. From the reduction in lift curve slope it can be concluded that the flow is separated at the higher angles of attack for flap deflections above 40 degrees. Figures 20 through 23 show the effect of flap deflection on incremental lift and section normal force coefficient. These curves were derived from the data of Figures 16 through 19 and verify the selection of a plain flap deflection of 40 degrees for testing with intermittent blowing.

The effectiveness of intermittent blowing was next investigated. The effect of varying the pulse frequency was determined at $\alpha = 0$ and $\alpha = 20$ degrees with the plain flap deflected 40 degrees. Figure 24 presents the variation of incremental section normal force coefficient with pulse frequency. The data show that as the pulse frequency is increased, the lift effectiveness increased up to a frequency of approximately 60 Hz. Additional increases in pulse frequency resulted in little or no gains in lift. This could be attributed to the viscous action of the vortex that entrains the surrounding air. As the pulse frequency is increased to 60 Hz, the surrounding air cannot react to the pulses and results in continuous entrainment.

Flap deflection and pulse frequency were optimized and the investigation was continued to determine the effectiveness of a pulsing jet to delay separation over a flapped airfoil. The pulse duration for these tests was approximately one-half the period. To obtain the same momentum coefficient for steady and pulsing, the steady blowing tests were conducted at approximately one-half the nozzle plenum pressure. This results in an instantaneous V_j, greater for the intermittent blowing than for the steady blowing. The higher V_j along with the vorticity resulting from the pulsing, tends to increase the extent of mixing and hence increases flap effectiveness at the same weight flow, or reduces the weight flow required for the same effectiveness. Figure 25 presents the results at $\alpha = 0$ and shows that in the range

of momentum coefficients normally considered for boundary layer control ($.01 < C_\mu < .14$), the same lift increment can be realized at a momentum coefficient that is approximately one-half that required for steady blowing. These data, when viewed with respect to weight flow as in Figure 26, show a similar savings in weight flow for the pulsing as compared to the steady blowing. This is quite significant when it is applied to an aircraft where the engine bleed requirements could be reduced by as much as 50 per cent.

It should be noted that the curves of Figure 25 tend to converge and no real gains in lift are indicated at values of momentum coefficient above .14.

At high angles of attack ($\alpha = 20°$) with the plain flap deflected 40 degrees, a comparison of steady and pulsing BLC is shown in Figure 27. The data indicate that at very low values of momentum coefficient ($0 < C_\mu < .07$) separation over the flap occurs with pulsed BLC. However, at the higher momentum coefficients ($.07 < C_\mu < .14$), the same lift increment can be realized at a reduced momentum coefficient (approximately 25 per cent).

The comparison of steady and pulsing BLC was made at a flap deflection of 0° and for angles of attack of 0° and 20°. These data, Figures 28 and 29, are external balance data. For $\alpha = 0$, the same lift increment can be realized at as much as 43 per cent reduction in the momentum flow coefficient when compared with steady blowing. At $\alpha = 20°$, even greater gains are shown. Approximately 50 per cent reduction in momentum coefficient will provide the same incremental lift coefficient.

A summary plot showing the variation of section normal force coefficient with angle of attack for the plain flap configuration is presented in Figure 30. The pulsing produced a 25 per cent increase in section normal force coefficient at $\alpha = 0$ with the lift curve slope being the same as for the steady blowing.

End plate effects were checked by conducting tests with and without the end plates. The results are presented in Figure 31. Pulsing the flow with the end plates off resulted in slightly less lift effectiveness than the steady blowing. The pressure distributions indicate flow separation now occurs on the wing ahead of the flap and requires extreme amounts of blowing to attach the flow over the flap.

A summary plot showing the total model force and moment data for no blowing, steady blowing, and pulsing is presented in Figures 32 through 34. The drag is reduced at a constant lift coefficient due to the reduction in the boundary layer losses with BLC. Pulsing BLC shows less boundary layer losses than the steady blowing condition. The variation of pitching moment coefficient about the quarter chord with lift coefficient substantiates the increased effectiveness with pulsing.

VELOCITY DISTRIBUTIONS

Velocity distributions taken at three chordwise stations for the plain flap deflected 40 degrees is shown in Figures 35 through 37. These measurements were obtained by utilizing a hot wire anemometer to measure the X-component of velocity. Comparisons are made between no BLC, steady blowing BLC, and pulsing BLC. The velocity distribution for the pulsing condition is presented for the maximum velocity (valve open) and minimum velocity (valve closed) during one cycle of valve operation. These data show that without BLC the flap flow is completely separated and that the steady blowing entrains the separated flow and provides flow attachment over most of the flap. With steady blowing, high jet velocity extends approximately 1/8-inch above the flap surface and reduces rapidly to a constant velocity approximately 1-inch above the surface. Local streamlines near the flap surface follow the flap contour but depart rapidly as the distance above the flap surface is increased. The velocity distributions for pulsing BLC indicates that the maximum jet velocity (valve open) distribution follows a somewhat similar variation as the steady blowing velocity distribution. The extent of mixing, however, is greater for the pulsing condition. This is evident from the velocity distribution at the instant the valve is closed. Only a slight reduction in the velocity is apparent at distances as great as eight inches from the flap surface. This implies that the higher jet velocity and vorticity due to pulsing when the valve is open is effective in entraining the flow even when the jet velocity goes to zero for a short instant of time. It is considered that once the entrainment pattern has been established, the inertia of the surrounding flow requires some time span before the flow can react. Assuming the pulse frequency is high enough, a continuous entrainment can be expected. Comparing the velocity distribution for the pulsing condition at each chordwise location, it is evident that the extent of mixing increases near the flap trailing edge, thus producing greater lift effectiveness when compared to the steady blowing. A sketch of the entrainment characteristics is shown below.

PULSING ON
(VALVE OPEN)

PULSING OFF
(VALVE CLOSED)

NO JET

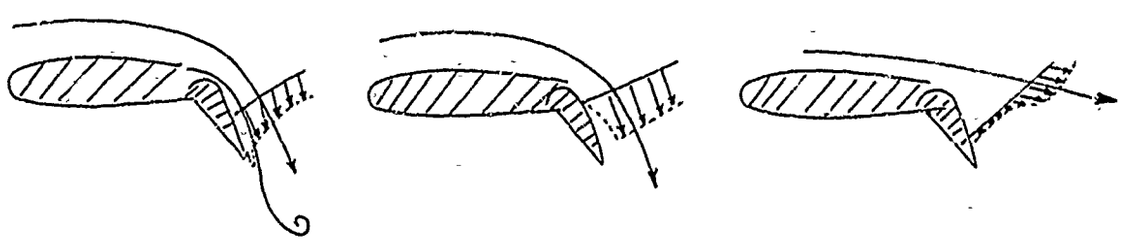

PRESSURE DISTRIBUTION

The pressure distribution data for the significant configurations and test conditions are presented in Figures 38 through 48. These data were obtained from surface pressure orifices located along the centerline of the two-dimensional channel and represent average values when pulsing the flow. For the plain flap configuration a number of pressure orifices located in the flap cove area were not exposed to the free stream flow and, therefore, resulted in discontinuities in the data. These orifices are identified as follows:

Flap Deflection	Location	
δ_F	x_f/c_w % c_w Flap Upper Surface	x/c_w % c_w Wing Lower Surface
0	0	50
	.5	52.5
	2.0	55
	4.5	60
	7.0	
20°	0	50
	.5	52.5
	2.0	55
	4.5	60
30°	0	50
	.5	52.5
	2.0	55
		60
40 & 50°	0	Same as above
	.5	Same as above

Figures 38 through 41 present the effect of flap deflection for steady and no blowing at angles of attack of zero and sixteen degrees. The constant pressure region indicates that with no blowing the flap flow is partially separated at flap deflection as low as 20 degrees and that no significant gain in maximum lift can be expected for flap deflections greater than 40 degrees. The steady blowing, however, attaches the flow over the flap for all flap deflections up to 50 degrees at $\alpha = 0$ as signified in Figure 40 by

the steep pressure gradient over the aft 50 per cent chord of the flap. At higher angles of attack ($\alpha = 16°$), little gain in lift is noted for flap deflections above 40 degrees. The 40 degree flap deflection was considered optimum for the plain flap and is used as a basic configuration for determination of the pulsing BLC effectiveness. The pulse frequency effect on the pressure distribution is shown in Figures 42 and 43 for zero and twenty degrees angle of attack, respectively. These data indicate that flow separation is completely eliminated over the flap at pulse frequencies of 60 Hz and greater. Pulsing the jet at the trailing edge of the wing affects the flow over the entire airfoil upper surface.

Figures 44 and 45 show the change in pressure distribution over the wing and flap with the variation of momentum coefficient (C_μ) for steady and pulsing BLC. A normal progression occurred with an increase in the momentum coefficient. Flow separation over the trailing edge of the flap was eliminated at a lower value of momentum coefficient for the pulsing than for the steady BLC. Pressure distributions for steady blowing and pulsing BLC are compared in Figure 46 for the plain flap configuration at constant C_μ. The pressure distribution over the flap for the steady blowing shows that the last 10 per cent chord of the flap is separated and that the pulsing jet eliminates this separation. The higher jet velocities of the pulsing system results in higher negative pressure coefficient over the entire airfoil upper surface.

Figures 47 and 48 are presented to aid in understanding the variation of incremental normal force coefficient (Δc_{n_t}) with momentum coefficient shown in Figure 27. The pressure distribution indicates that at $C_\mu = .06$ the pulsing jet does not prevent separation and is actually less effective than the steady blowing. Increasing the momentum coefficient to $C_\mu = .08$, however, results in flow attachment for the pulsing with only slight alteration to the steady blowing pressure distribution. This was only observed at the high angle of attack ($\alpha = 20°$) condition.

The effect of removing the end plates and blowing over only a 12-inch section of the wing resulted in a loss in effectiveness for both steady and pulsing BLC, as depicted in Figure 49. With the end plates off, the pulsing jet was slightly less effective in delaying separation over the flap than the steady blowing. It should not be concluded from these data that the pulsing would not be effective for a three-dimensional application, however, since the blowing was local over only one-fourth of the model span.

FLOW VISUALIZATION

Flow visualization was accomplished by using the neutrally buoyant helium bubble technique. This technique is relatively new and consists of introducing helium-filled bubbles into the airstream (via a small probe), ahead of the model. The bubbles are photographed with special high speed film and lighting. The technique and equipment is described in Reference (e). Figures 50a through 50b present photographs comparing the basic flap (no blowing), steady blowing, and pulsing. These photographs were taken from above the model looking through a plexiglass end plate. What appears to be a step on the center of the upper surface is actually the bracket that attaches the end plate to the model and is outside the flow channel.

In comparing conditions at a constant C_μ, Figure 50a, ($\delta_F = 40°$, $\alpha = 0$, $P_{T_c} = 30$ psia to $\delta_F = 40$, $\alpha = 0$, $P_{T_c} = 60$ psia, $\omega = 60$ Hz), and after careful analysis using the pressure distribution data as a guide, it appears the surrounding flow is affected to a greater extent with the pulsing jet. A discrete vortex produced by the pulse was not evident in the photographs. This was understandable when considering that at the free stream test velocity (75 ft/sec) each vortex would be only partially formed during the time interval which the vortex had to travel the distance equal to the flap chord. It should be noted here that the free stream velocity for the flow visualization tests was reduced to stay within the operational limits of the bubble generator. The limits of the bubble generator were set in order to obtain the highest quality photographs for this particular test.

TIME-DEPENDENT DATA

Figures 51a through 51g present typical outputs from the surface dynamic (Kulite) transducers and the hot wire anemometer. These data were obtained for each vertical position of the hot wire probe and at three chordwise stations along the flap. The data presented are at a chordwise station of 27 per cent c_w, $\alpha = 0$, $\delta_F = 40°$. These data cannot be analyzed in detail from the oscillograph traces, but will require reduction from magnetic tapes which are not considered part of this study scope. Some interesting trends are evident, however, and are discussed as follows: 1) the transducer at the leading edge of the wing did respond to the pulsing at the trailing edge flap, indicating that the circulation around the complete airfoil is affected by the pulses over the flap upper surface, 2) the character of the static pressure pulse changes as the distance downstream from the nozzle exit is increased for a given vertical height above the flap, 3) the hot wire anemometer output shows that as the probe height above the flap surface increased, the peak jet velocity decreased and that minimum velocity (valve closed) increased. The outputs of the surface transducers on the flap at chord stations 1.25, 5.75, and 10.75 per cent c_w show a large decrease in static pressure when the valve is in the open position. This is due to the high jet velocity. Further downstream at flap chord station of 19.5 and 29.5 per cent c_w, the static pressure increased at the same valve position (open). The mechanics of the vortex action that causes this phenomenon is not obvious from these data.

Section V

CONCLUSIONS

An experimental investigation conducted on a two-dimensional model has shown that intermittent blowing over the knee of a plain flap decreases the required weight flow. The pulsing BLC method requires less weight flow in the jet momentum coefficient range ($0 < C_\mu < .14$) to produce the same section normal force coefficient as the steady blowing. The saving amounts to as much as 50 per cent.

The effectiveness of the pulsing jet to entrain the surrounding flow is evident and can be attributed to increased mixing rate and greater jet velocity produced for a given mass flow. Also, the inertia of the entrained flow requires a time span for the flow to react, resulting in essentially continuous entrainment even between pulses.

The extent of the mixing increases as the vortex moves downstream and delays the separation over the flap trailing edge when compared to the steady blowing case.

The ability of the pulsing BLC to delay separation over the plain flap was found to be primarily a function of pulse rate and jet velocity. Lift effectiveness was increased as the pulse rate was increased to a frequency of approximately 60 Hz. Little gain in lift effectiveness was realized beyond this point.

The gains with the pulsing BLC were realized for the range of momentum coefficients (C_μ) applicable for BLC systems ($0 < C_\mu < .14$). Higher values of C_μ were not covered in this study, but indications are that the gains in lift effectiveness would not extend beyond this range for the conditions of this investigation.

Section VI

RECOMMENDATIONS

The present experimental study has demonstrated the ability of a pulsing BLC concept to produce significant reduction in air flow rates in a BLC application compared to that for steady blowing. However, these gains were not evident as the momentum coefficient was increased beyond the range of normal BLC application. It is recommended that additional study be conducted to improve the understanding of the flow mechanism of the pulsing system. This study should include detailed analysis of the mixing process between the jet and the surrounding flow. Once the flow mechanism is understood, the benefits of the pulsing method for entraining flow might be applied to other systems such as augmentor wings, jet flaps, and ejectors.

Work should be done to determine suitable means of achieving intermittent blowing on an aircraft. One potential way would be by use of fluidic principles wherein the flow at the engine is steady and the flow alternates at a pair of nozzles.

Section VII

REFERENCES

(a) Lachman, G. V., Editor, Boundary Layer and Flow Control, Its Principles and Application, Vol I, Pergamion Press, London 1961

(b) Verhoff, August, "Steady and Pulsing Two-Dimensional, Turbulent Wall Jets in a Uniform Stream," Princeton University Report No. 723, March 1970 (AD 705235)

(c) Plasterer, D., "Structural Analysis Wind Tunnel Model for a Pulsing Boundary Layer Control Study," North American Rockwell Report No. NR71H-253, dated 10 June 1971

(d) Oyler, Ted E., "Pretest Information for Pulsing Boundary Layer Control Tests at Ames Research Center," North American Rockwell Report No. NR71H-293, dated 22 July 1971

(e) SAI Bubble Generator Model 3 - Sage Action, Inc., Ithaca, New York, 1 Jan 1972

Note: Copies of References (c) and (d) can be obtained by submitting requests directly to North American Rockwell Corporation.

Section VIII

TABLES AND FIGURES

Table I

AIRFOIL COORDINATES
(UNFLAPPED)

ler/c = 0.0428	$x/c)_{ler}$ = 0.0428	y/c_{ler} = 0.00
x/c	$y/c)_{upper}$	y/c_{lower}
0.0	0.000	0.000
0.0125	0.0304	-0.030
0.0250	0.0401	-0.0408
0.0375	0.0469	-0.048
0.0500	0.0519	-0.0533
0.075	0.0595	-0.0611
0.100	0.0652	-0.0664
0.125	0.06963	-0.0704
0.150	0.07325	-0.0735
0.175	0.07625	-0.0760
0.200	0.07890	-0.0779
0.250	0.0832	-0.0807
0.300	0.0363	-0.0819
0.350	0.08825	-0.0820
0.400	0.0891	-0.0810
0.450	0.08893	-0.0786
0.500	0.08783	-0.0748
0.550	0.08568	-0.0690
0.575	0.08423	-0.0652
0.600	0.08248	-0.0607
0.625	0.08043	-0.0554
0.650	0.07811	-0.0495
0.675	0.07541	-0.0431
0.700	0.07233	-0.0366
0.725	0.06881	-0.0301
0.750	0.06476	-0.0240
0.775	0.0602	-0.0184
0.800	0.0553	-0.0134
0.825	0.0499	-0.0093
0.850	0.0440	-0.0060
0.875	0.0376	-0.0036
0.900	0.0308	-0.0021
0.925	0.0236	-0.0017
0.95	0.0160	-0.0025
1.00	0.00	-0.0080

Table II

FLAP COORDINATES

$\frac{x_f}{c}$	$\frac{y_{upr}}{c}$	$\frac{y_{lwr}}{c}$
0.0	-.03722	-.03722
0.5	-.00443	-.05369
1.0	.00861	-.05783
1.25	.01371	-.05903
1.50	.01823	-.05986
1.75	.02231	-.06006
2.00	.02603	-.060
5.00	.05498	-.05444
10.00	.07232	-.04200
12.00	.07232	-.0366
17.00	.06476	-.0240
22.00	.0553	-.0134
27.00	.0440	-.0060
32.00	.0308	-.0021
37.00	.0160	-.0025
42.00	.0000	-.0080

NOTE: c is total wing chord (3 ft.)

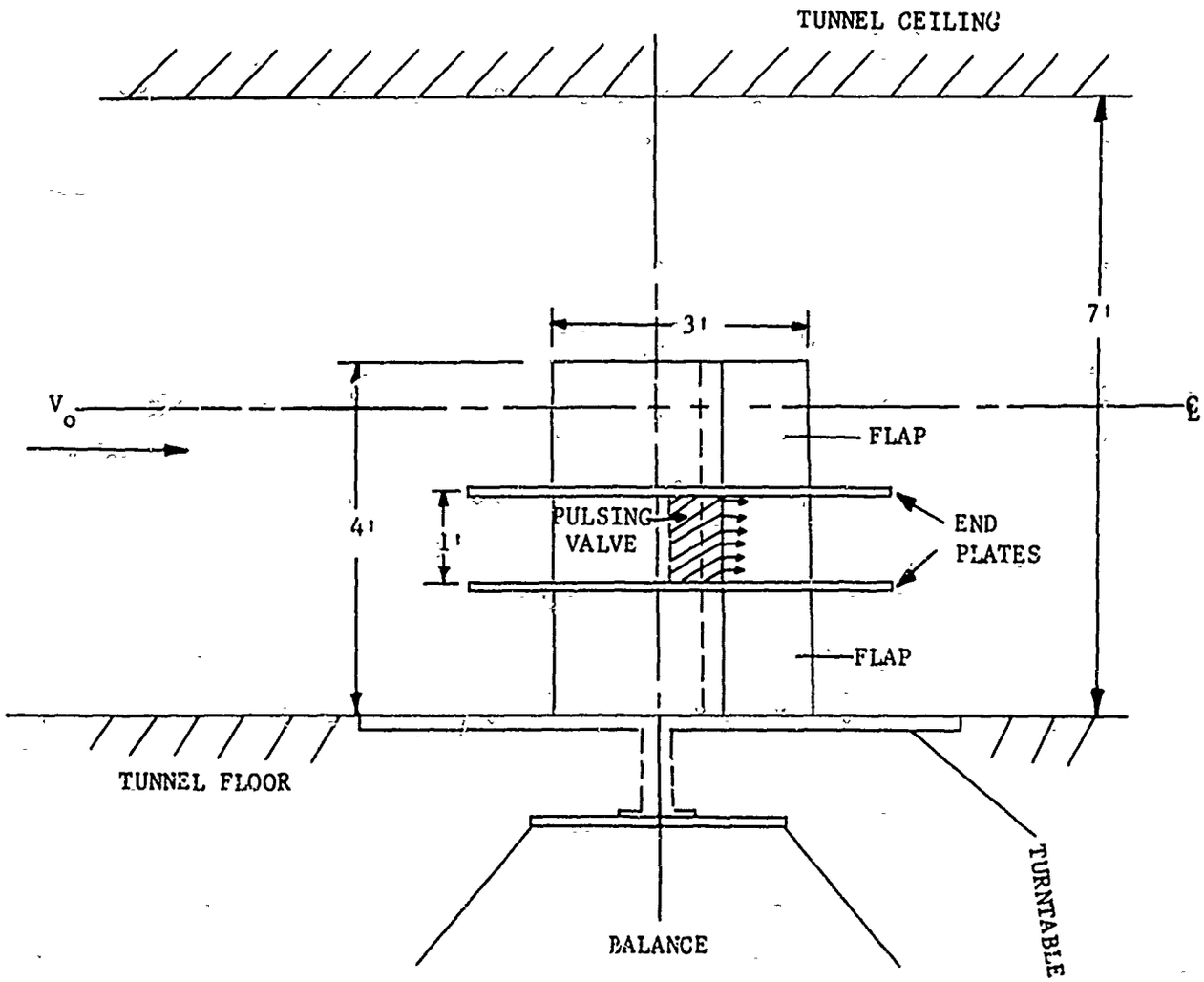

Figure 1 . Installation Sketch

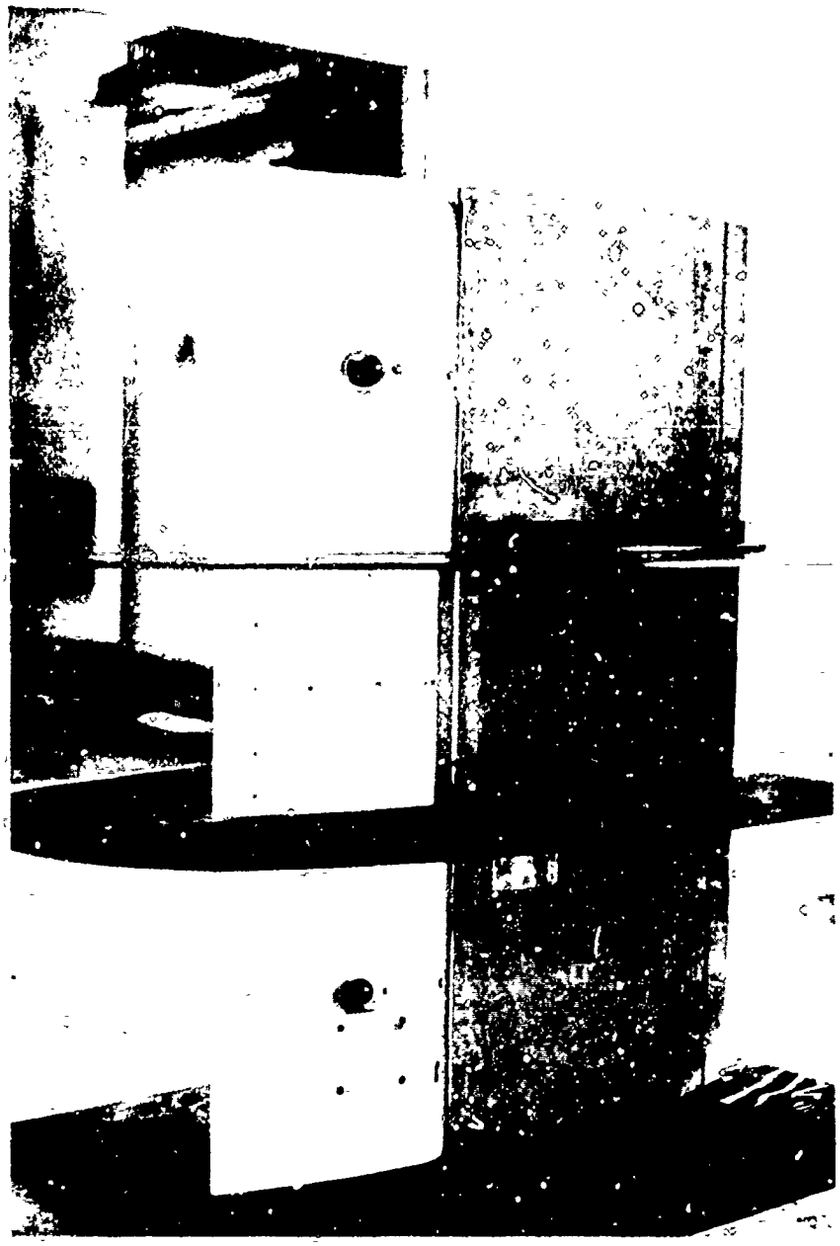

Figure 2 . View of Model Installed in the Test Section
F = 0

Figure 3 . Aft View of Model in the Test Section

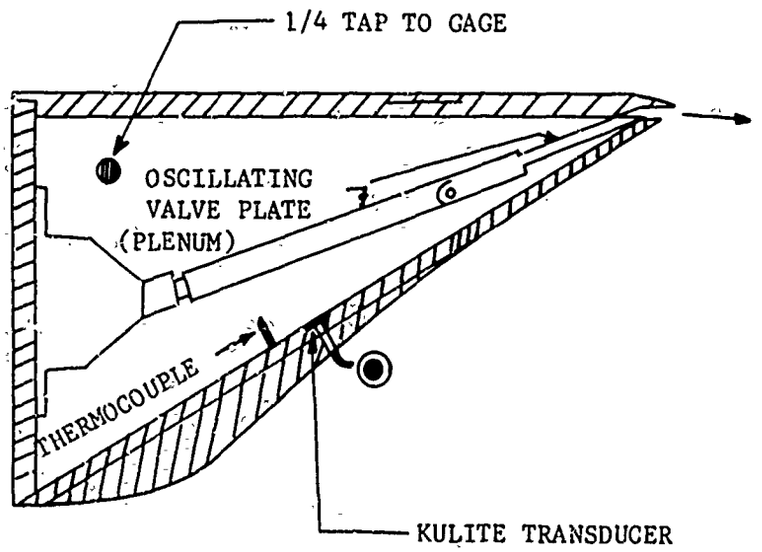

Figure 4 . Sketch of Pulsing Valve

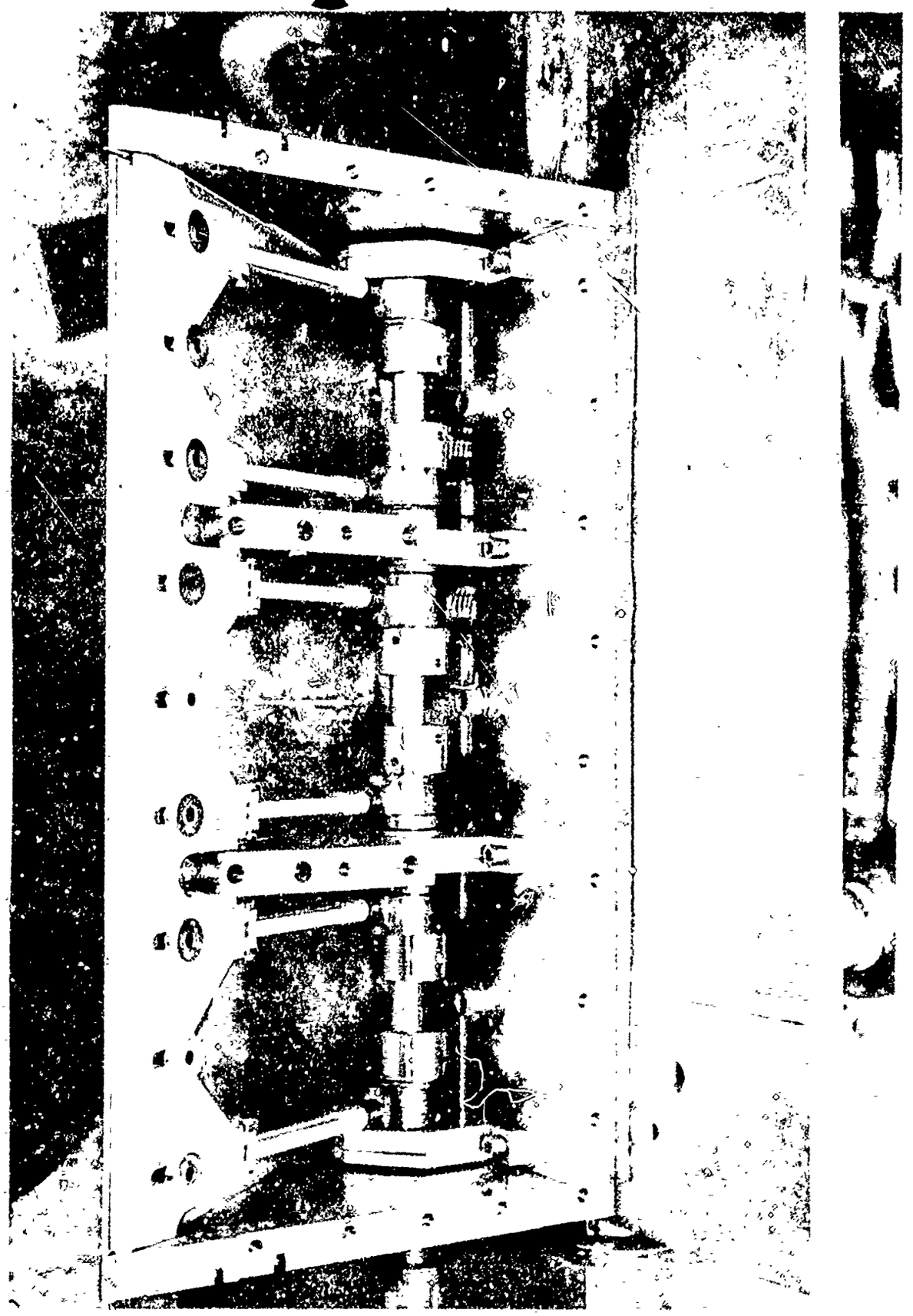

Figure 5. Photograph of Pulsing Valve Mechanism

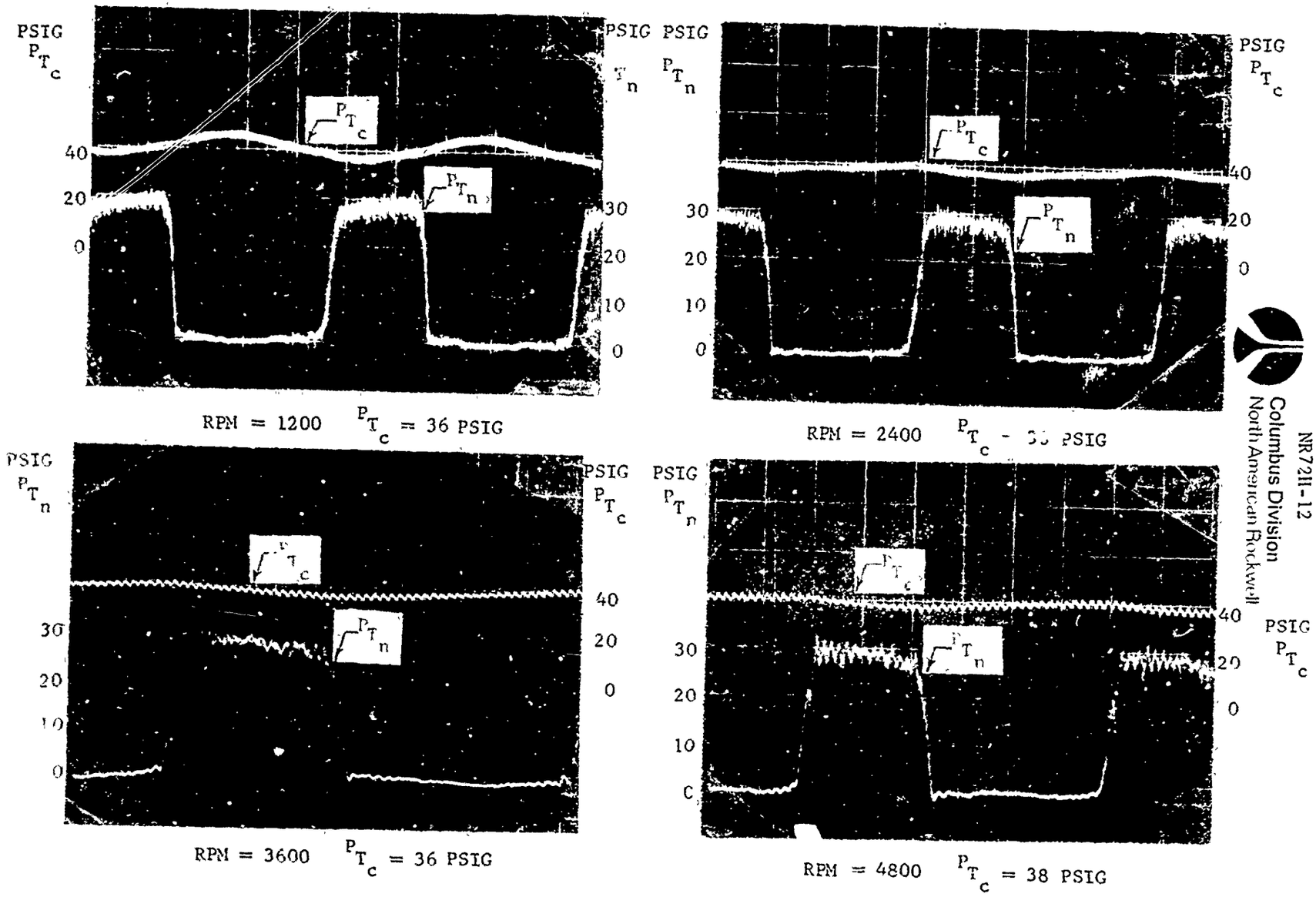

Figure 6 . Typical Wave Shapes

Columbus Division
North American Rockwell
NR72H-12

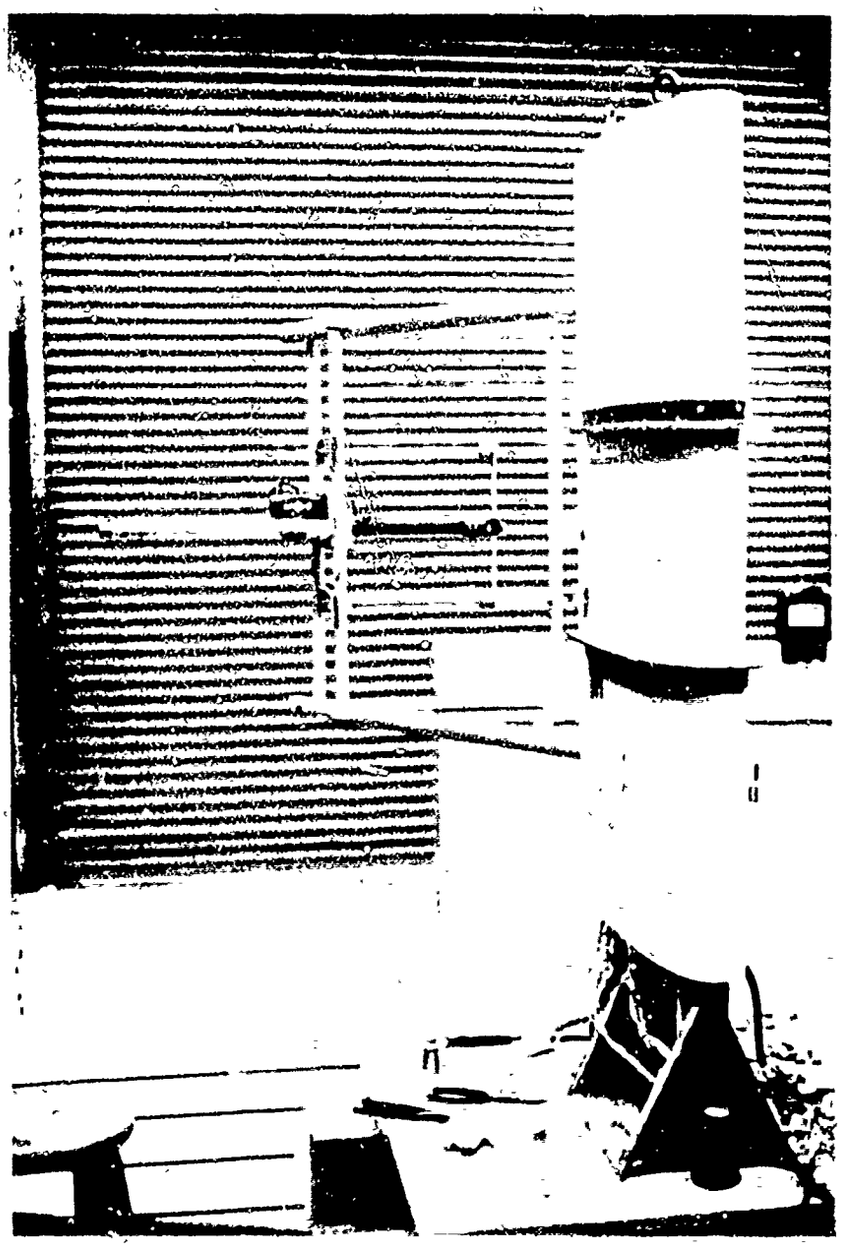

Figure 7 . Front View of Traversing Mechanism

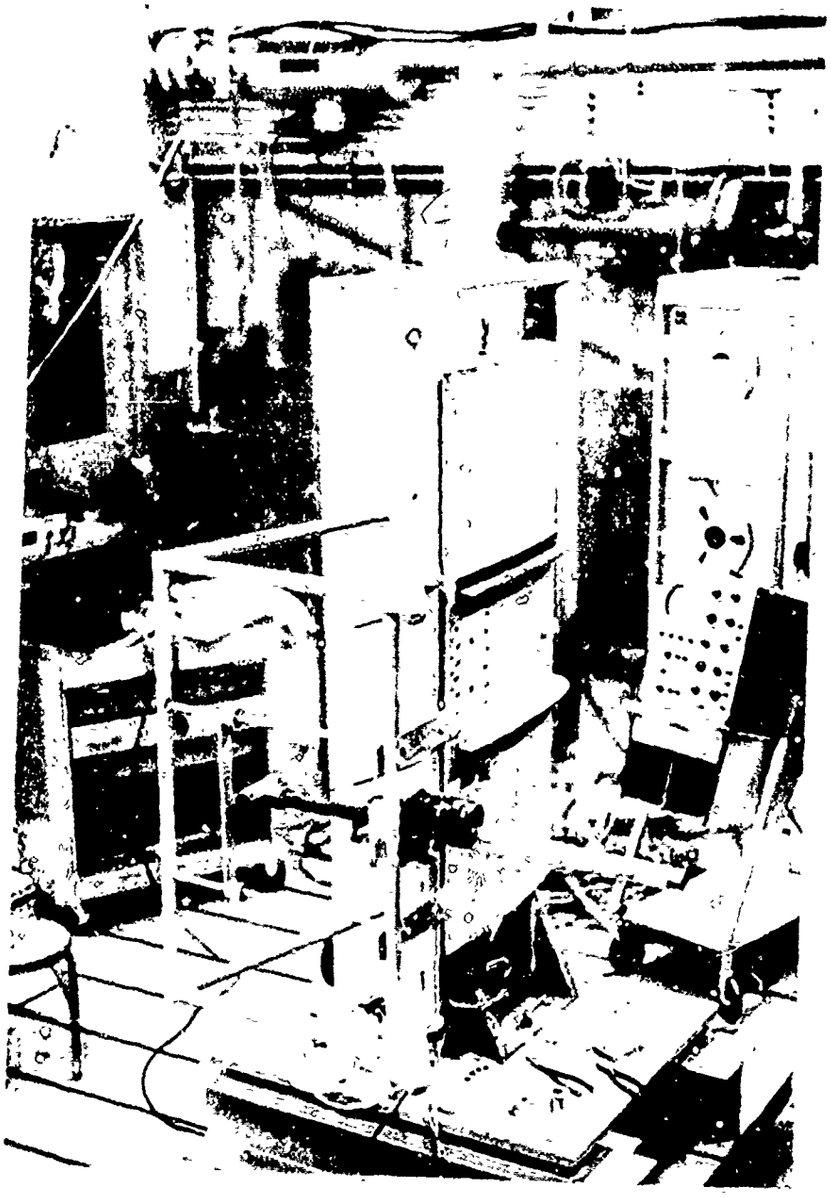

Figure 8 . Aft View of Traversing Mechanism

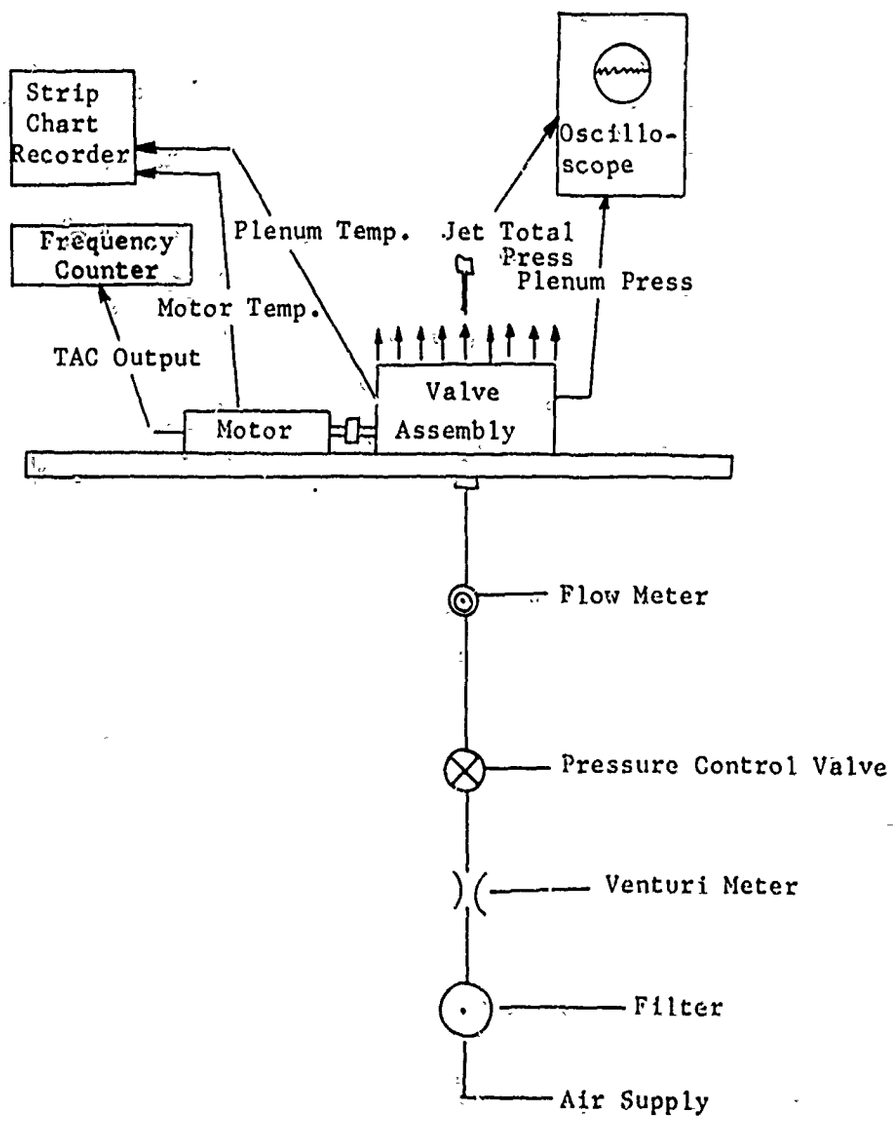

Figure 9 . Schematic of Bench Test Set-Up

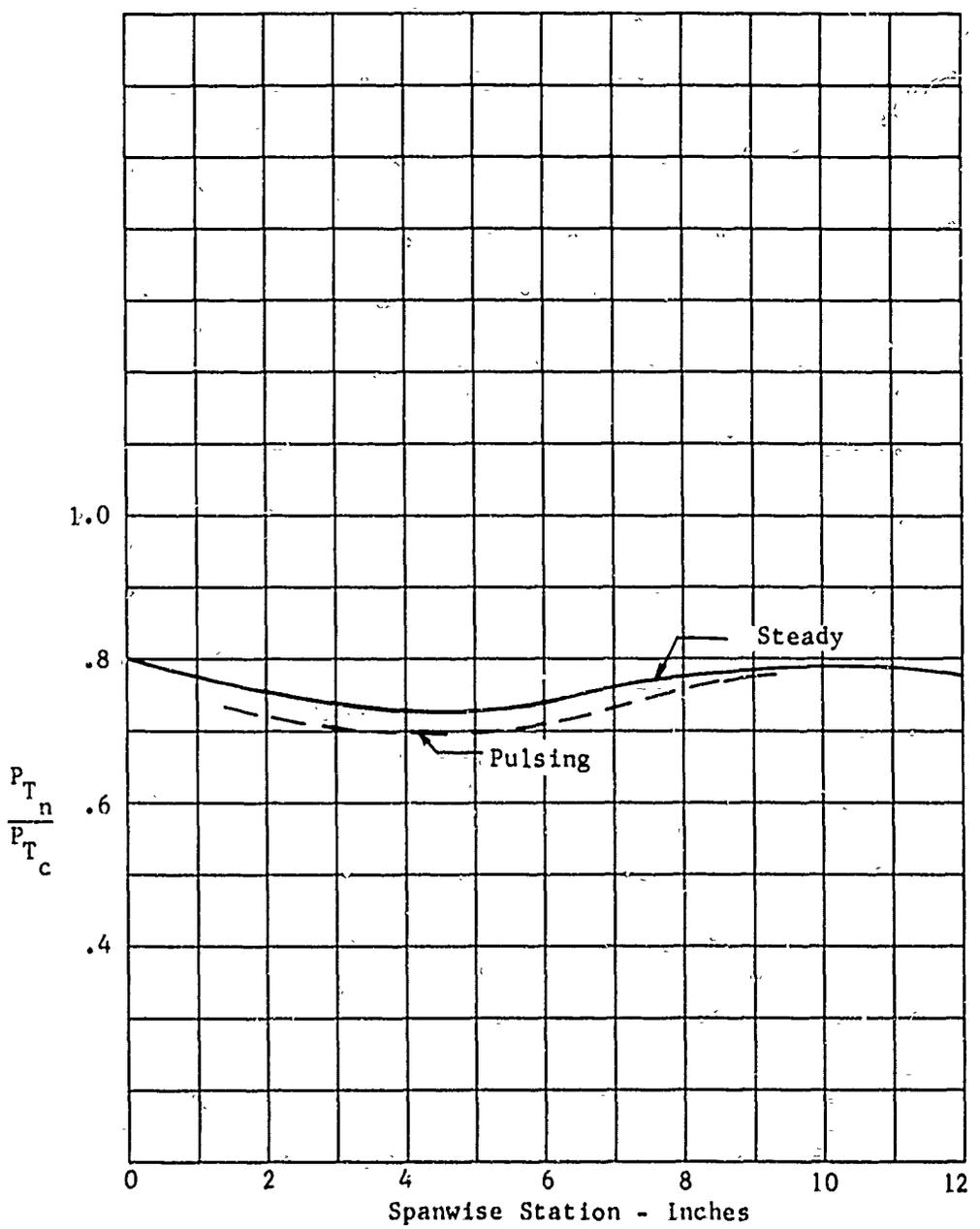

Figure 10. Spanwise Pressure Variation for BLC Nozzle

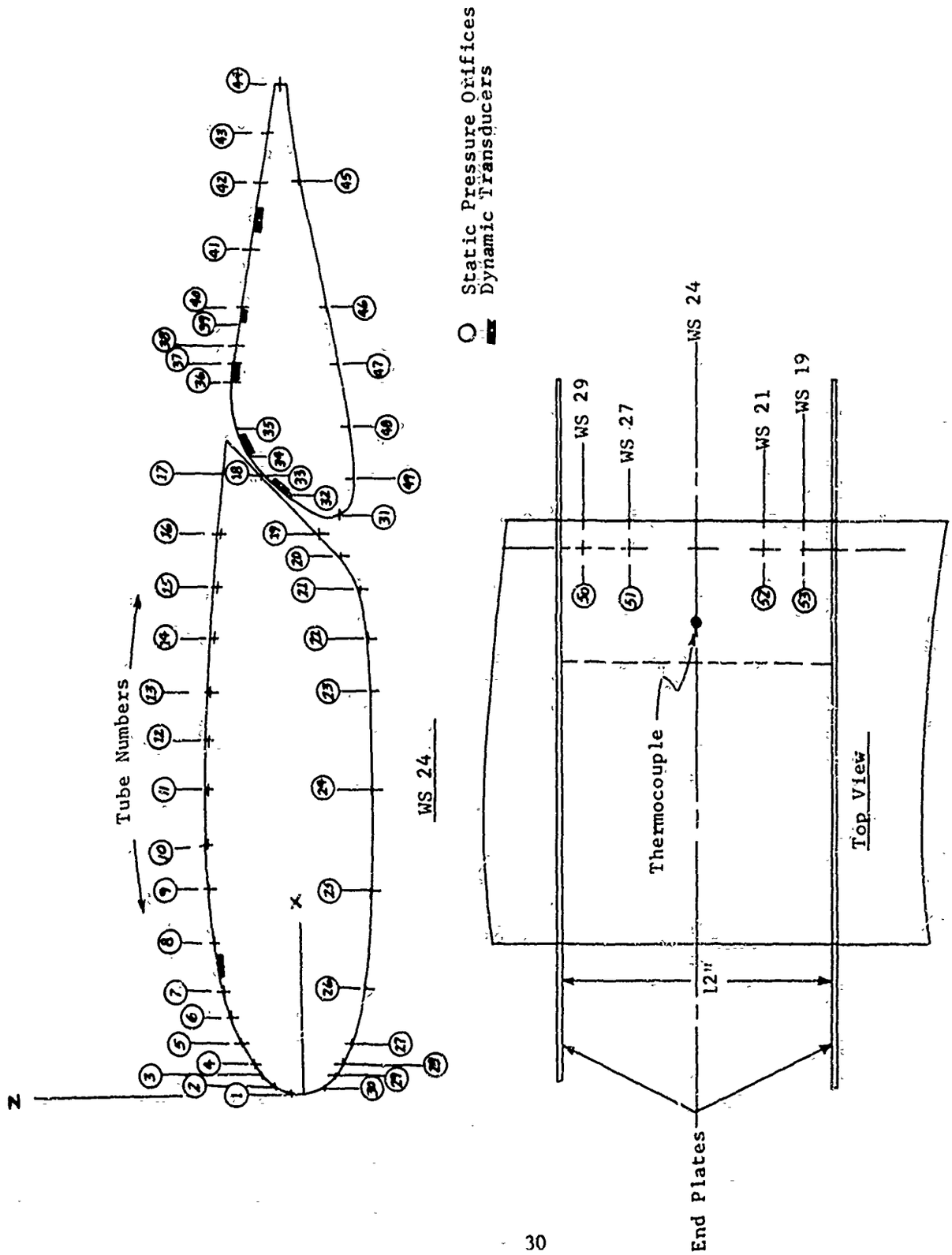

Figure 11. Instrumentation Sketch

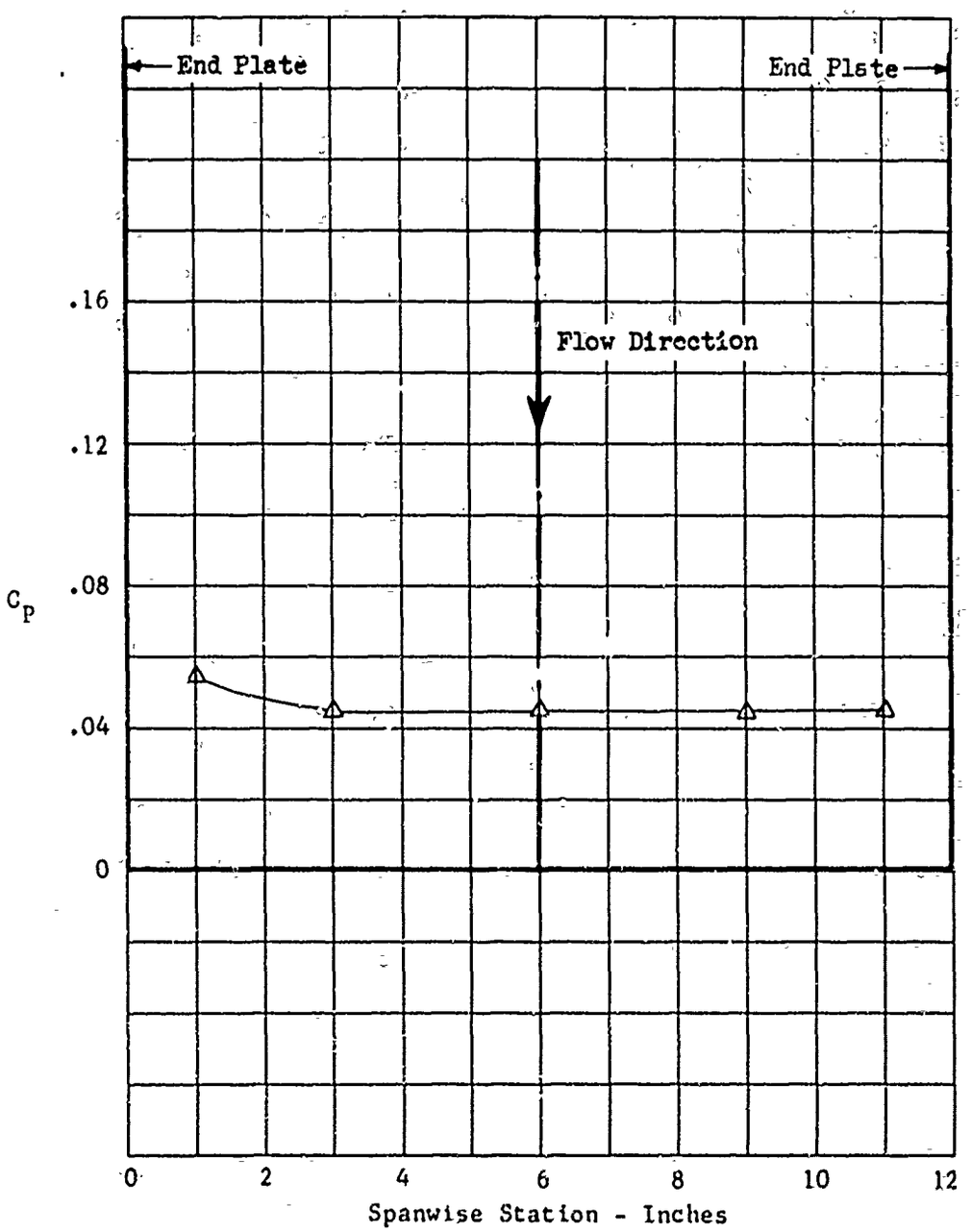

Figure 12. Flow Channel Spanwise Pressure
$\alpha = 0 \quad \delta_F = 0$

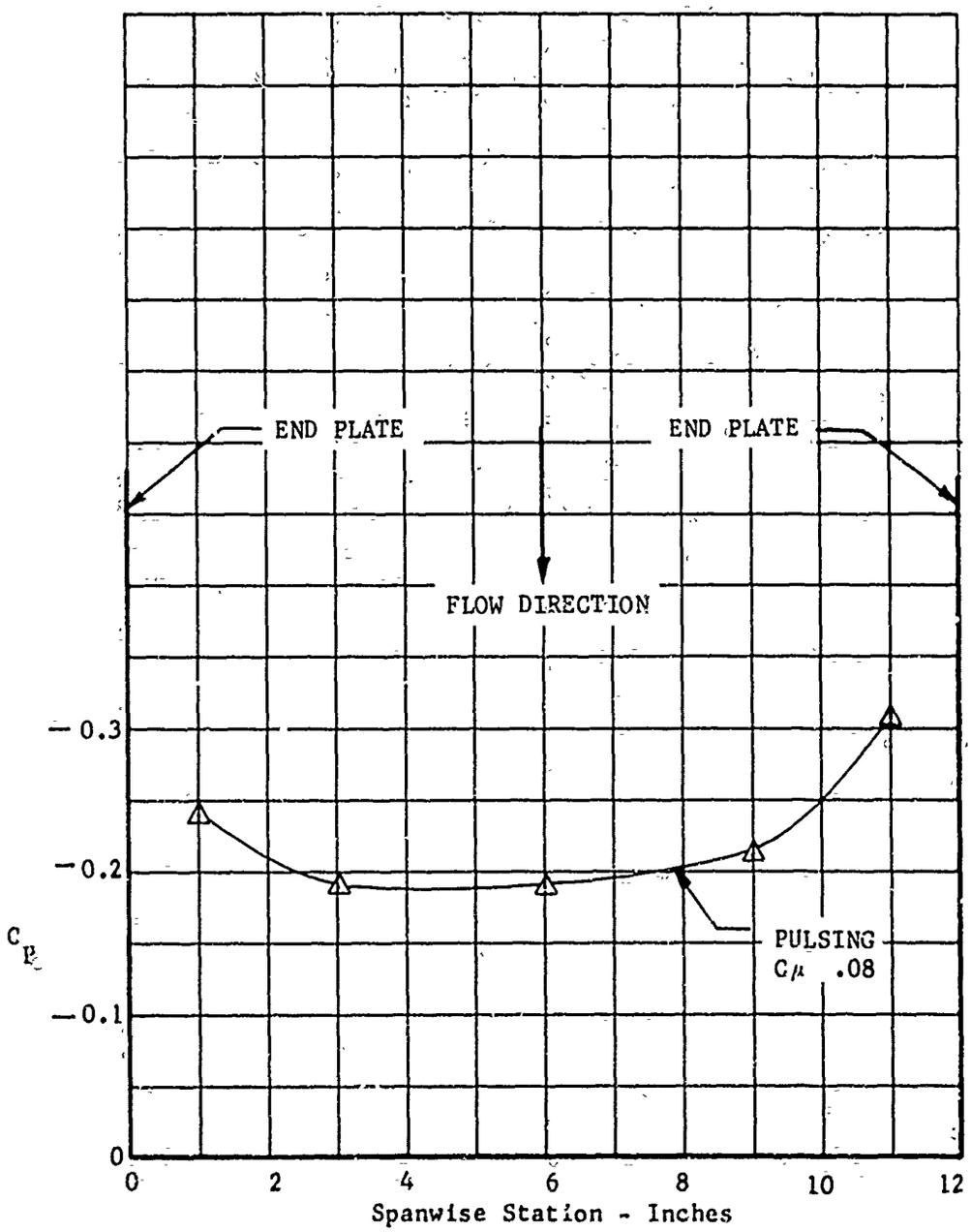

Figure 13. Flow Channel Spanwise Pressure Variation
$\alpha = 0 \quad \delta_F = 40°$

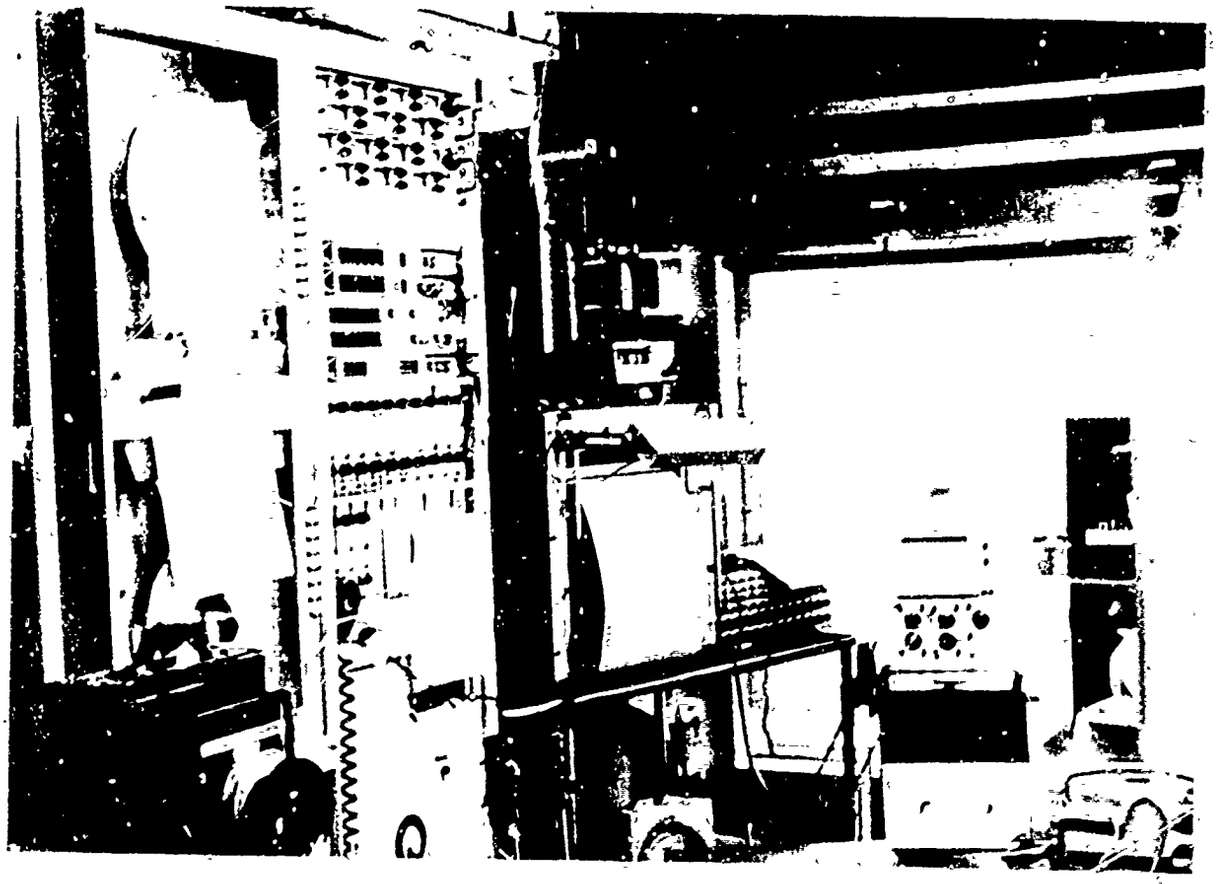

Figure 14. Photograph of Recording Equipment

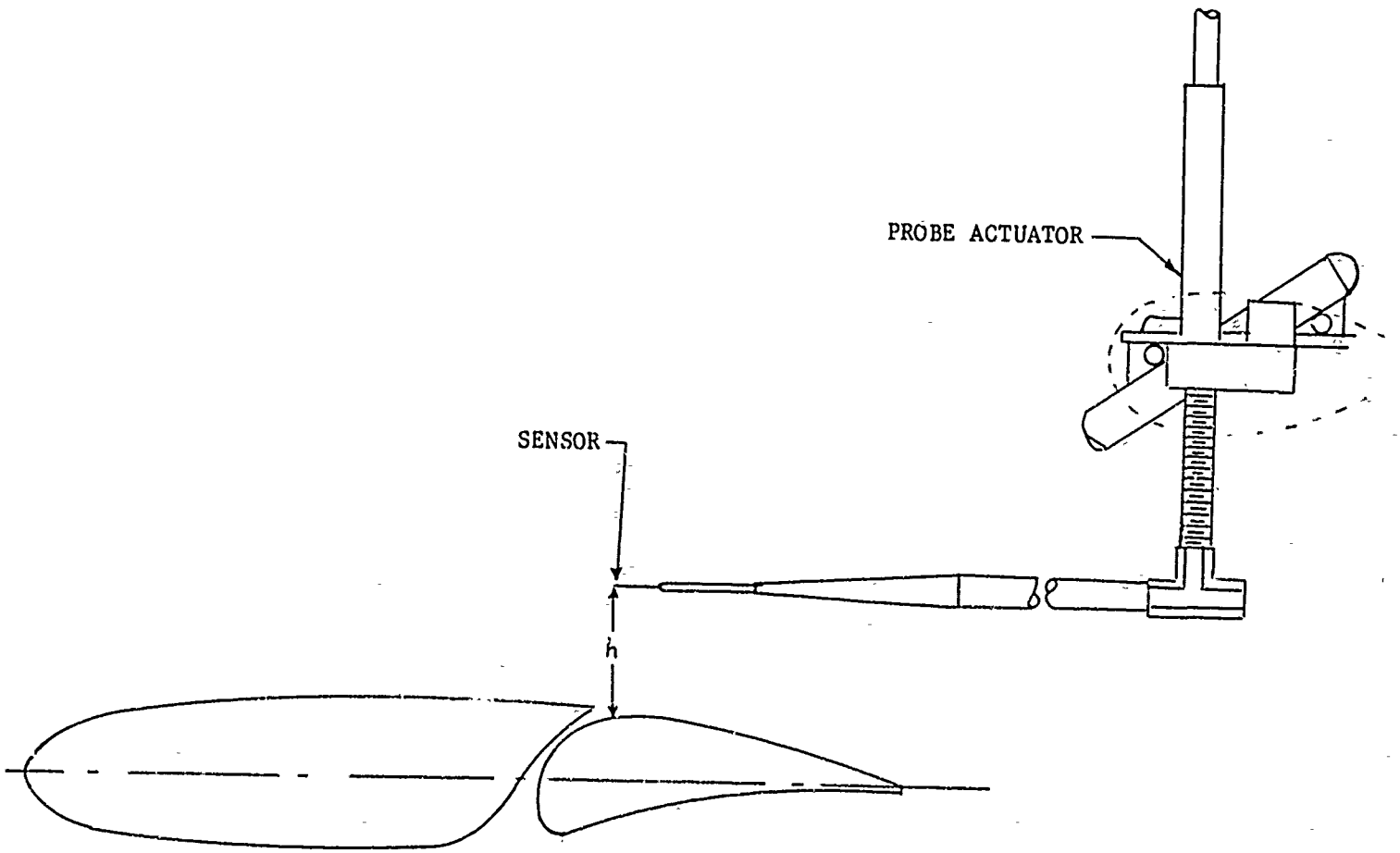

Figure 15. Sketch of Probe Assembly

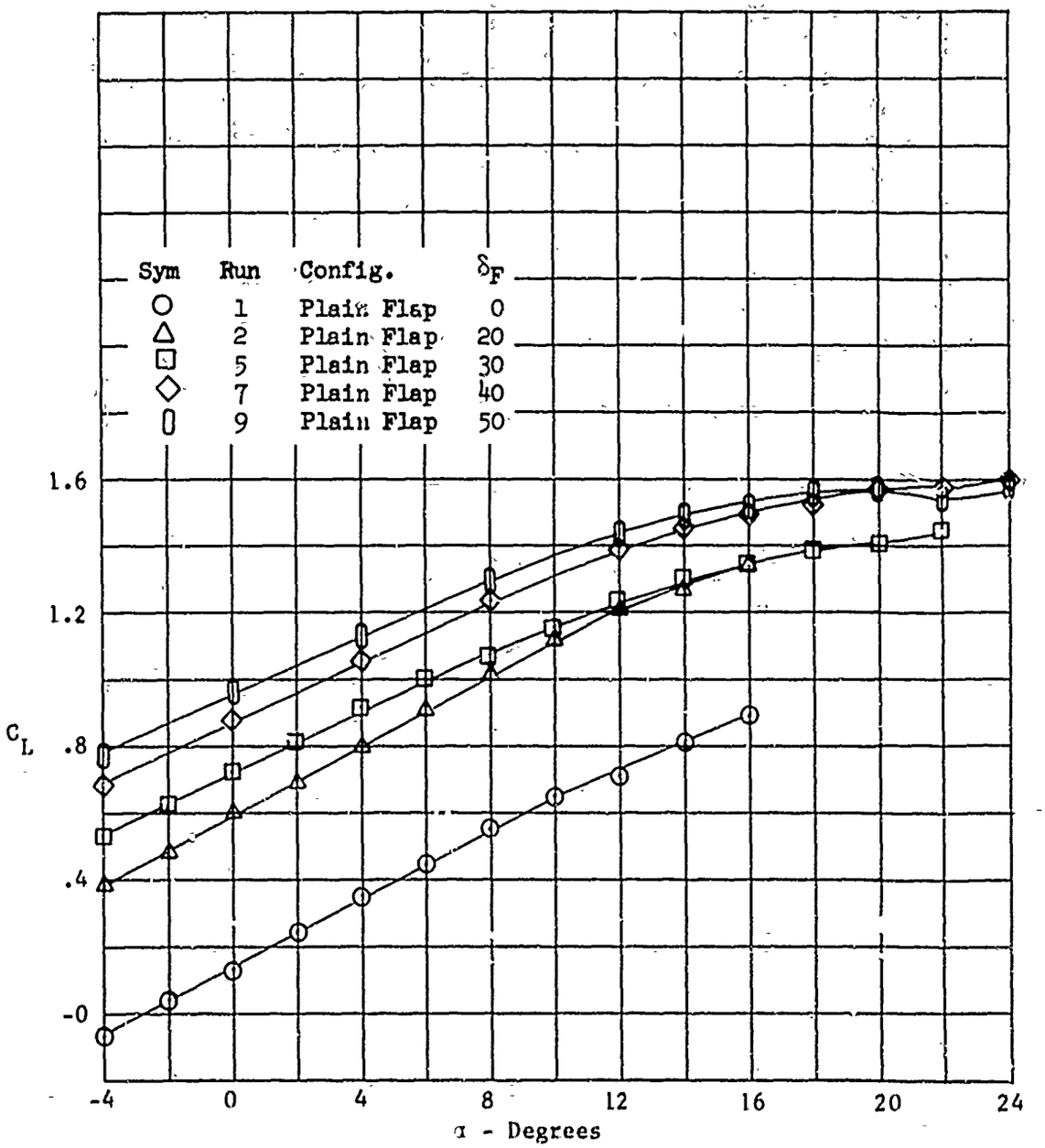

Figure 16 . Variation of Lift Coefficient With Angle of Attack
$C_\mu = 0$

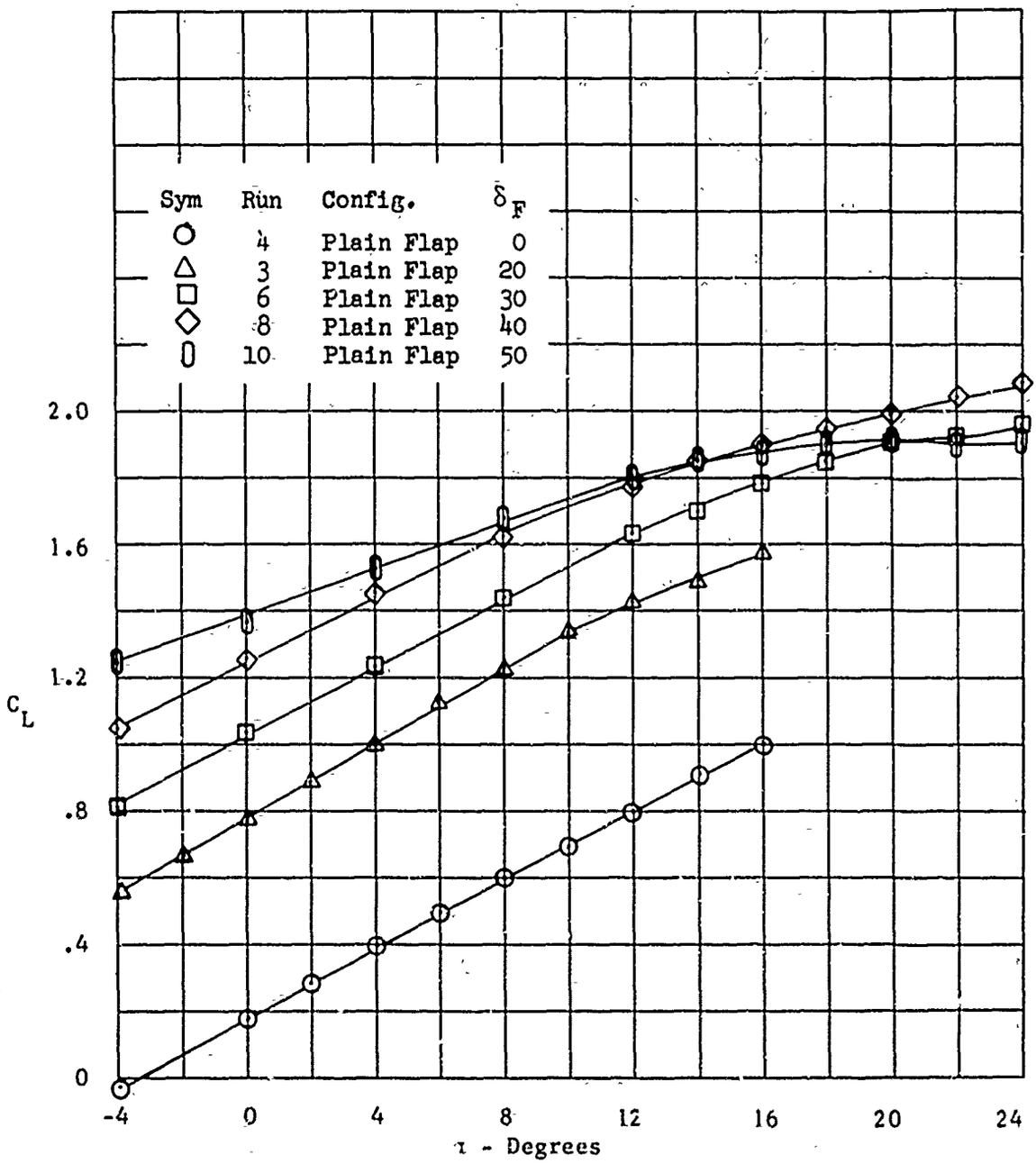

Figure 17. Variation of Lift Coefficient With Angle of Attack
$C_\mu = .165$

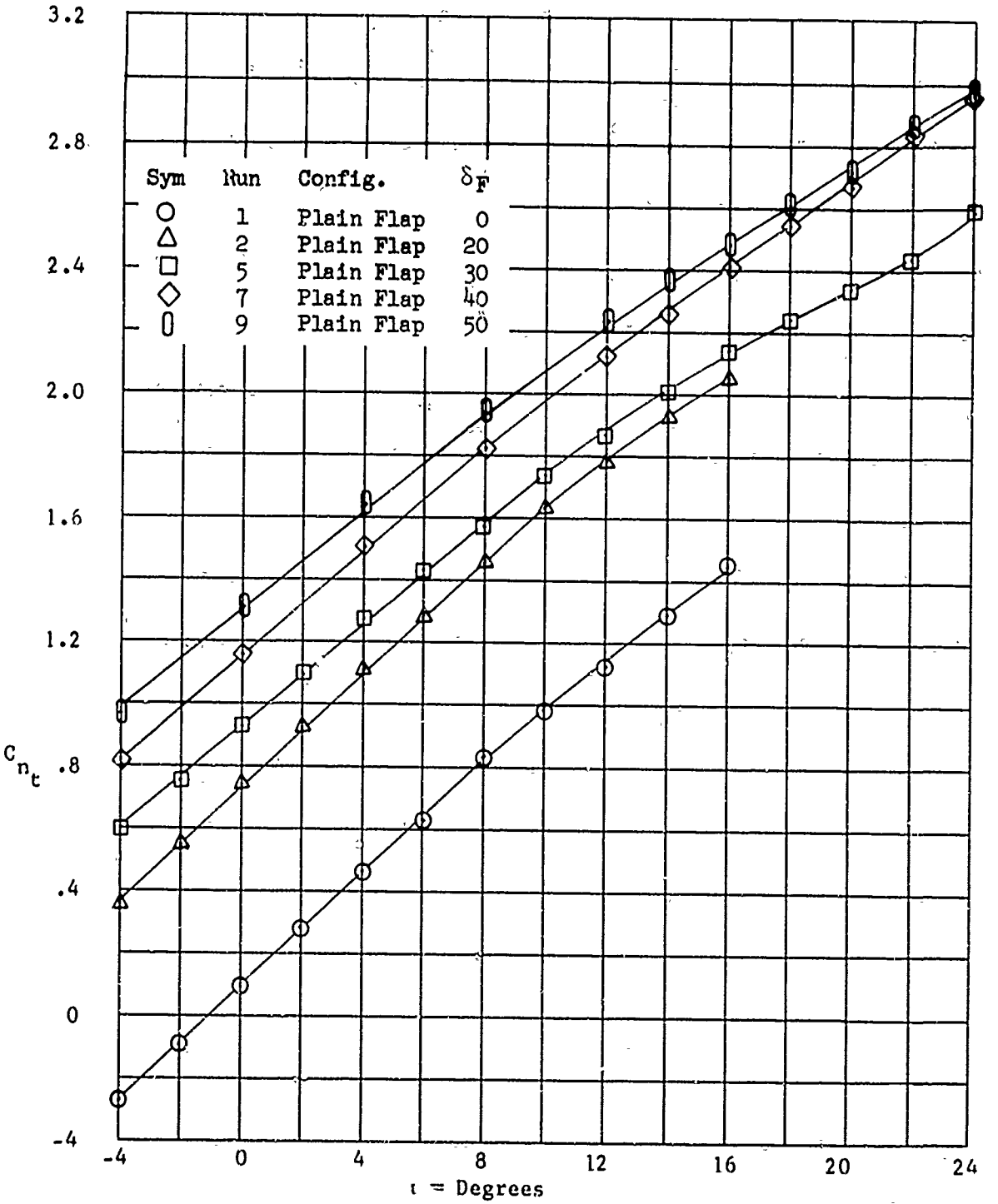

Figure 18. Variation of Section Normal Force Coefficient With Angle of Attack

$C_\mu = 0$

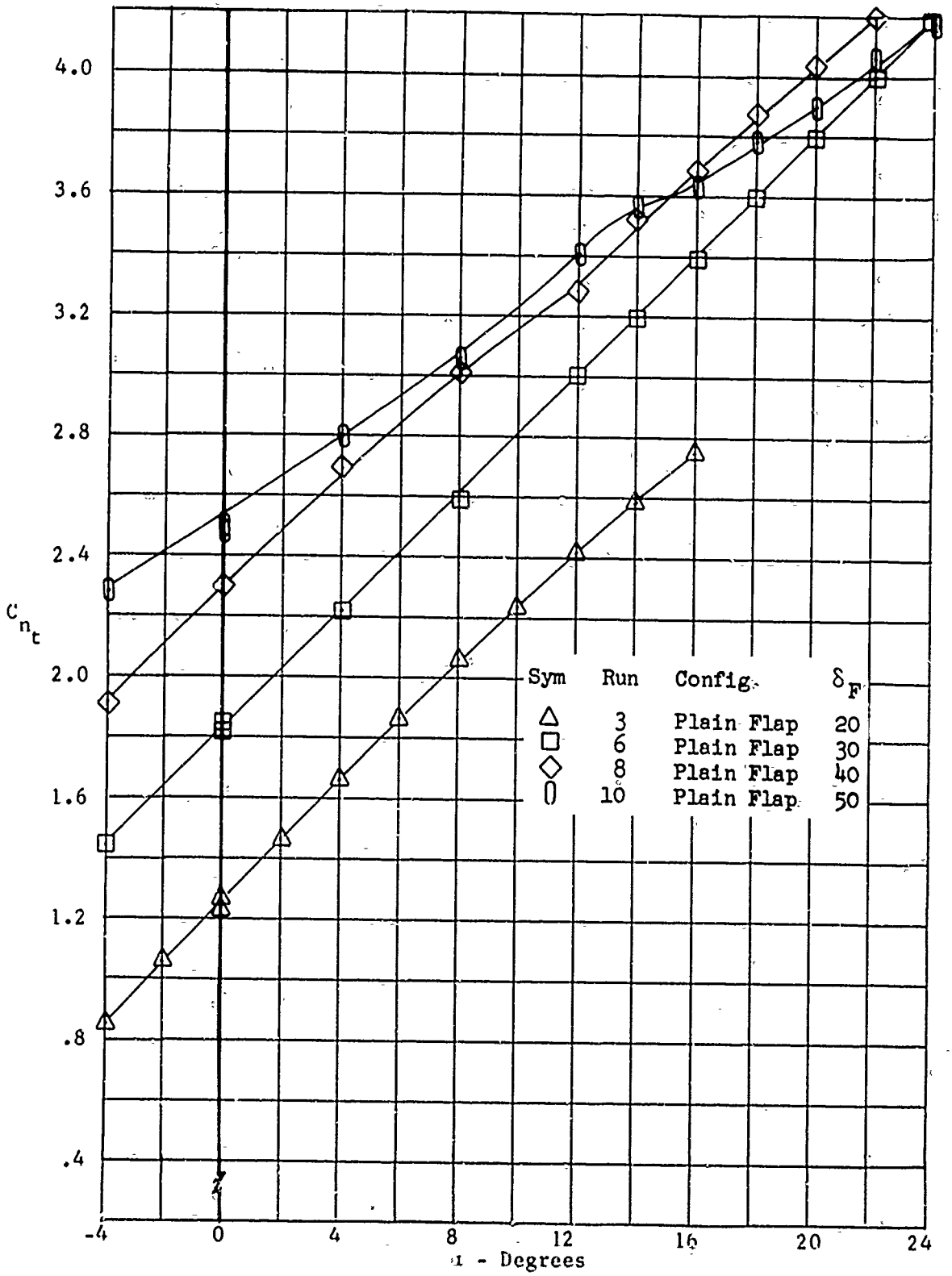

Figure 19. Variation of Section Normal Force Coefficient With Angle of Attack

$C_\mu = .165$

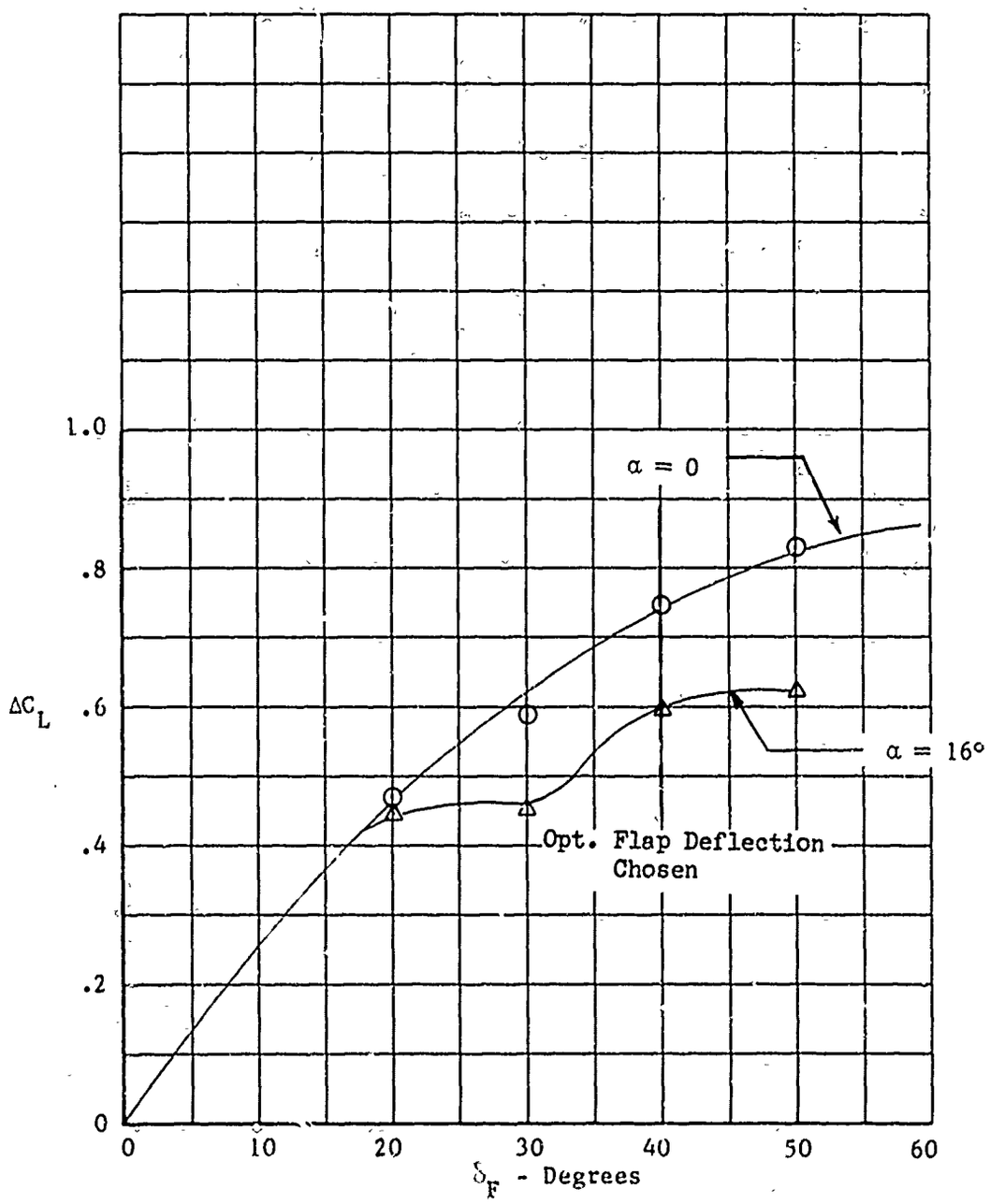

Figure 20. Variation of Incremental Lift With Flap Deflection
$C_\mu = 0$

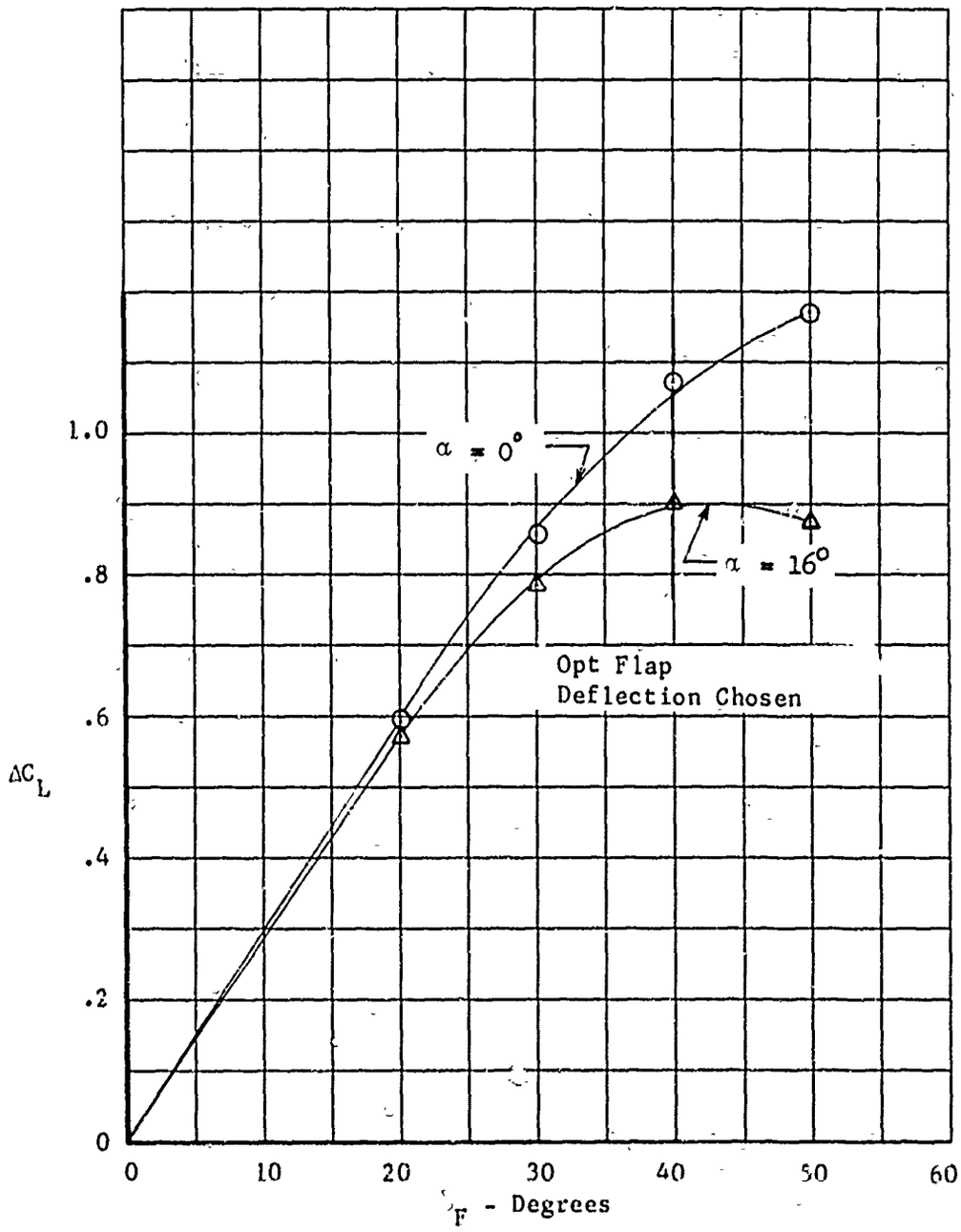

Figure 21. Variation of Incremental Lift With Flap Deflection
$C_\mu = .165$

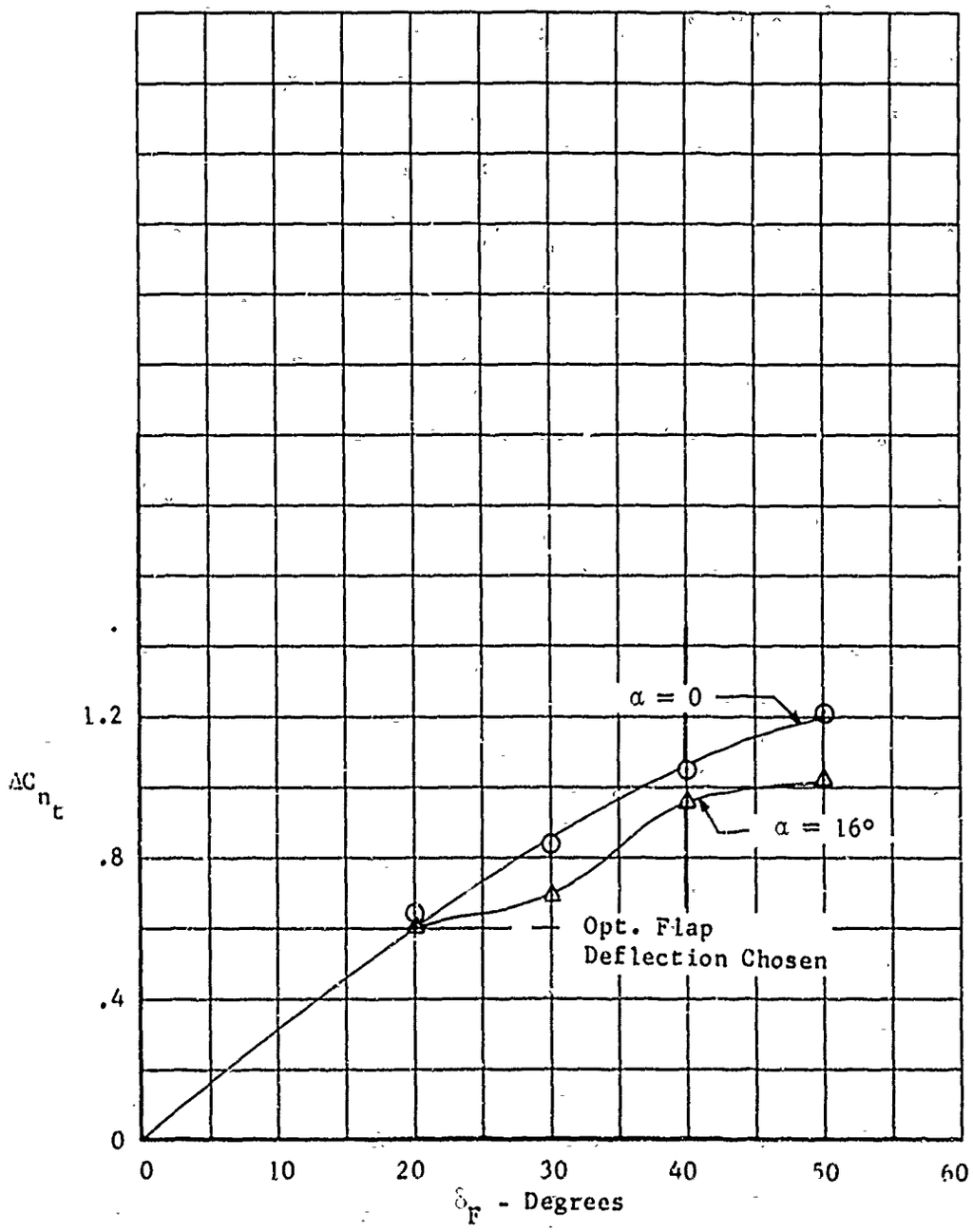

Figure 22. Variation of Incremental Section Normal Force Coefficient With Flap Deflection
$C_\mu = 0$

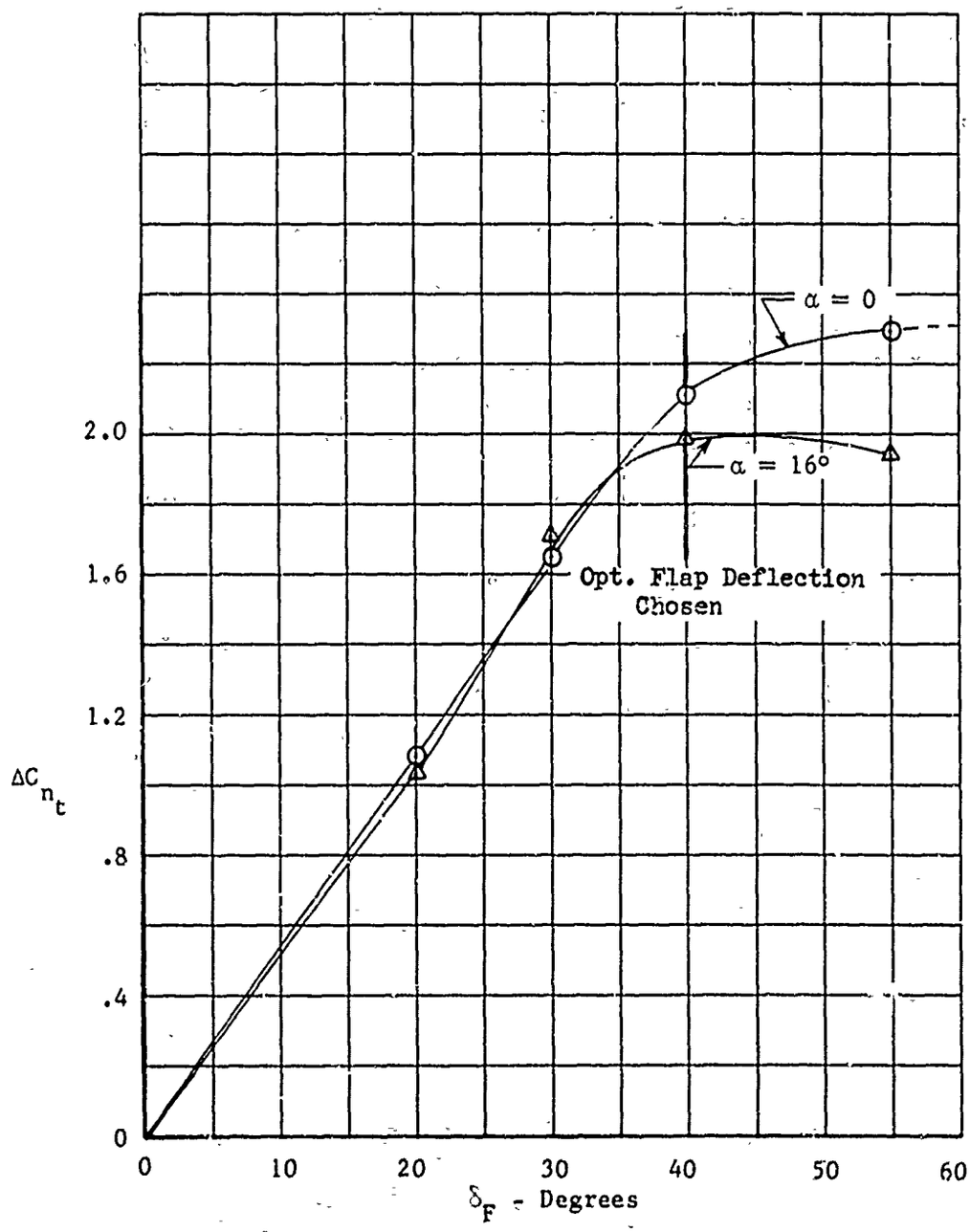

Figure 23. Variation of Incremental Section Normal Force Coefficient With Flap Deflection
C_μ = .165 (Steady Blowing)

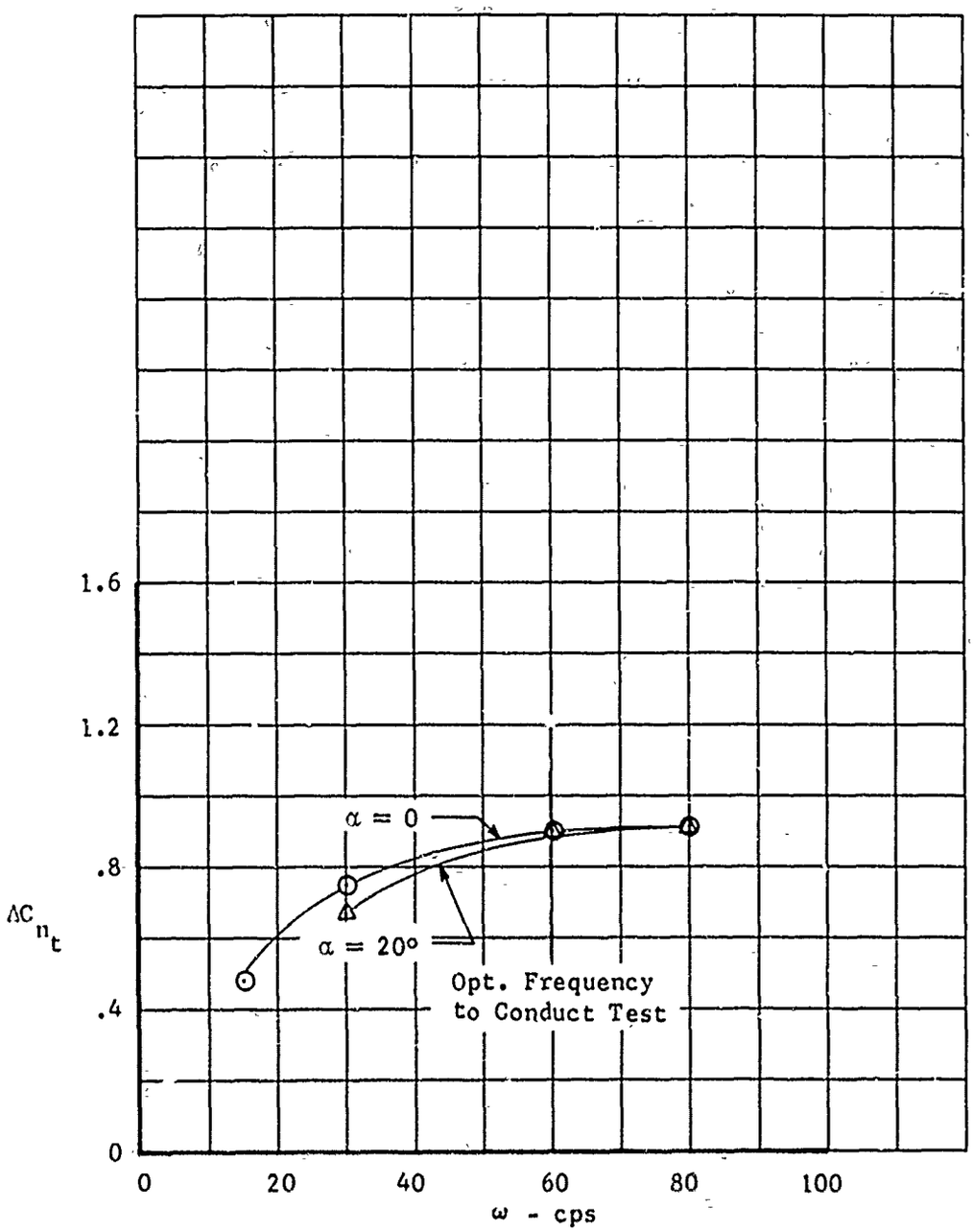

Figure 24. Variation of Incremental Section Normal Force Coefficient With Pulse Frequency

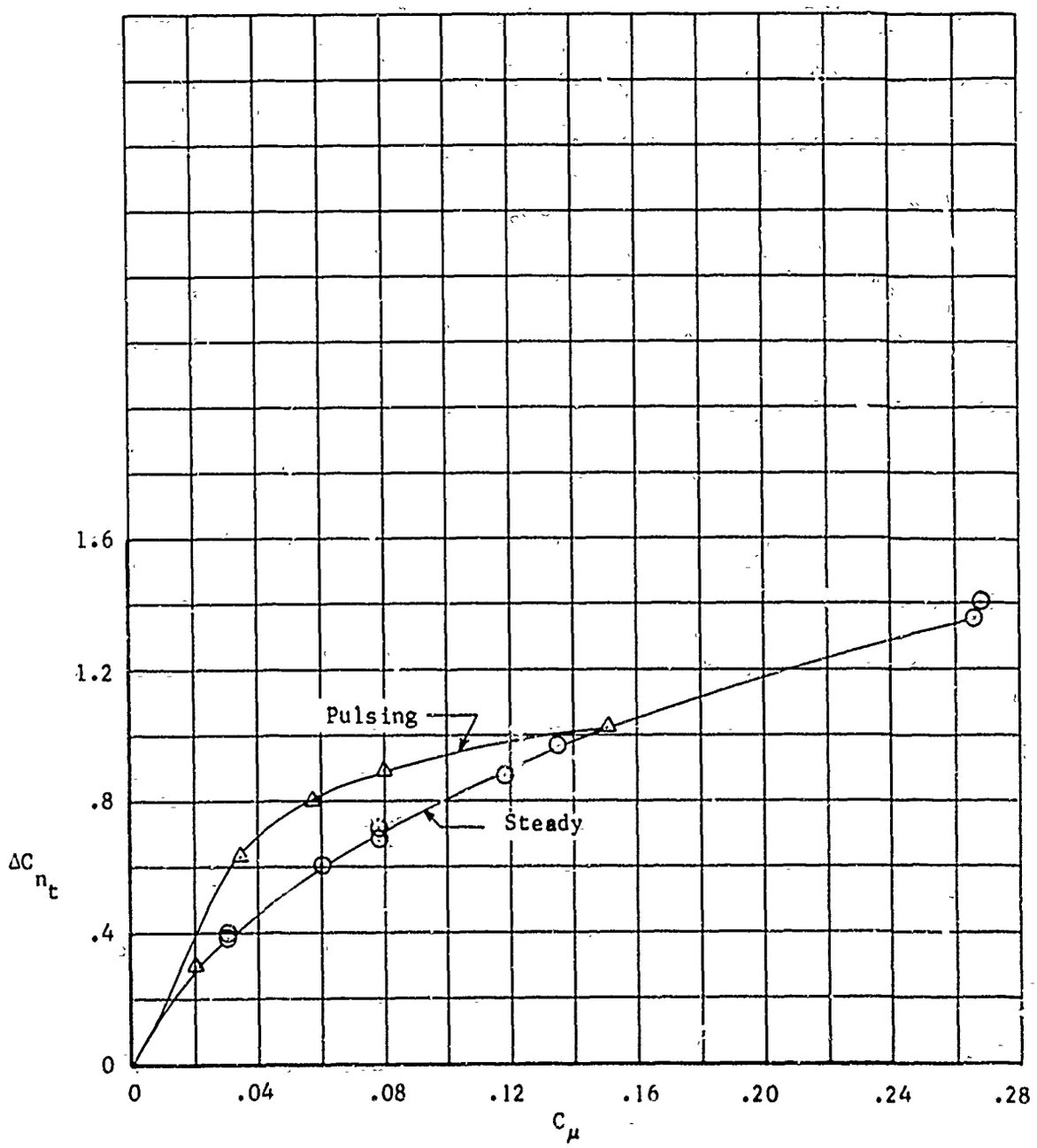

Figure 25. Variation of Incremental Section Normal Force Coefficient With Momentum Flow Coefficient
$\alpha = 0 \quad \delta_F = 40°$

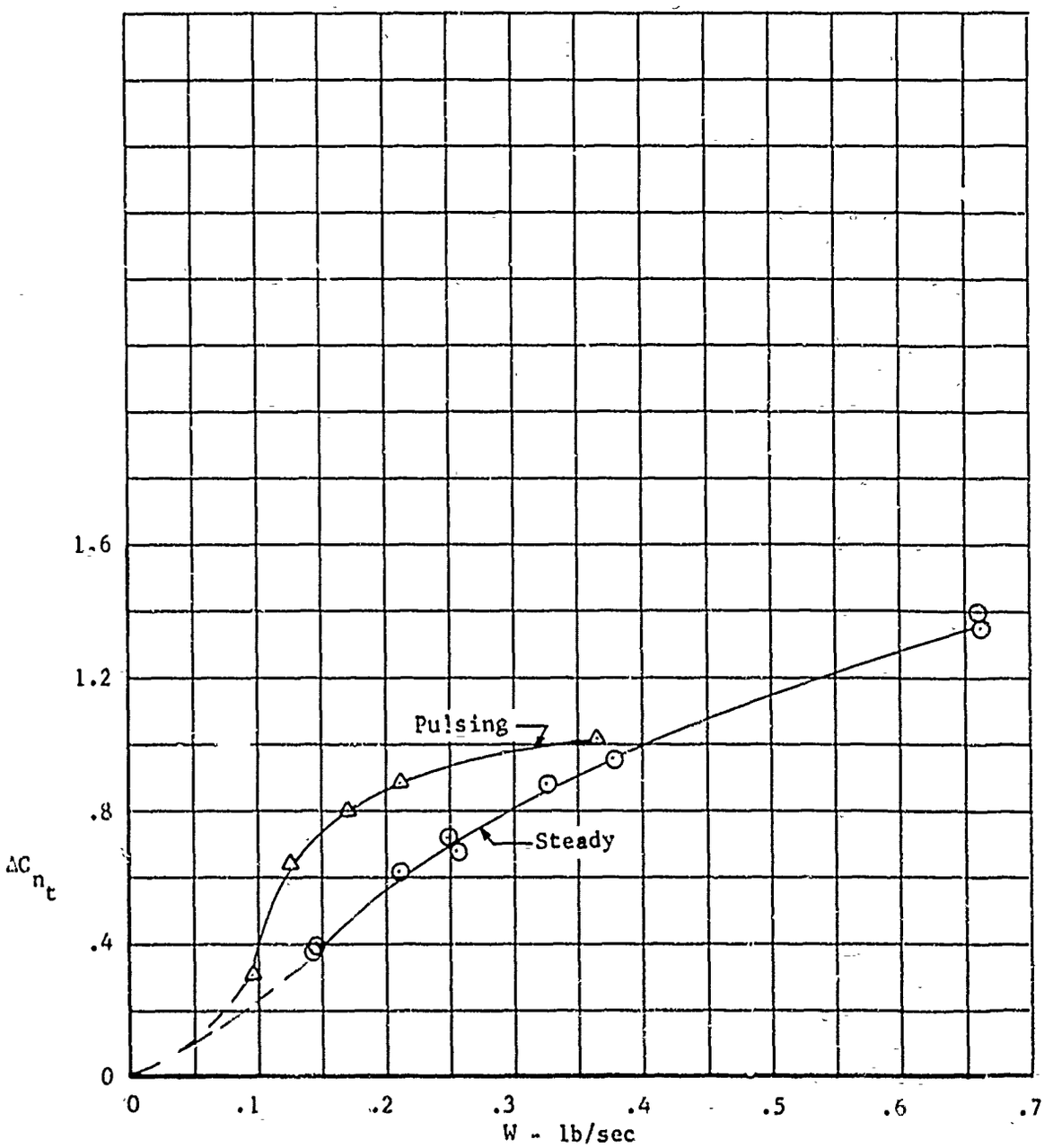

Figure 26. Variation of Incremental Section Normal Force Coefficient With Weight Flow
$\alpha = 0 \quad \delta_F = 40°$

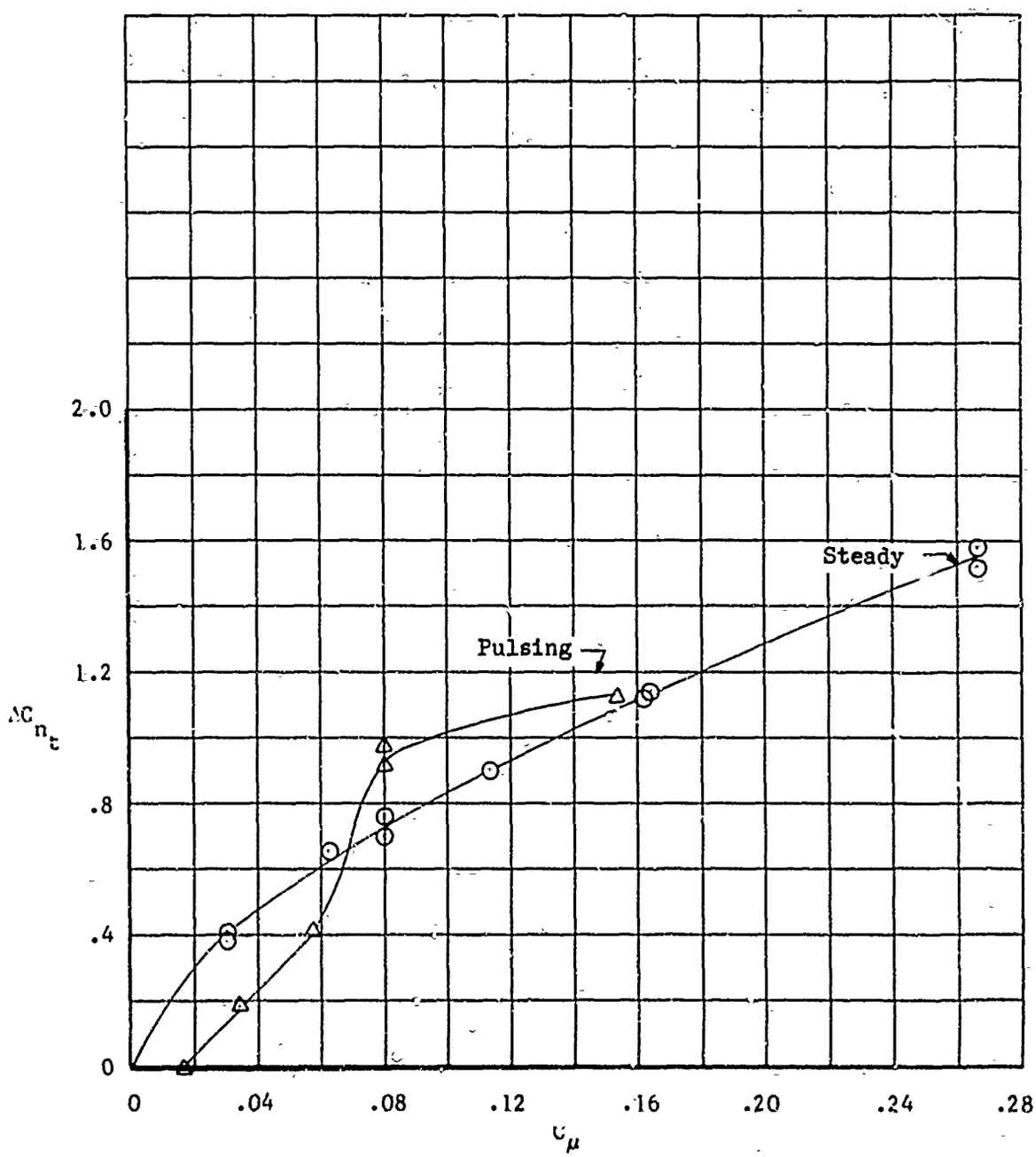

Figure 27. Variation of Incremental Section Normal Force Coefficient With Momentum Coefficient
$\alpha = 20°$ $\delta_F = 40°$

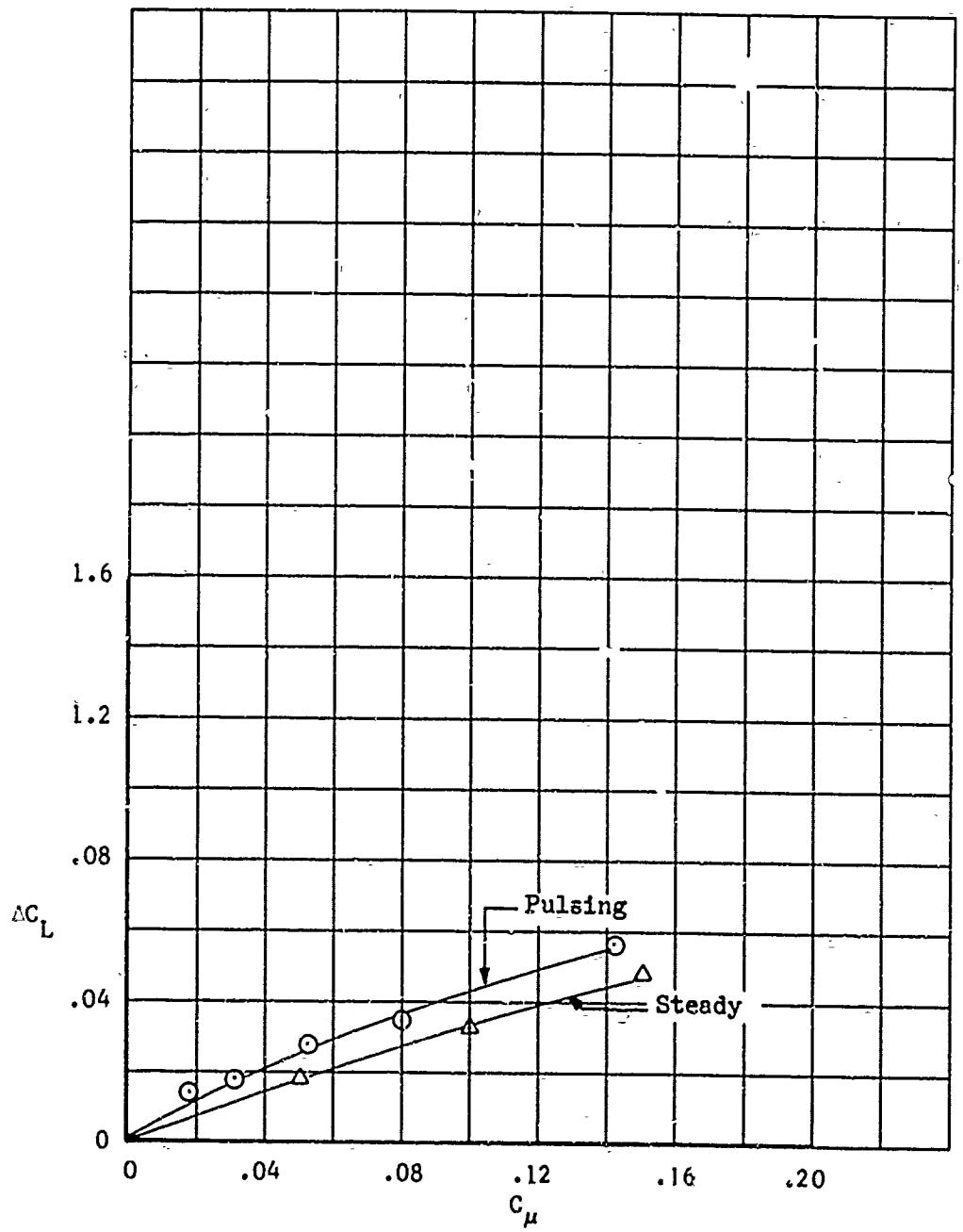

Figure 28. Variation of Incremental Lift Coefficient With Momentum Coefficient
$\alpha = 0 \quad \delta_F = 0$

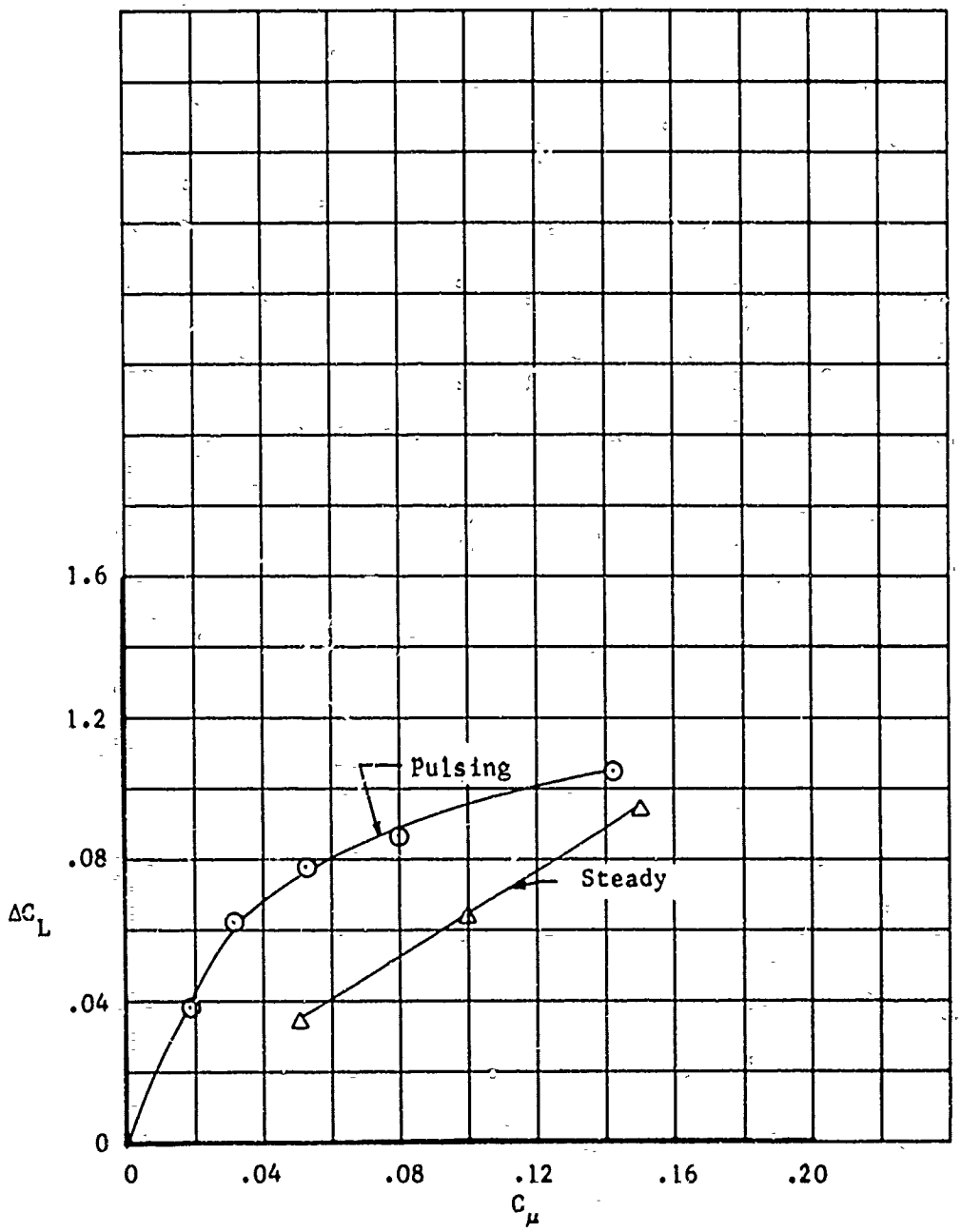

Figure 29. Variation of Incremental Lift Coefficient With Momentum Coefficient
$\alpha = 20°$ $\delta_E = 0°$

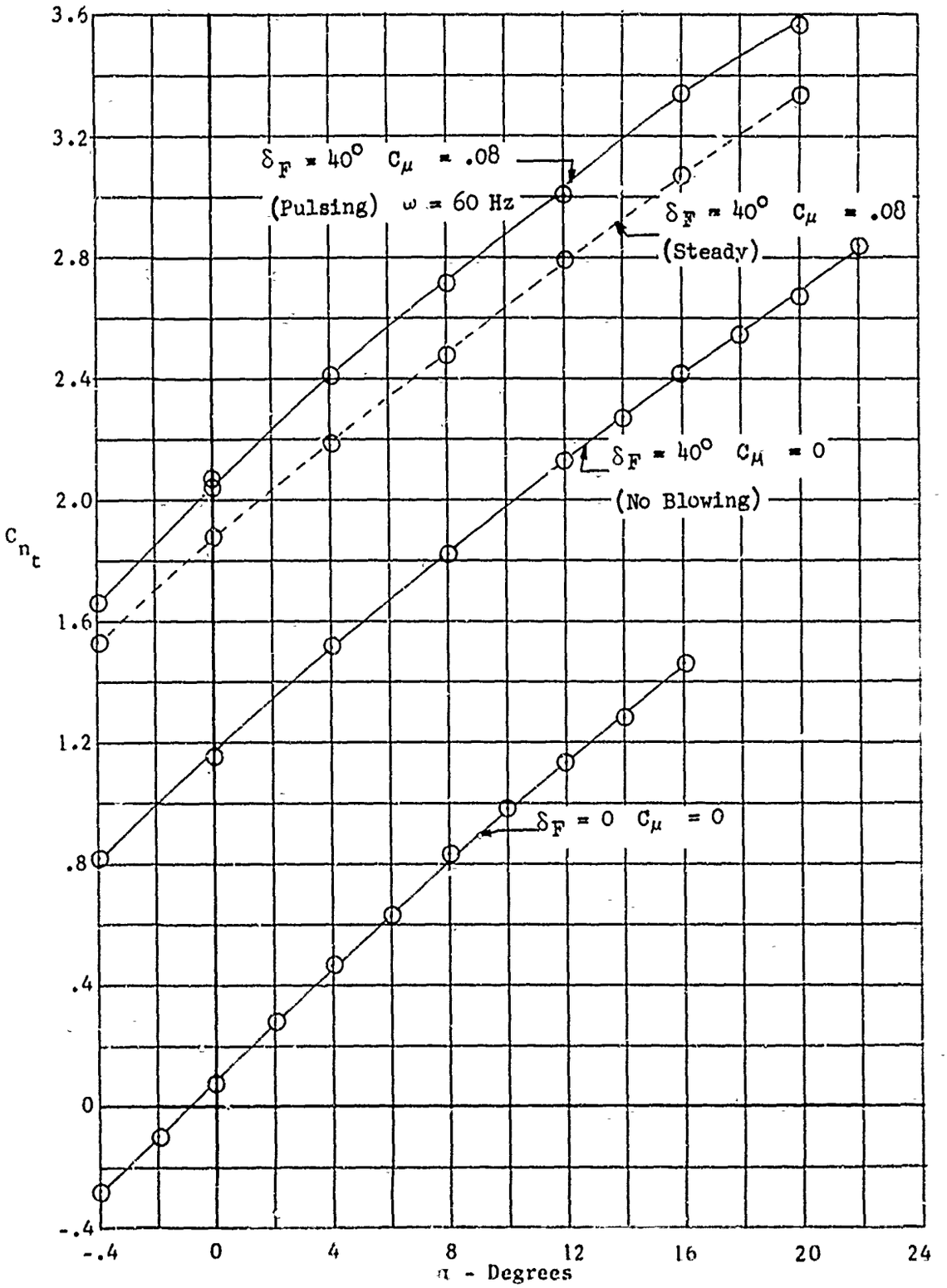

Figure 30. Variation of Section Normal Force Coefficient With Angle of Attack

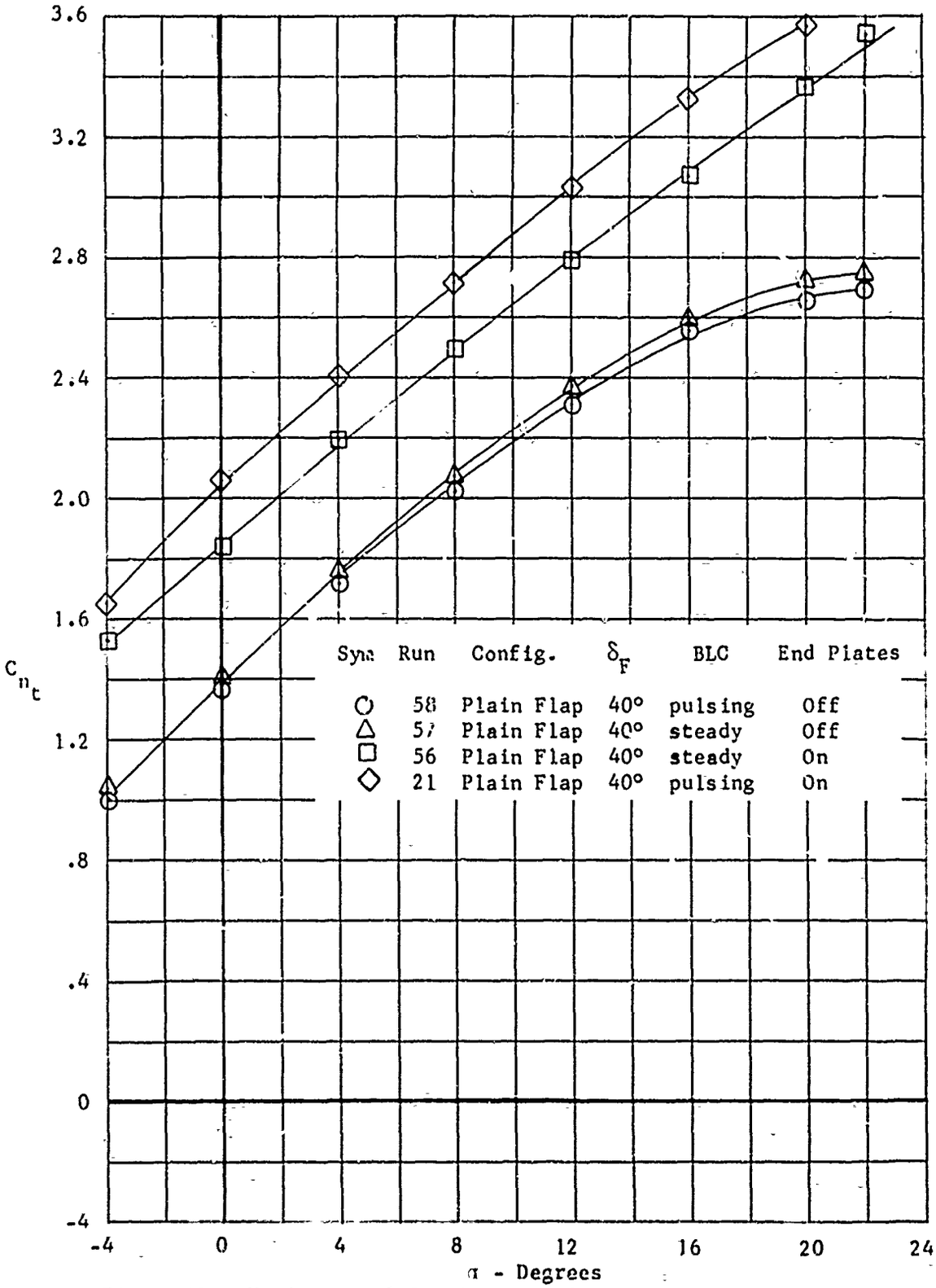

Figure 31. Variation of Section Normal Force Coefficient With Angle of Attack With and Without End Plates
$\delta_F = 40°$

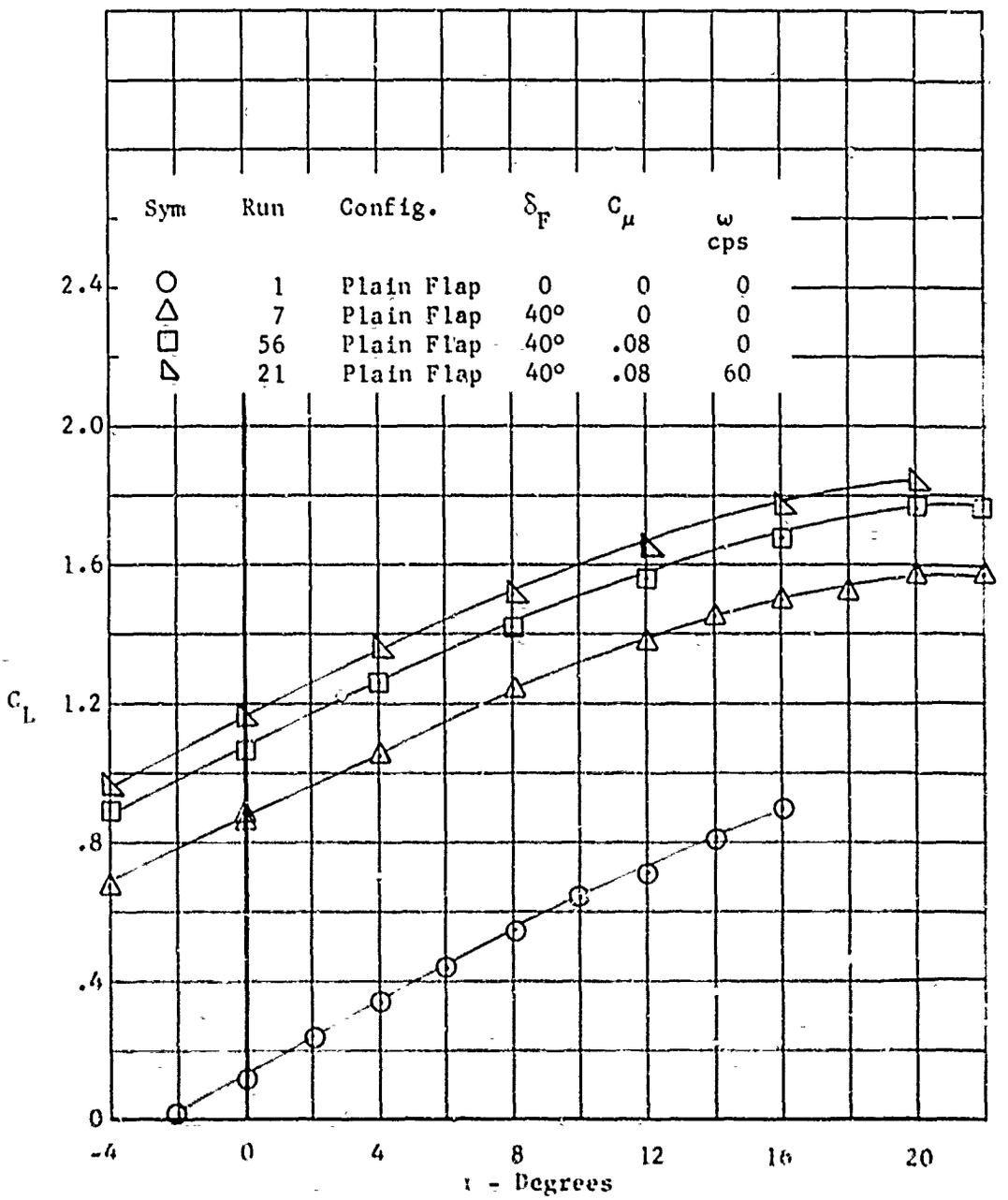

Figure 32. Variation of Lift Coefficient With Angle of Attack

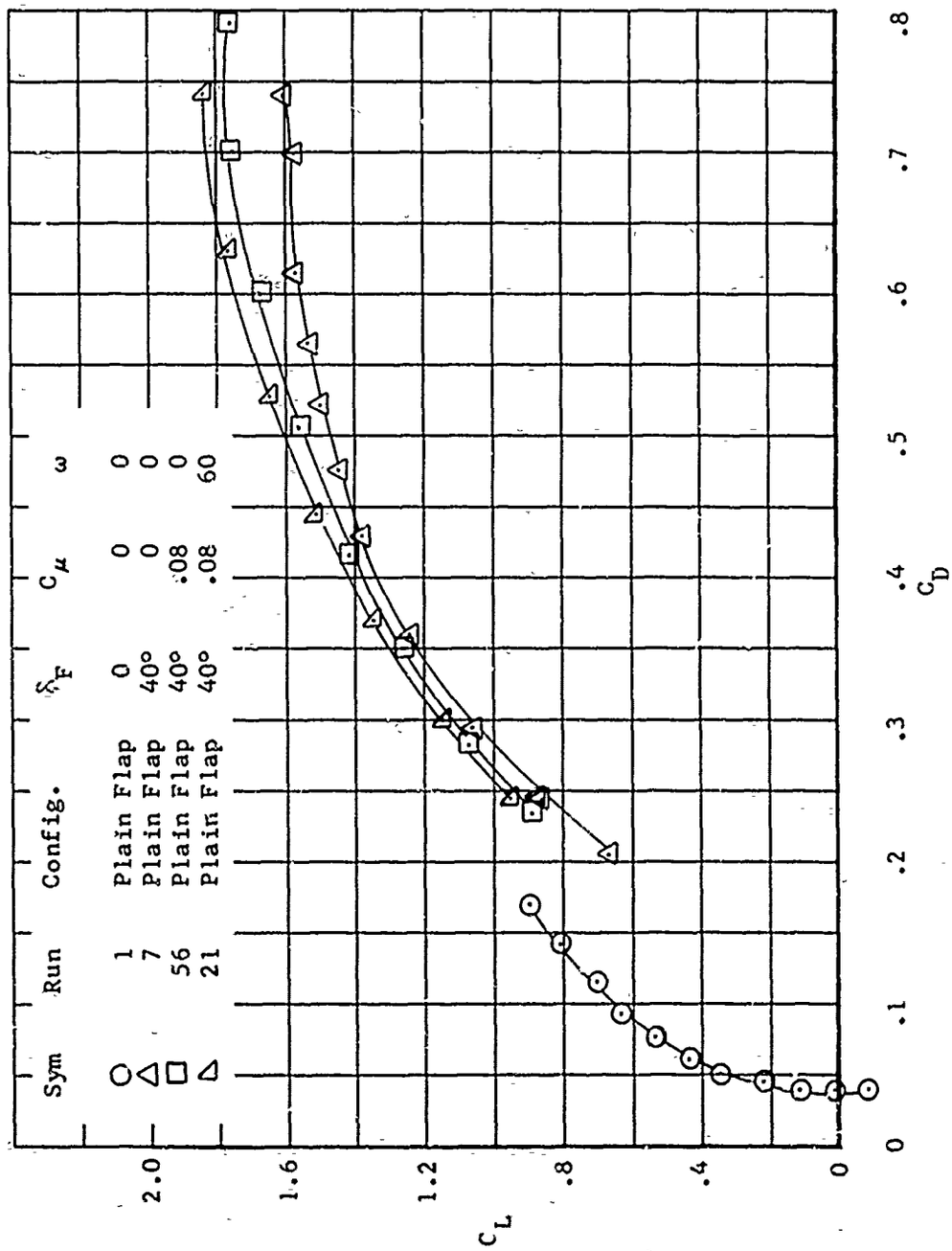

Figure 33. Variation of Drag Coefficient With Lift Coefficient

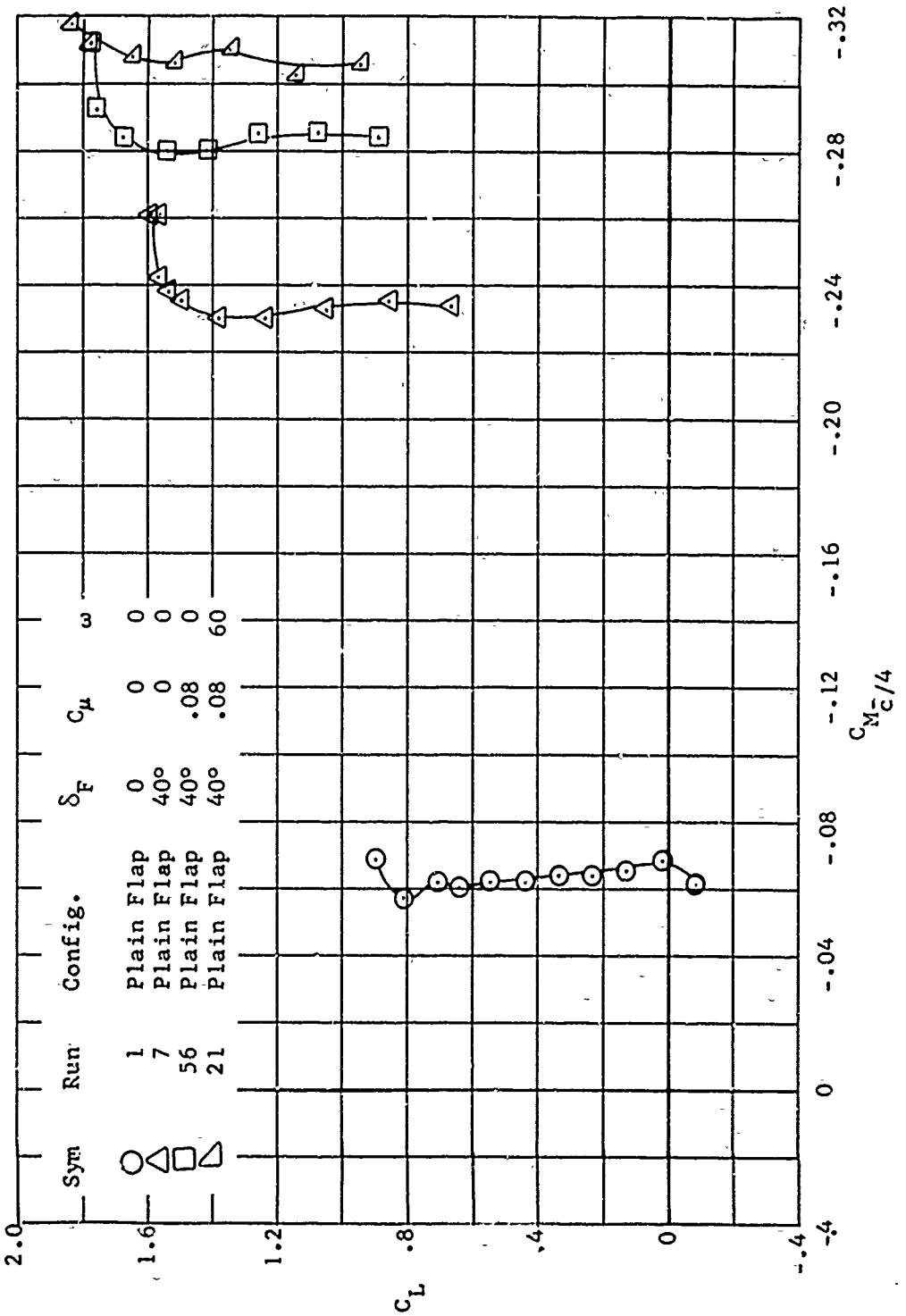

Figure 34. Variation of Pitching Moment Coefficient With Lift Coefficient

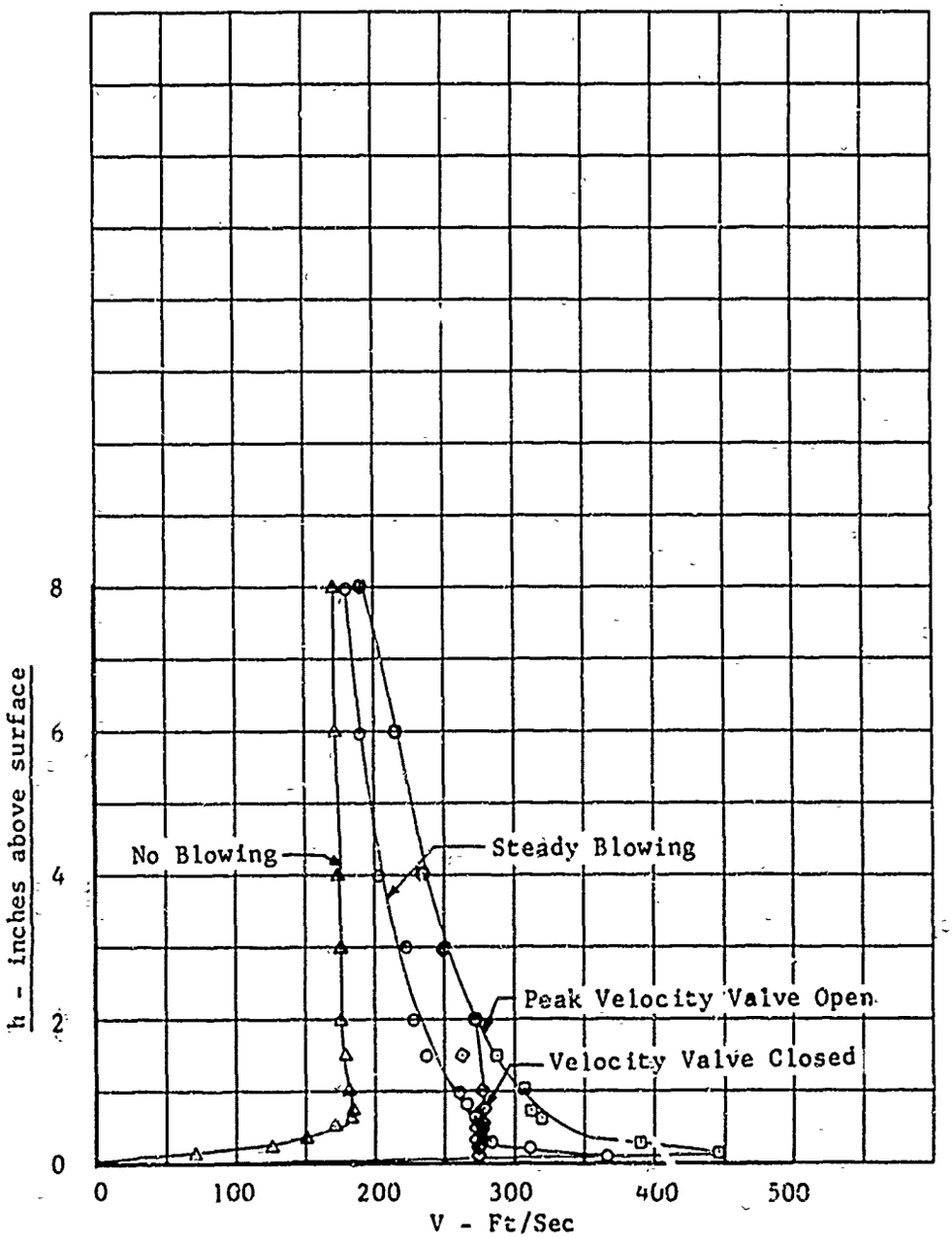

Figure 35. Longitudinal Velocity Distribution Normal to the Flap Chord Plane
Flap Chord Station - 9.3% c_w
$\alpha = 0$ $\delta_F = 40°$

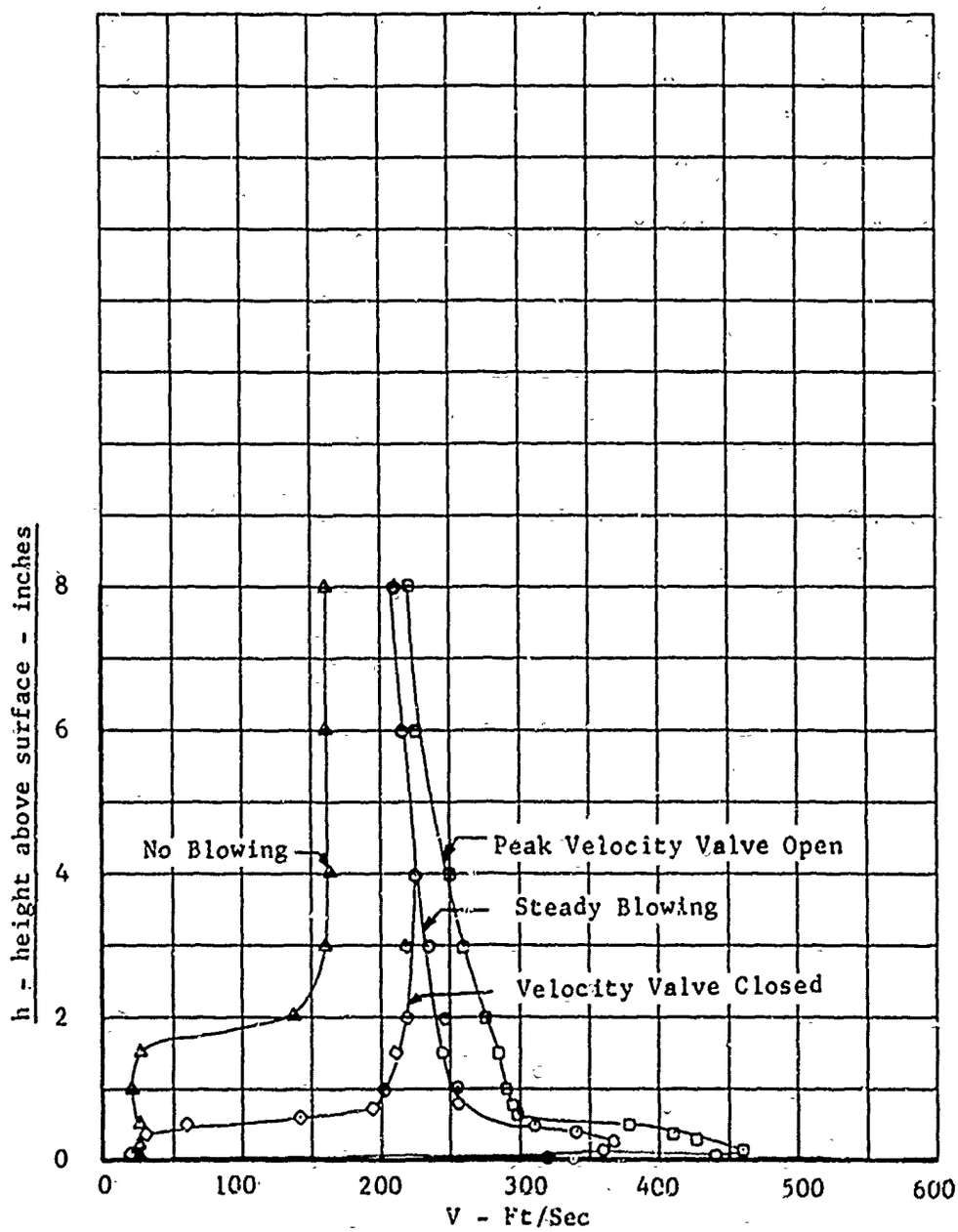

Figure 36. Longitudinal Velocity Distribution Normal to the Flap Chord Plane

Flap Chord Station 17% c_w

$\alpha = 0 \quad \delta_F = 40°$

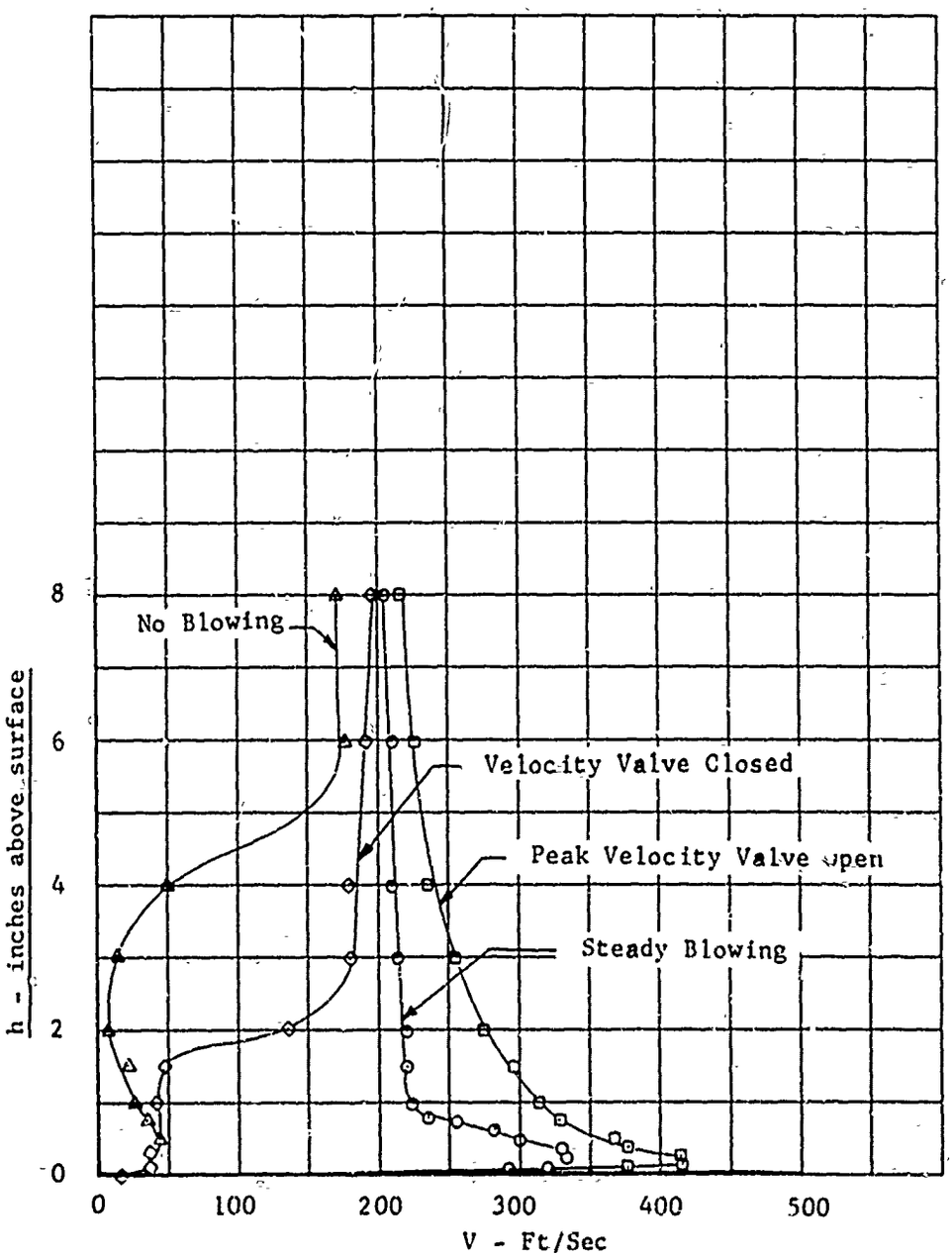

Figure 37. Longitudinal Velocity Distribution Normal to the Flap Chord Plane
Flap Chord Station - 27% c_w
$\alpha = 0$ $\delta_F = 40°$

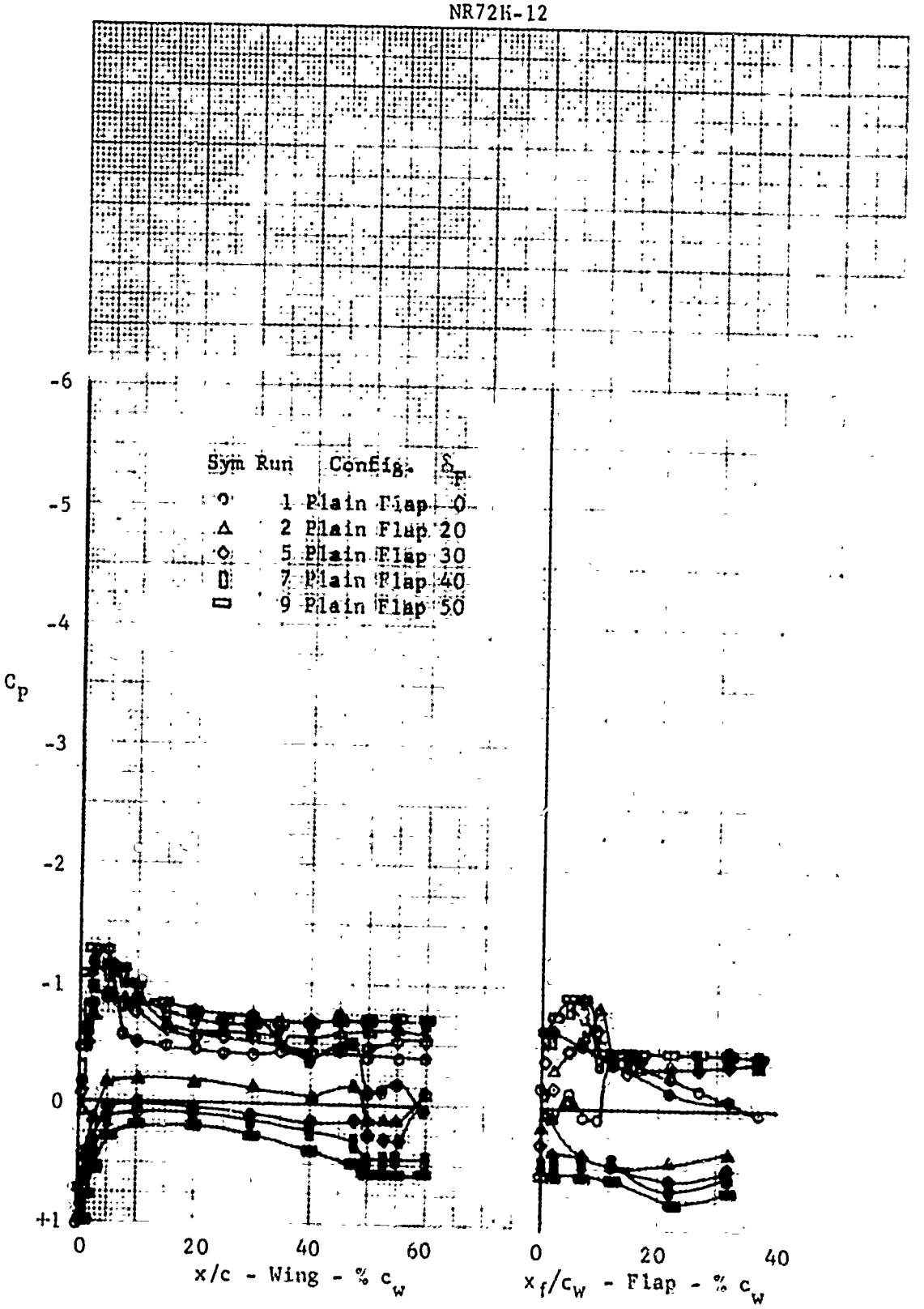

Figure 38. Effect of Flap Deflection
$C_\mu = 0$, $\alpha = 0$

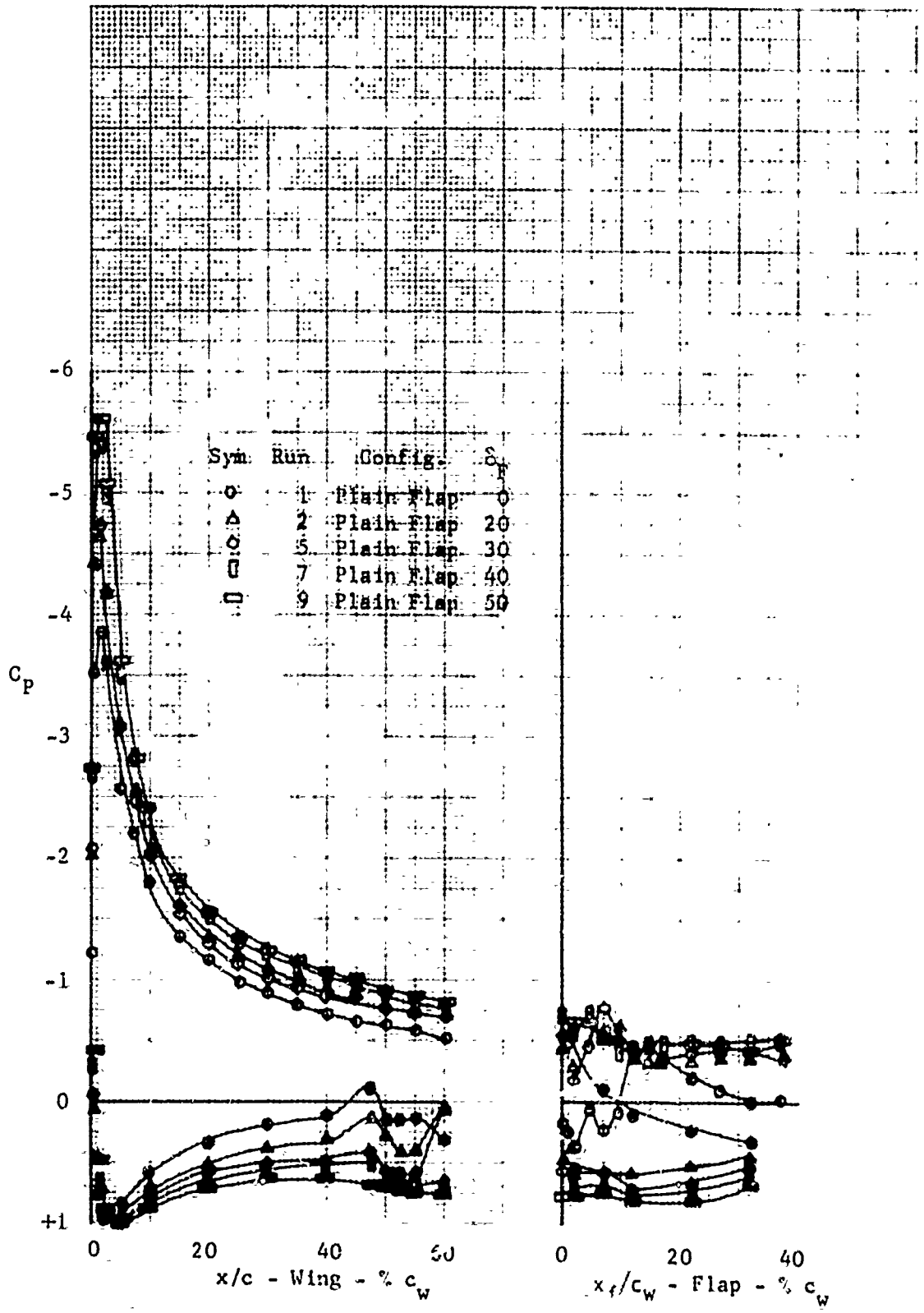

Figure 39 . Effect of Flap Deflection
$C_\mu = 0 \quad \alpha = 16°$

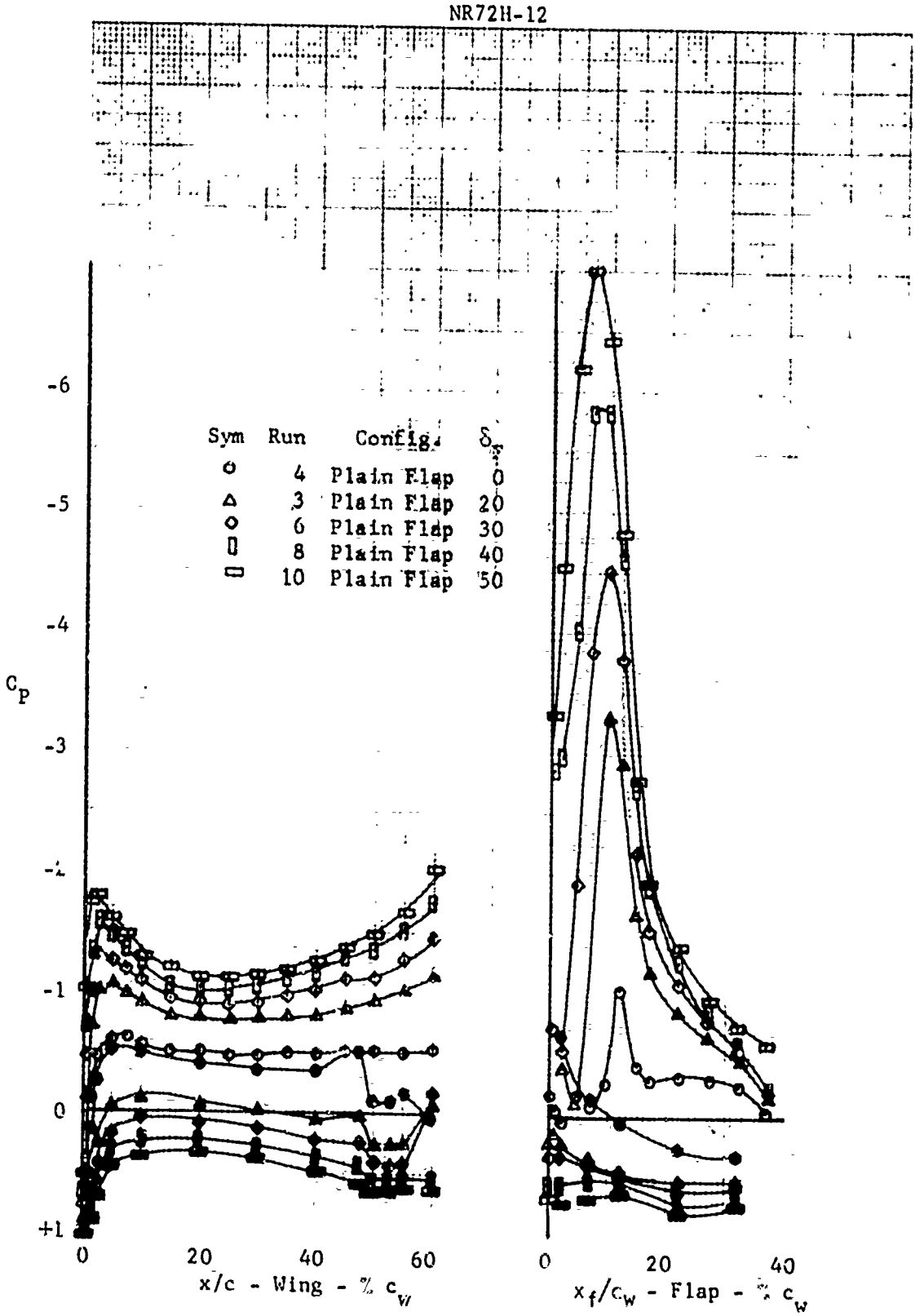

Figure 40. Effect of Flap Deflection
$C_\mu = .16 \quad \alpha = 0$

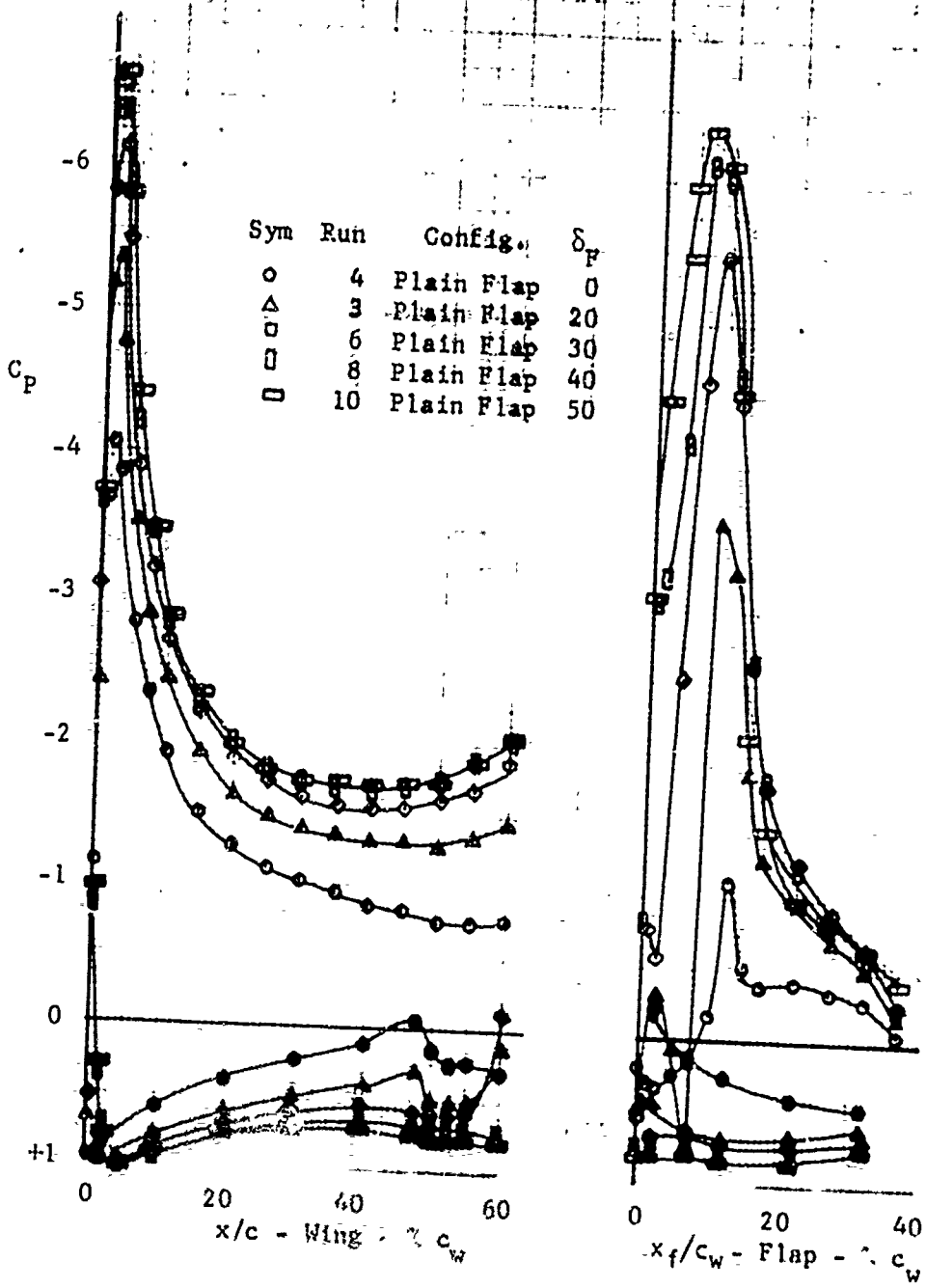

Figure 41. Effect of Flap Deflection
$C_\mu = .16$ $\alpha = 16°$

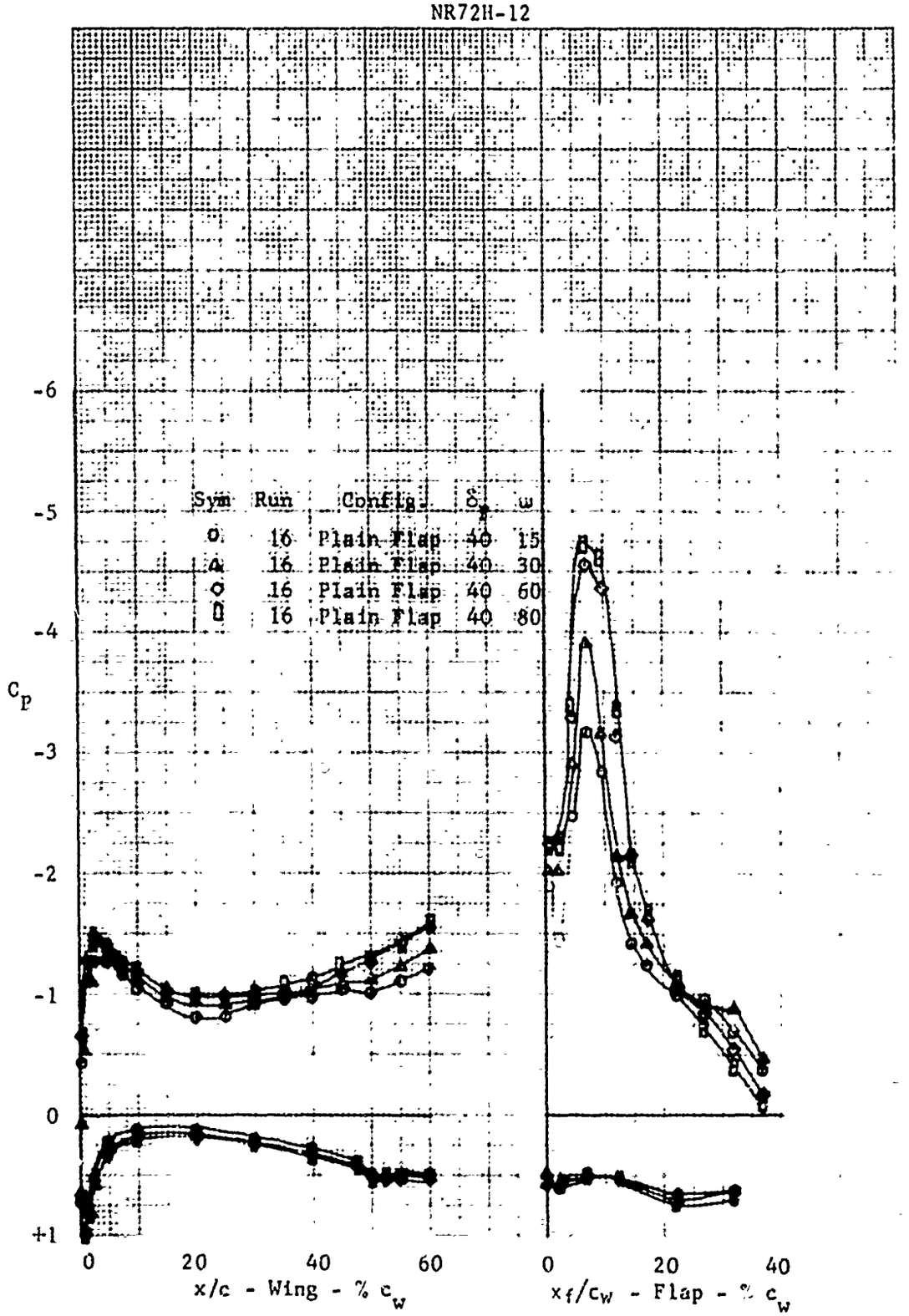

Figure 42. Effect of Pulse Frequency
$C\mu = .16 \quad \alpha = 0$

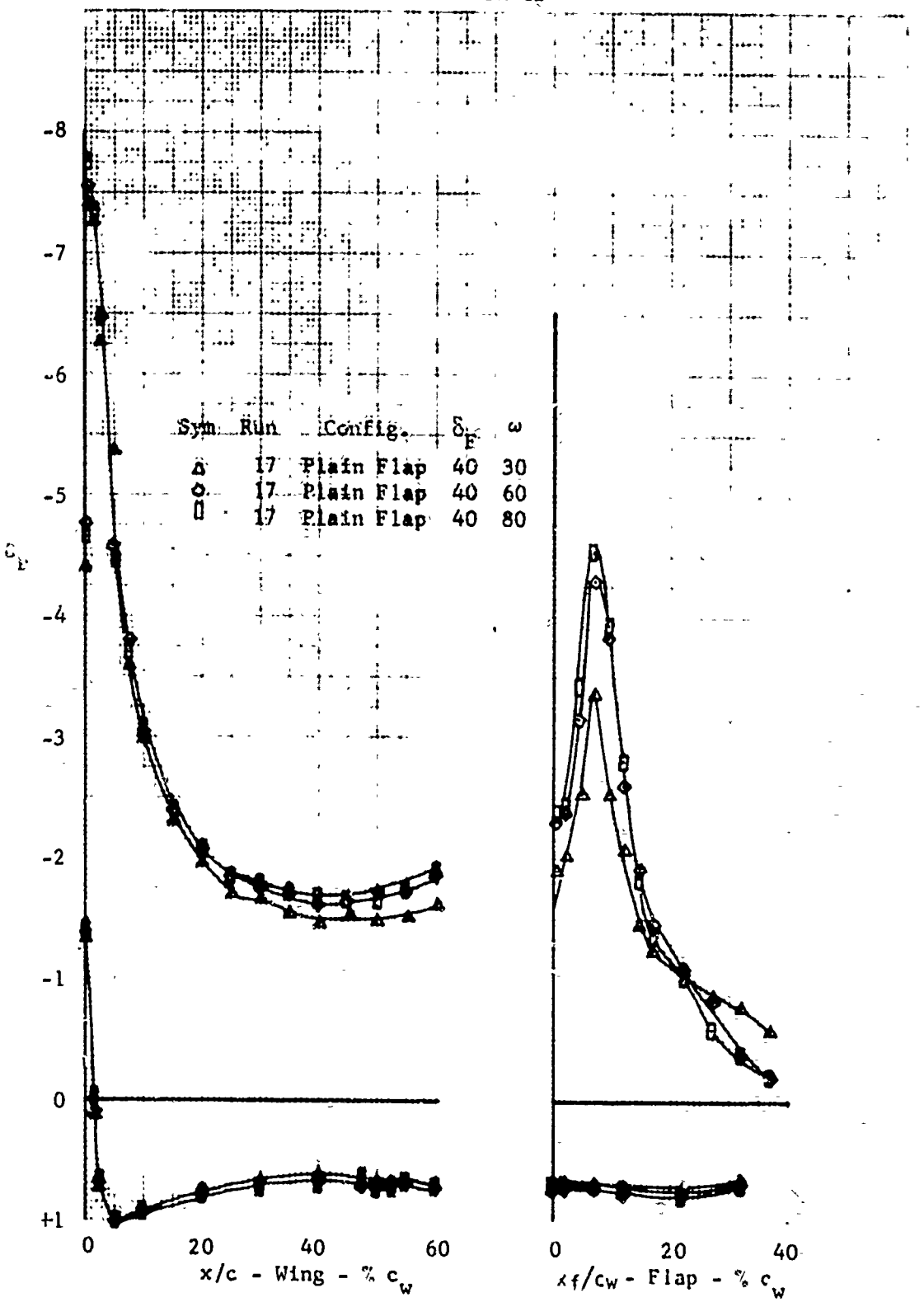

Figure 43. Effect of Pulse Frequency
$C_\mu = .160$ $\alpha = 20°$

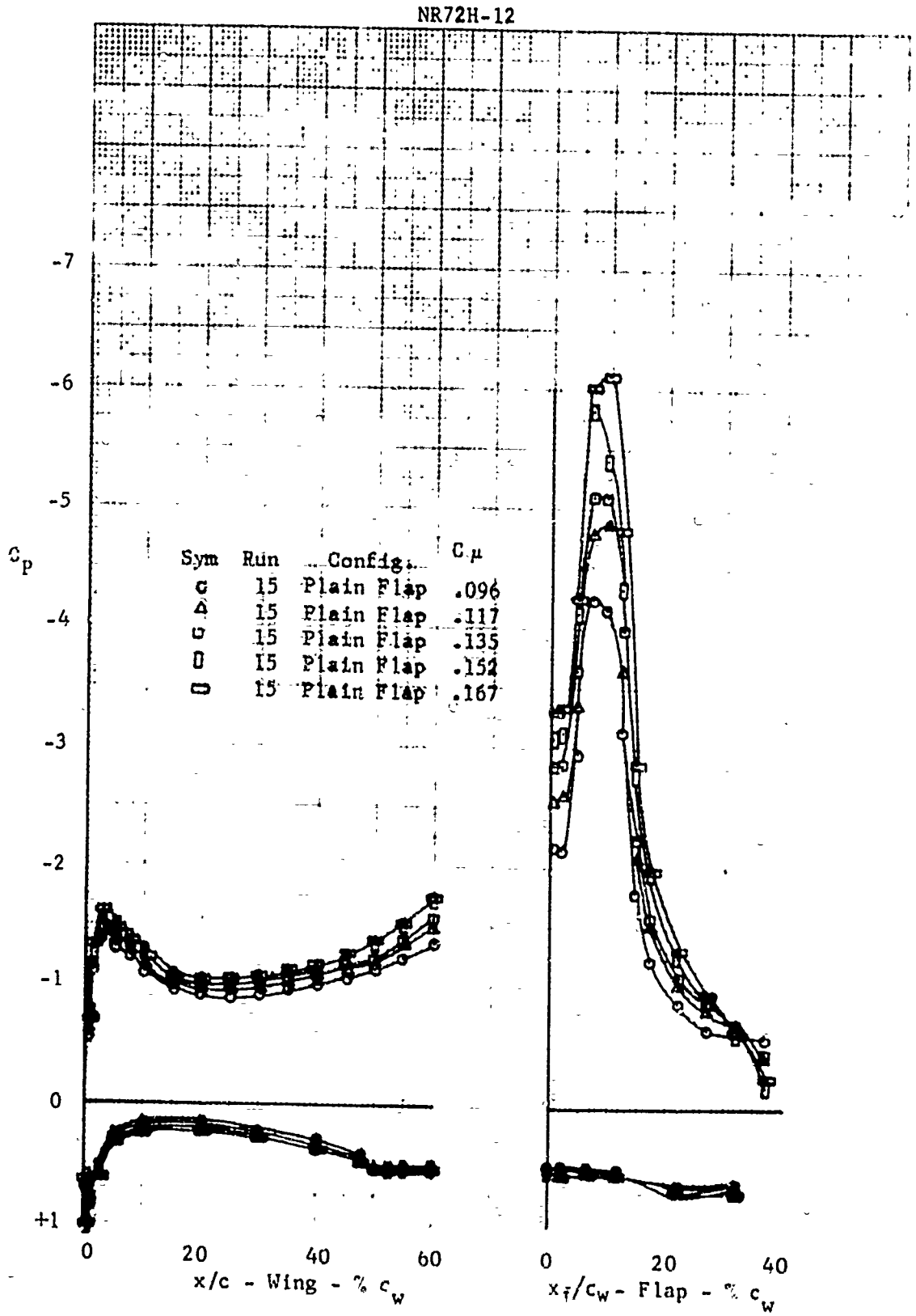

Figure 44. Effect of Momentum Coefficient steady blowing, $\alpha = 0$, $\delta_F = 40°$

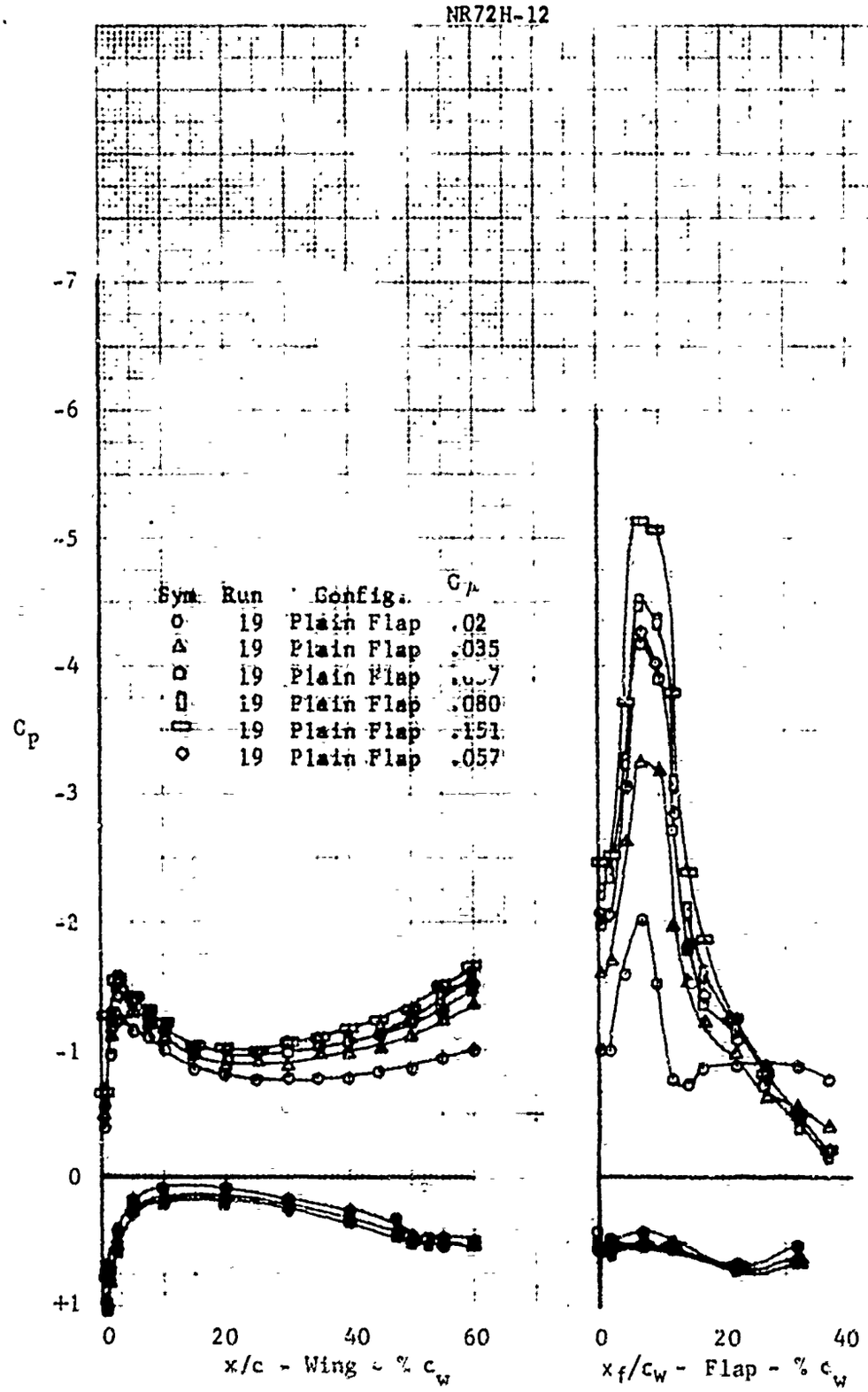

Figure 45. Effect of Momentum Coefficient

pulsing BLC, $\alpha = 0$, $\omega = 60$ Hz, $\delta_F = 40°$

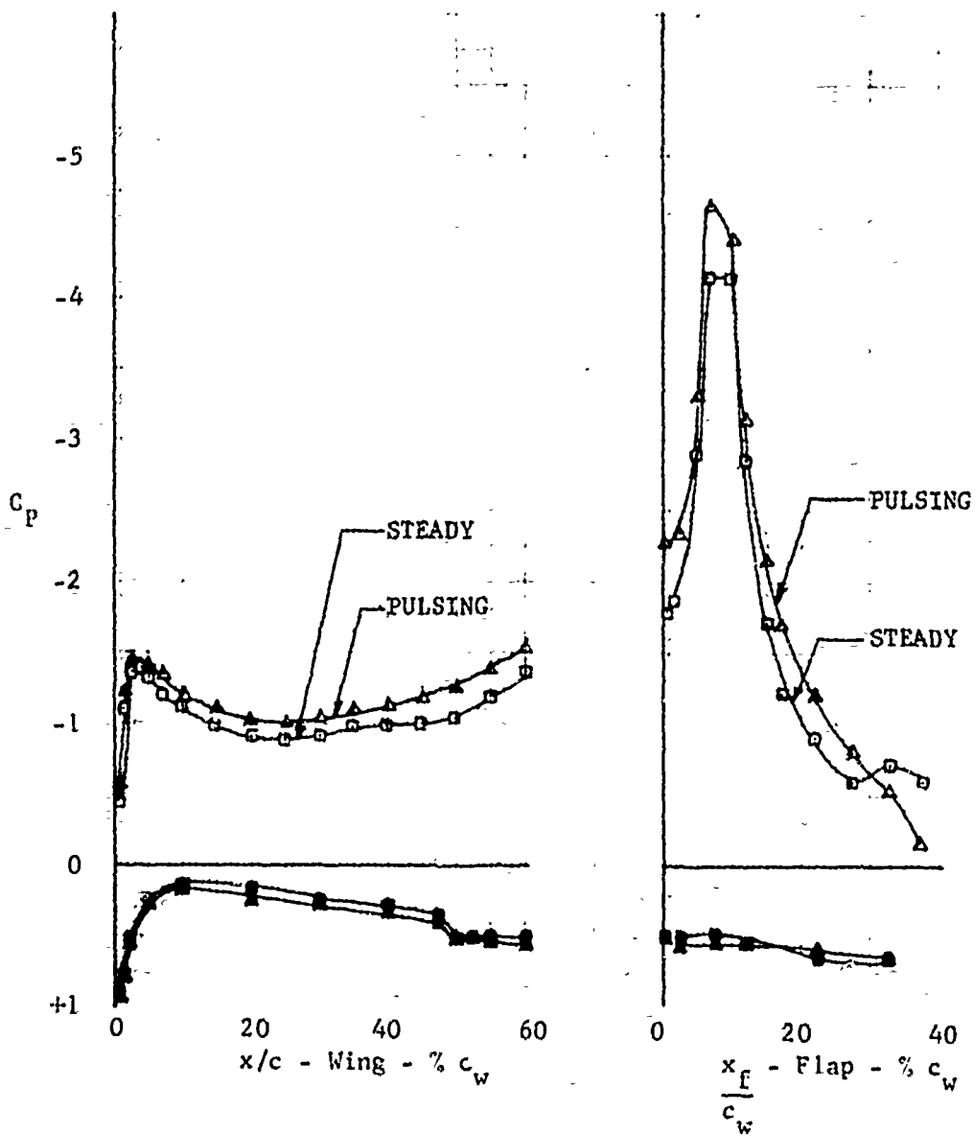

Figure 46. Comparison of Steady and Pulsing BLC
$\alpha = 0 \quad \delta_F = 40°$

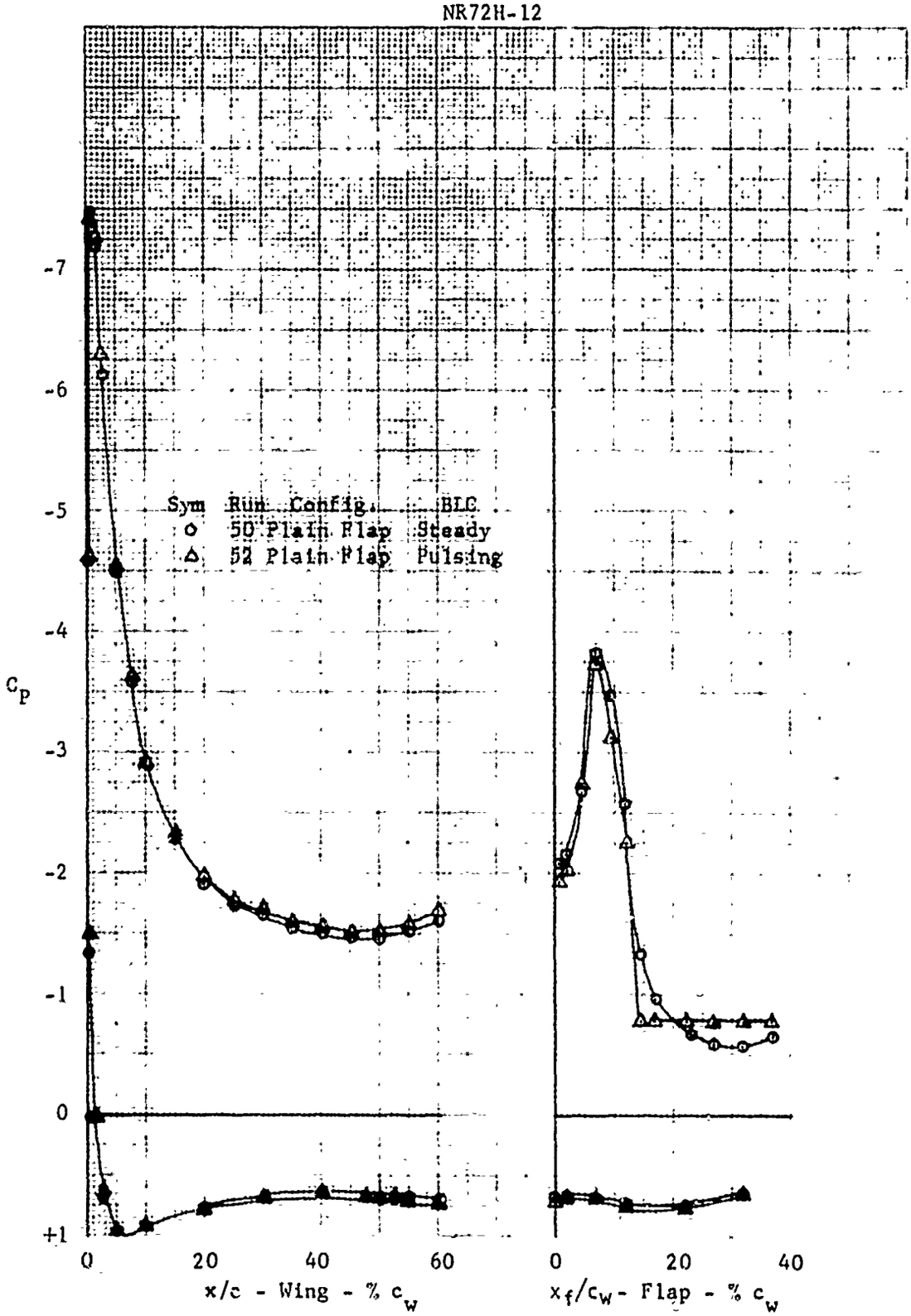

Figure 47. Comparison of Steady and Pulsing BLC
$C\mu = .06$, $\alpha = 20°$, $\delta_F = 40°$

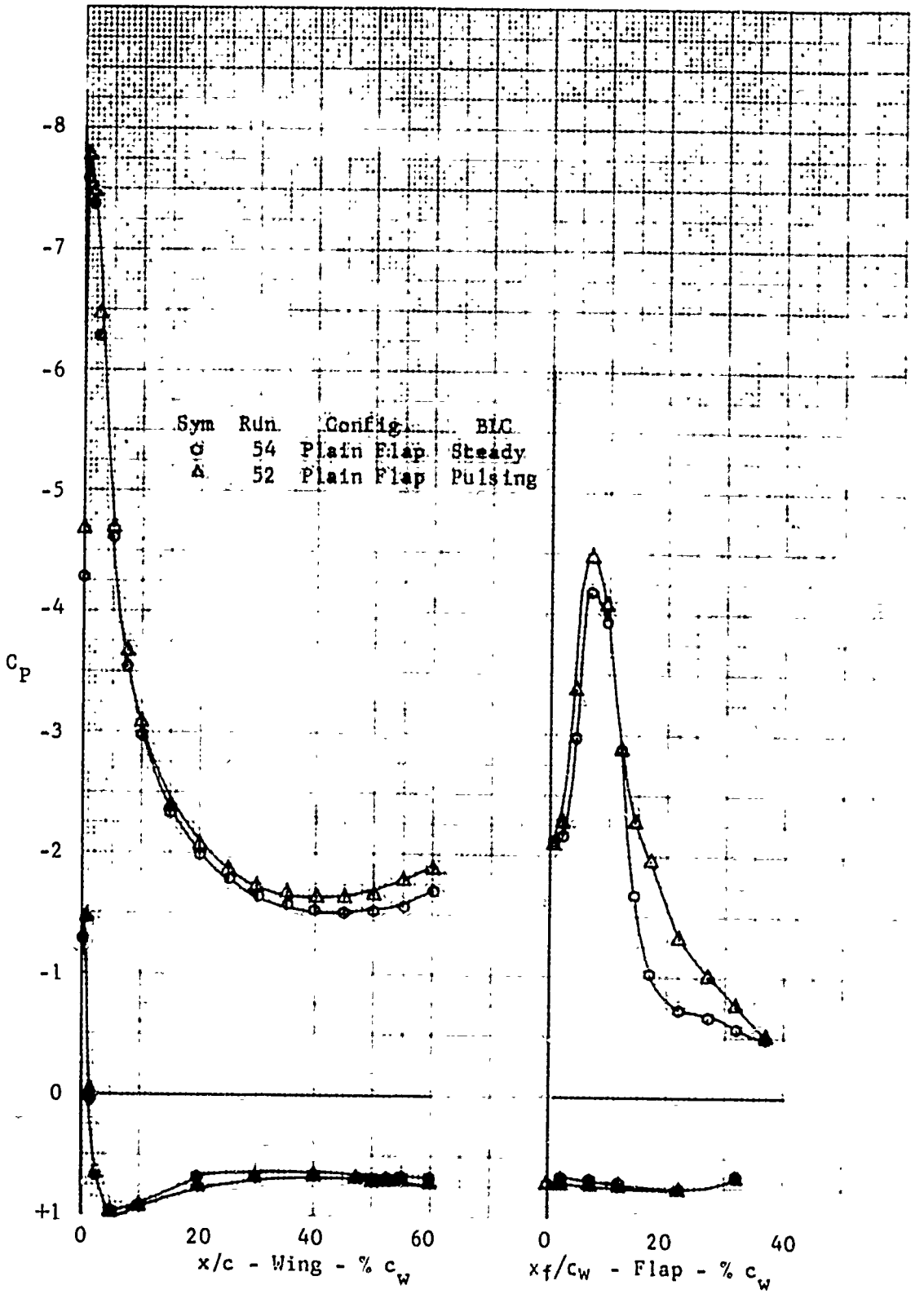

Figure 48 . Comparison of Steady and Pulsing BLC
$\alpha = 20°$, $C_\mu = .08$, $\delta_F = 40°$

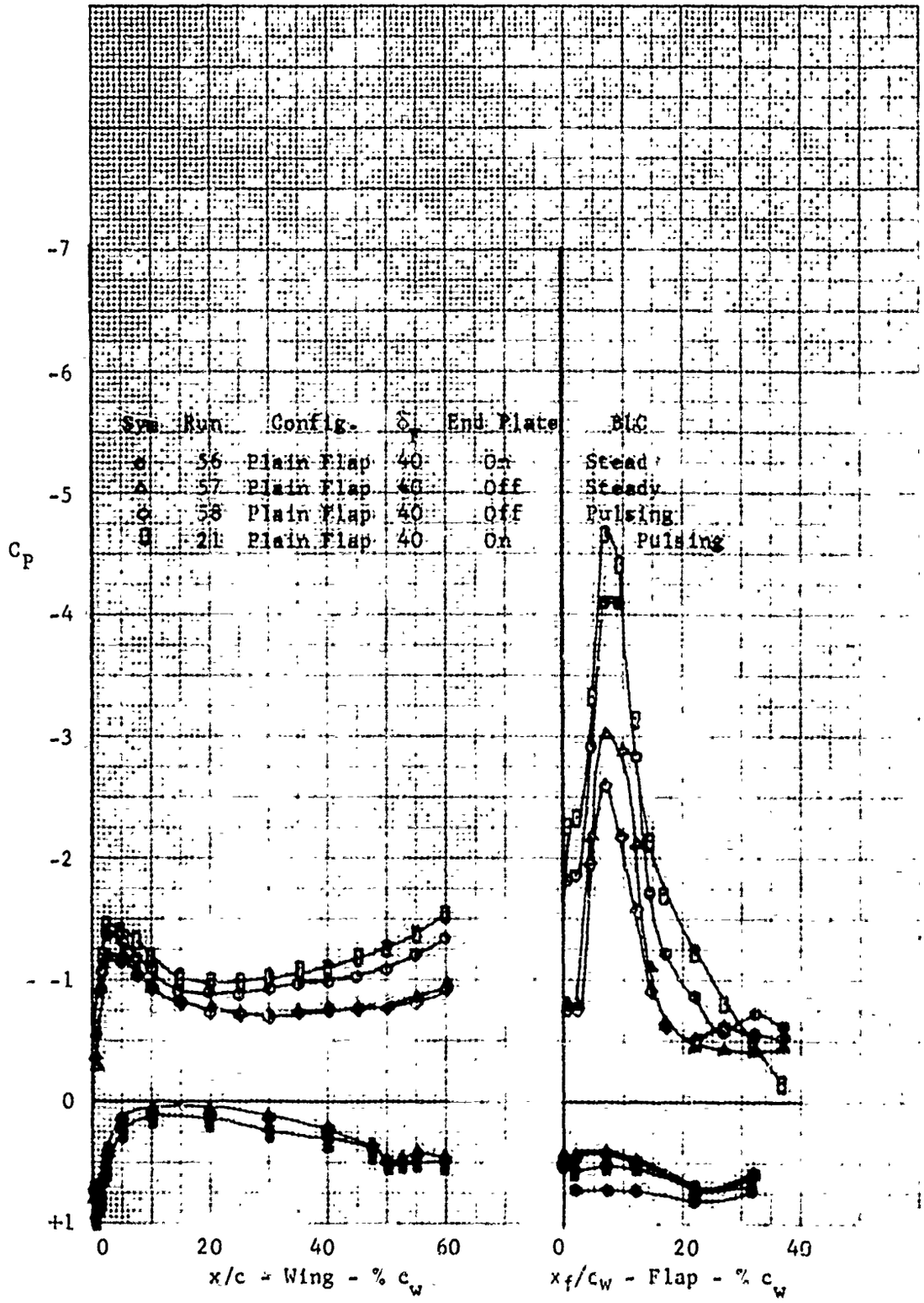

Figure 49. Effect of End Plates for Steady and Pulsing BLC
$\alpha = 0$

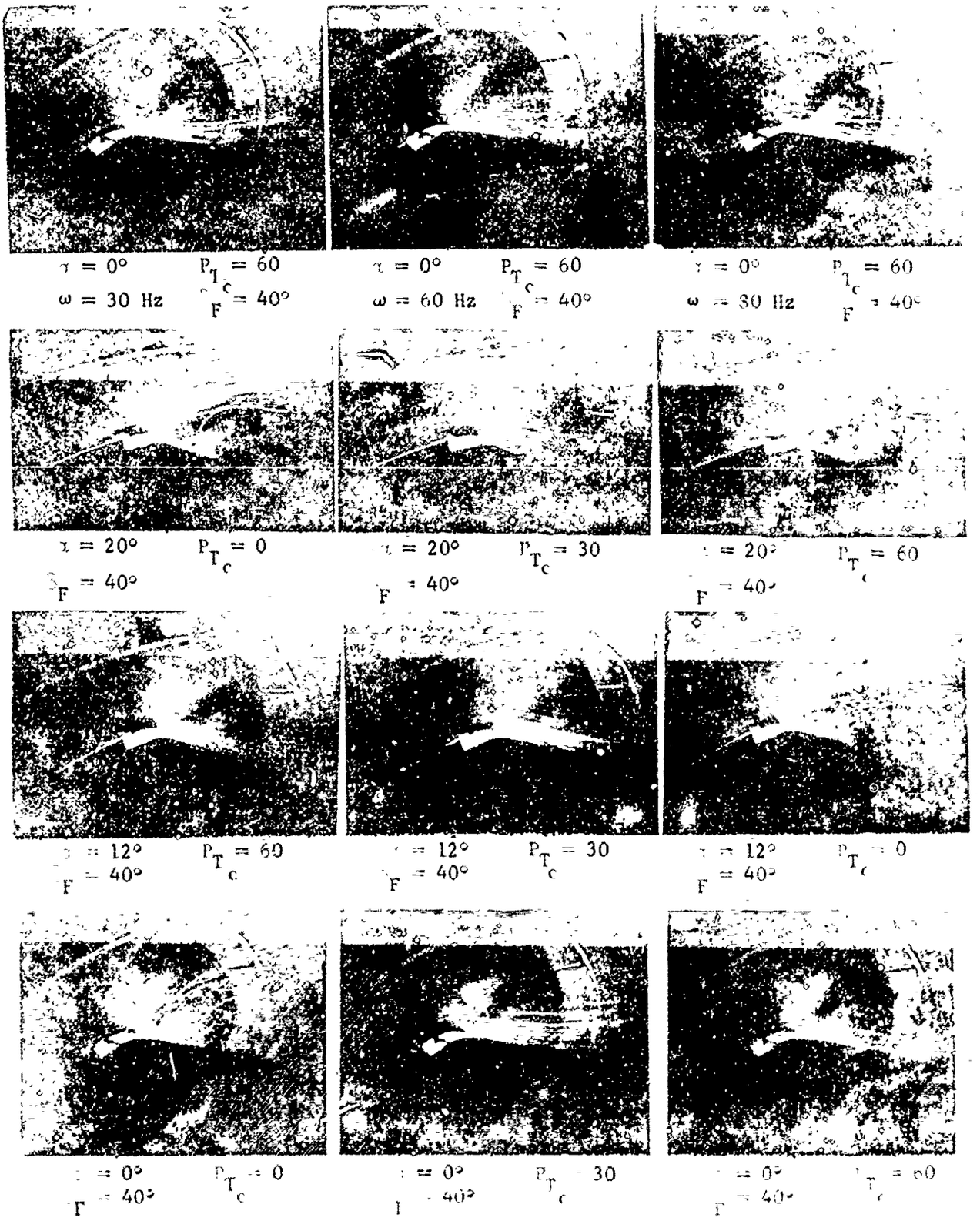

Figure 50a. Typical Flow Visualization Photographs

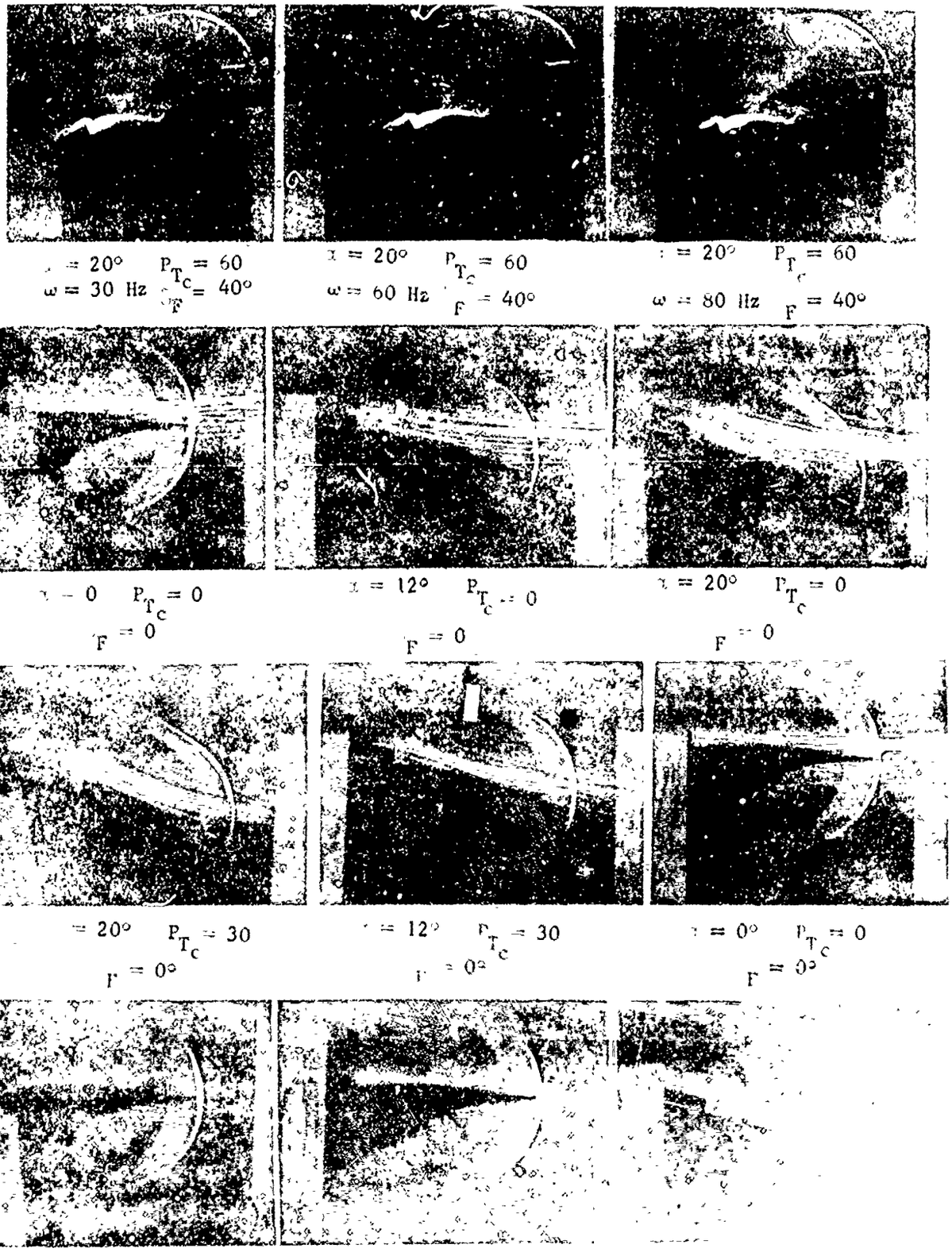

FORM 351-F

Figure 50b. Typical Flow Visualization Photographs

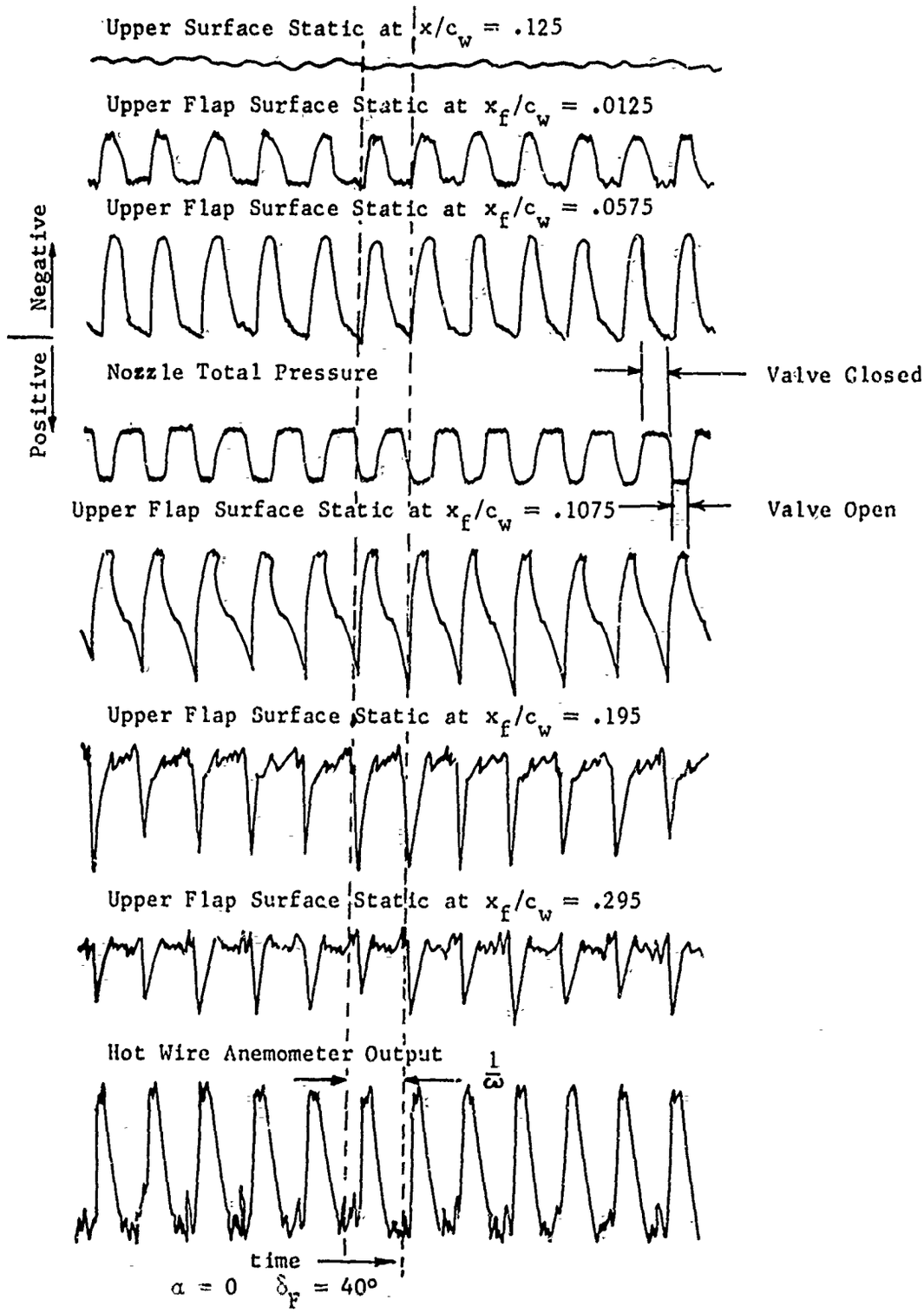

Figure 51a. Typical Outputs From Dynamic Transducers and Hot Wire Anemometer

h = 1/16" Flap Chord Station x_f/c_w = .27, ω = 60 Hz P_{T_c} = 60 psia

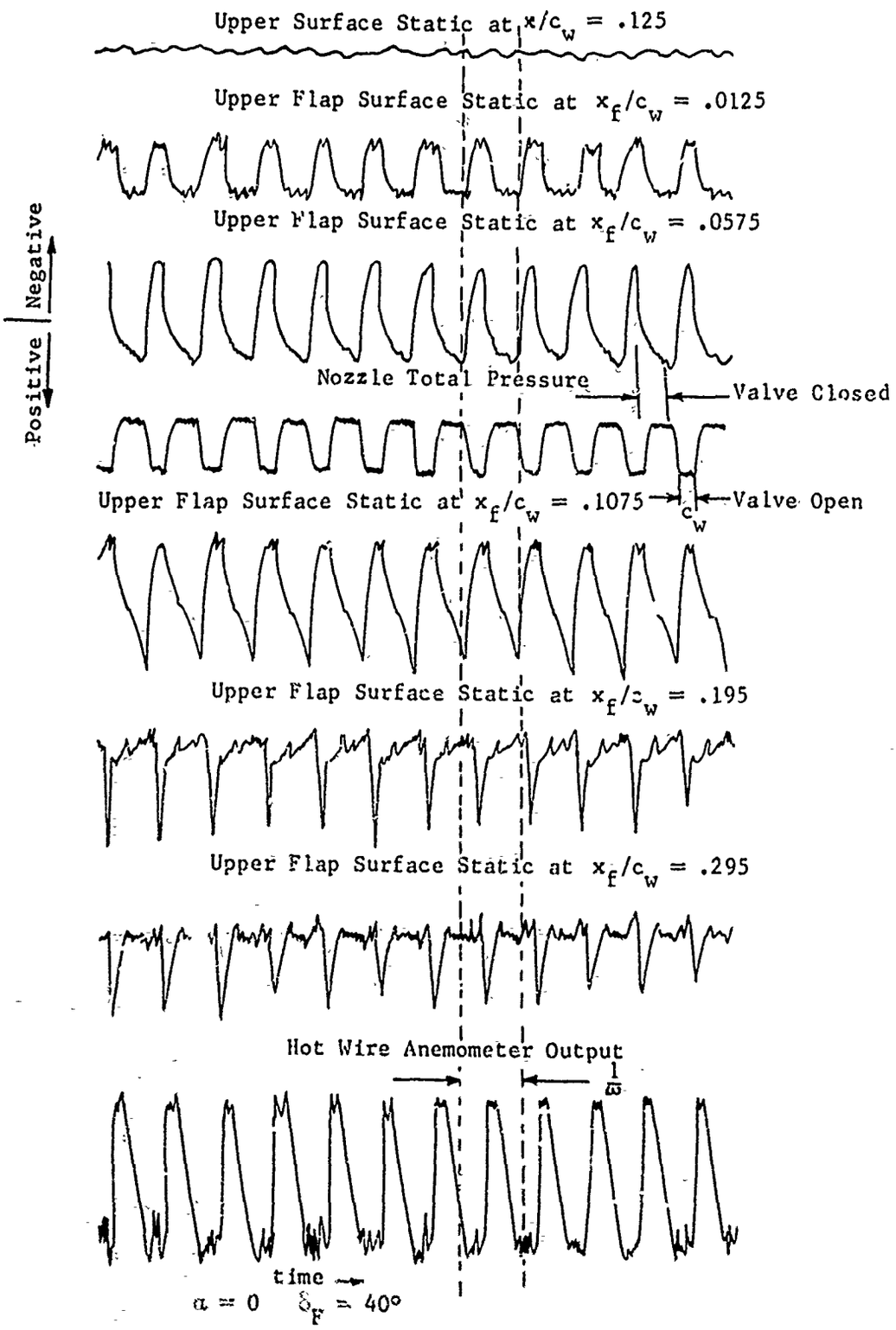

Figure 51b Typical Outputs from Dynamic Transducers and Hot Wire Anemometer

h = 1/8" Flap Chord Station x_f/c_w = .27, ω = 60 Hz P_{T_c} = 60 psia

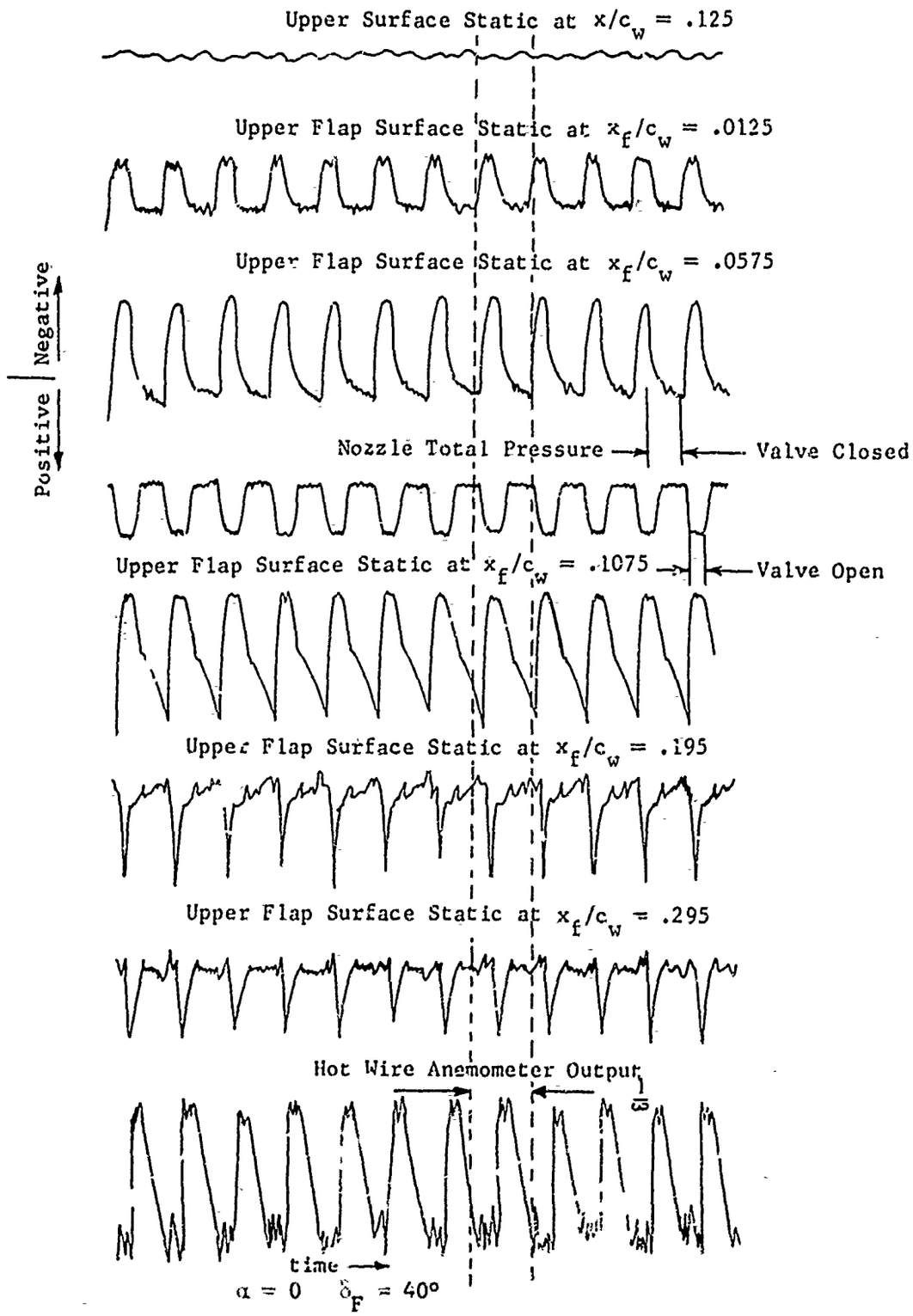

Figure 51c. Typical Outputs From Dynamic Transducers and Hot Wire Anemometer

h = 1/4" Flap Chord Station x_f/c_w = .27, ω = 60 Hz P_{T_c} = 60 psia

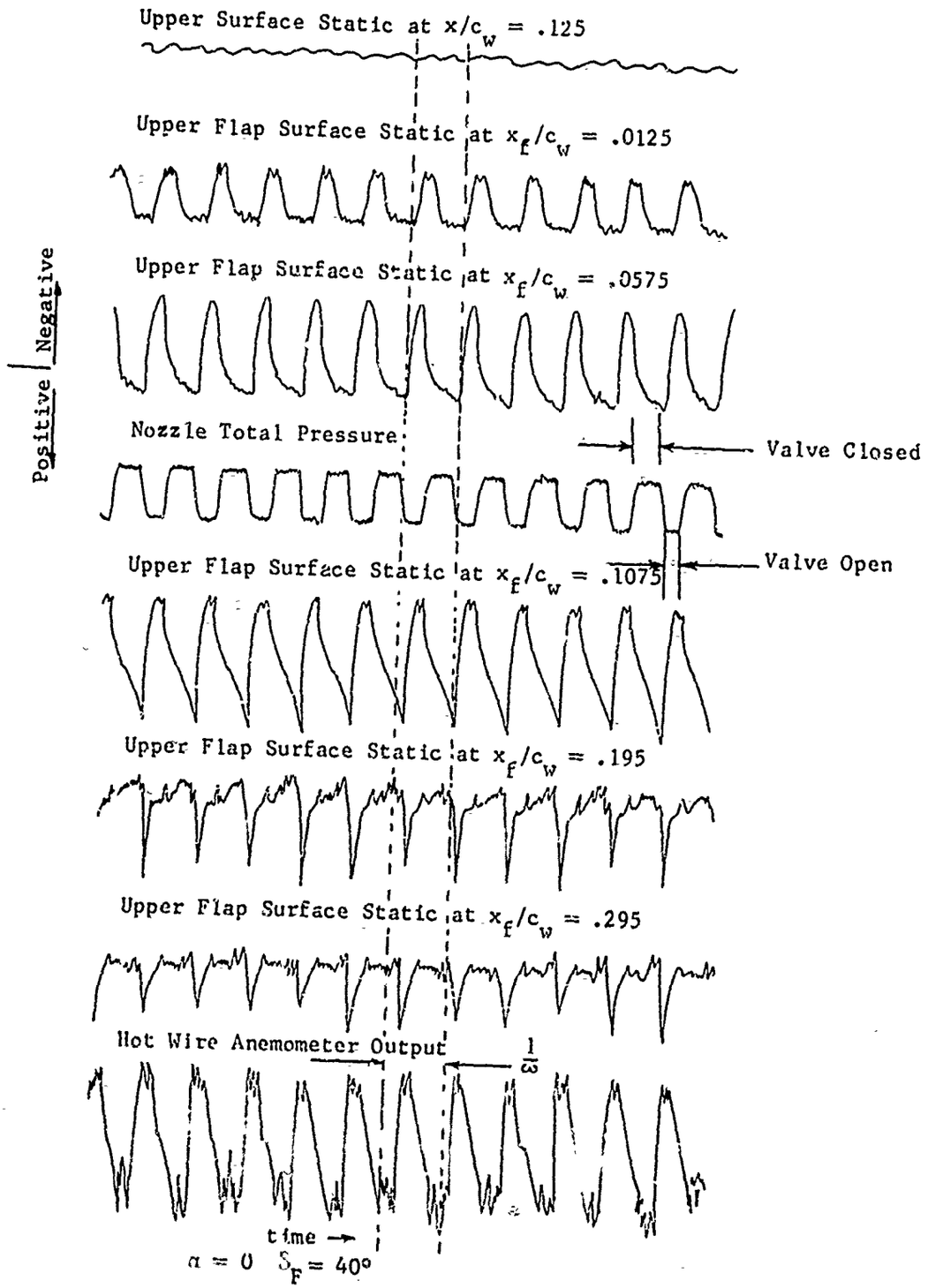

Figure 51d. Typical Outputs From Dynamic Transducers and Hot Wire Anemometer
h = 3/8" Flap Chord Station x_f/c_w = .27, ω = 60 Hz P_{T_c} = 60 psia

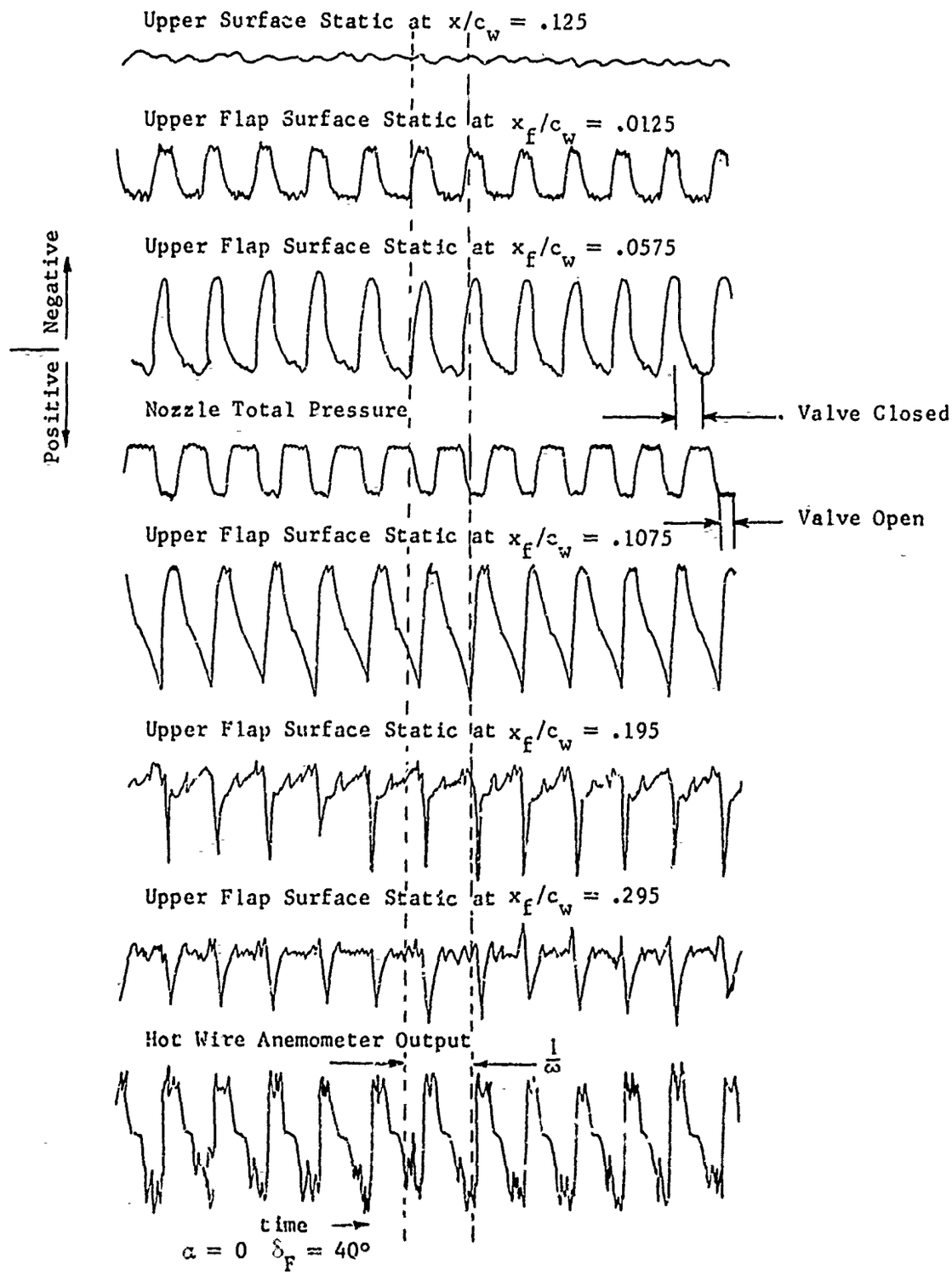

Figure 51e. Typical Outputs From Dynamic Transducers and Hot Wire Anemometer

$h = 1/2"$ Flap Chord Station $x_f/c_w = .27$, $\omega = 60$ Hz $P_{T_c} = 60$ psia

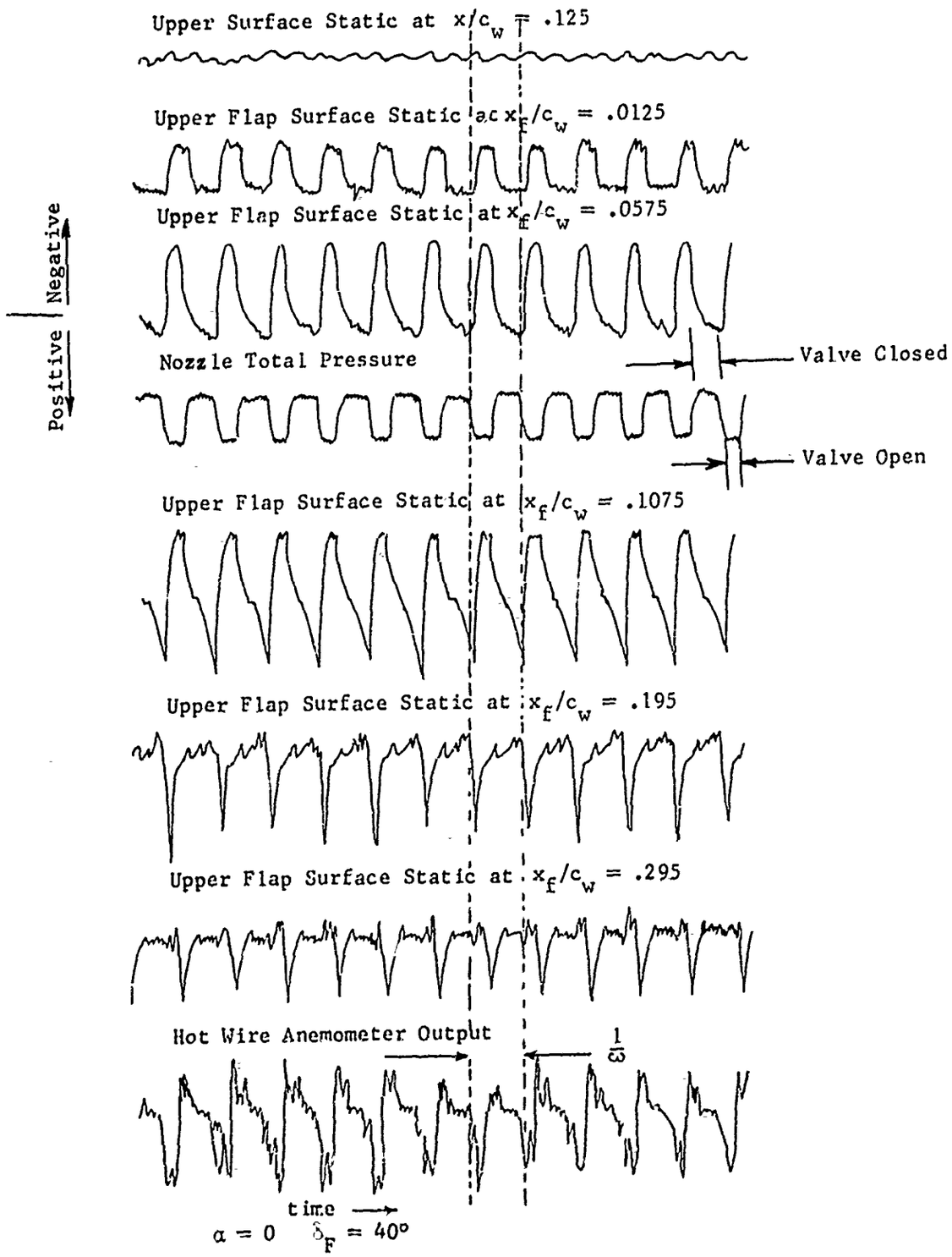

Figure 51f. Typical Outputs From Dynamic Transducers and Hot Wire Anemometer
h = 3/4" Flap Chord Station x_f/c_w = .27, ω = 60 Hz P_{T_c} = 60 psia

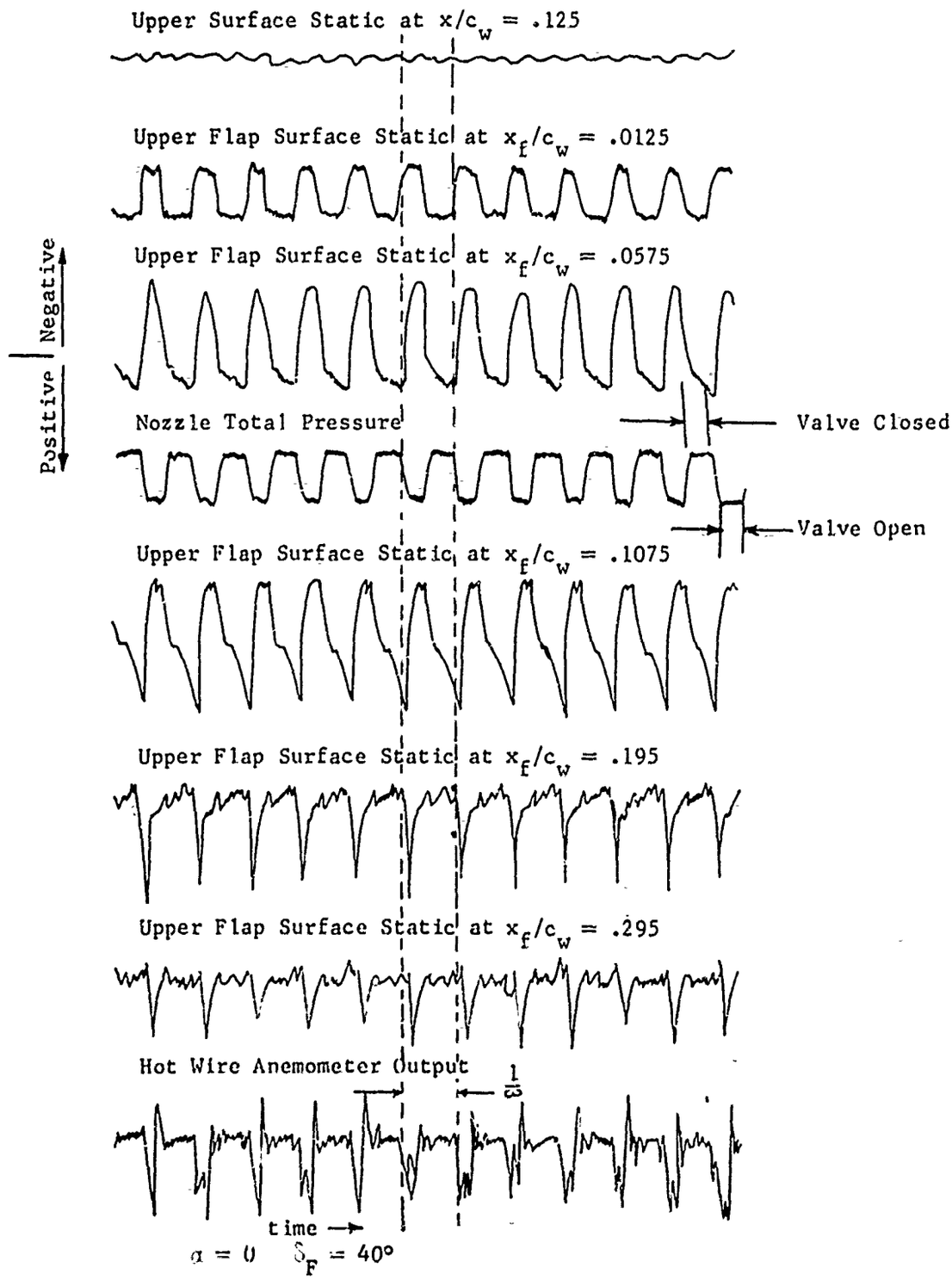

Figure 51g. Typical Outputs From Dynamic Transducers and Hot Wire Anemometer

FORM 351-F h = 1.0" Flap Chord Station x_f/c_w = .27, ω = 60 Hz P_{T_c} = 60 psia